

Improving seismic site response analysis for non-standard sites

Carolina Volpini

Thesis submitted to the Department of Civil and
Environmental Engineering, University of
Strathclyde, Glasgow, in fulfilment of the
requirements for the degree of:

Doctor of Philosophy

In

Civil and Environmental Engineering

Declaration of authenticity and author's right

This thesis is the result of the author's original research. It has been composed by the author and has not been previously submitted for examination, which has led to the award of a degree.

The copyright of this thesis belongs to the author under the terms of the United Kingdom Copyright Acts as qualified by University of Strathclyde Regulation 3.50. Due acknowledgement must always be made of the use of any material contained in, or derived from, this thesis.

Signed:

Date: June 2019

Acknowledgements

First, I would like to express my sincere gratitude to my advisor, Dr. John Douglas, for his support and patience throughout my PhD. His knowledge and guidance helped me, during these three years. He always encouraged me to believe in my research. I could not have imagined having a better supervisor. For this, thank you, John!

I would like to thank my second advisor, Prof. Alessandro Tarantino, for his insightful advices, during the whole period.

Besides my advisors, I am very grateful to Andreas H. Nielsen for his knowledge and incomparable help with codes. Thank you Andreas!

A special thanks goes to “University of Strathclyde for the Engineering: the future scholarship” for the opportunity to undertake this experience.

My sincere thanks also goes to CH2M/Jacobs team for the advices they gave me throughout my PhD, for the moments of discussion we shared and for the access to FLAC3D they provided for.

I would like to thank the reviewers of our Journal of Earthquake Engineering and Bulletin of Earthquake Engineering papers for their precious comments.

I would like to thank my Glasgow Family: all of you, guys! You made this journey so special!

Thank you to Emma, Manu and Fede for always being there for me.

Thank you to my sisters, Laura & Marea. You are my rocks!

A special thank goes to Andrea, without whom I could not arrive till this point. Thank you for supporting me, for helping me, for always being there for me. Thank you!

Last but not least, I thank my family for believing in me and supporting me throughout this path.

To my Parents

Abstract

Earthquake engineering aims to design and analyse structures to avoid damage in minor earthquakes and to prevent collapse in major earthquakes. An important aspect of assessing the ground motions that could occur at the basis of a structure is how the seismic waves will be affected by travelling through soil deposits near the surface. In fact, these near-surface layers act as a filter modifying (amplify/de-amplify) the input motion and leading to modified ground motions at the ground surface. Hence, the study of the effect of these near-surface layers on seismic waves is important for earthquake engineers designing and analysing structures in earthquake-prone regions.

The main issues connected with assessing earthquake ground motions are the uncertainties connected with many aspects of this phenomenon: from the knowledge of the fault rupture generating the seismic waves, through the overall travel path of these waves, to the modification of the waves near the surface. In this work, I concentrate my attention on the uncertainties connected with the near-surface soil deposits. In particular, I focus on aspects of site response analysis, i.e. the modelling of the modulation of seismic waves by soil deposits. The main goal of the thesis is to improve site response analysis for “non-standard” sites, which are those for which the general assumptions of shallow (<50m deep) perfectly horizontal layers breakdown.

Firstly, I focus on the importance of the stratigraphy; in particular, I undertake an analysis of the possible two-dimensional effects of quasi-horizontal layers. In general, there are two macro-worlds of interests: a) sites with marked one-dimensional characteristics (flat and parallel layers) and b) sites with pronounced two-dimensional characteristics (valleys and canyons). In this thesis, I conduct parametric site response analyses for sites at the boundaries between these two worlds after carefully checking the validity of my calculations by comparing the results of various

software packages. Based on these analyses I propose guidelines on the best way to analyse such sites.

Secondly, I carry out a detailed study on the uncertainties related to poor knowledge of the geotechnical characteristics of the soil, in particular its stiffness (shear-wave velocity). The main question I try to answer is when the lack of information on these characteristics has a significant impact on the computed site amplification. In particular, I focus on uncertainties connected with the deep portion (>50m) of soil profiles. Very often, it is difficult to have sufficient and/or reliable in-situ measurements of the characteristics of this part of soil deposits. Therefore, it is common to take advantage of the quarter-wavelength method to assess site amplifications for these profiles because it does not need a detailed shear-wave velocity profile. In this thesis, I develop a procedure to generate randomized profiles for use within the standard site response analysis technique used for shallow deposits. This procedure uses basic information obtained from a large database of real shear-wave velocity profiles, such as length of the deep portion of the profile, the thickness of the layers and the presence of softer layers below the seismic bedrock. Finally, I compare the site amplifications using this procedure and those computed using the quarter-wavelength method and draw conclusions about when our lack of knowledge is important.

Journal papers:

- 1- Guidance on Conducting 2D Linear Viscoelastic Site Response Analysis Using a Finite Element Code, Carolina Volpini, John Douglas & Andreas Hvidtfelt Nielsen (2019), *Journal of Earthquake Engineering*, DOI: 10.1080/13632469.2019.1568931. (basis of Chapter 2)
- 2- An accessible approach for the site response analysis of quasi-horizontal layered deposits, Carolina Volpini & John Douglas (2019), *Bulletin of Earthquake Engineering*, **17**(3), 1163-1183, DOI: 10.1007/s10518-018-0488-4. (basis of Chapter 3)
- 3- The influence of limited knowledge of deep (>100m) shear-wave velocities on estimated site amplifications, Carolina Volpini & John Douglas (2019), *not yet submitted*. (basis of Chapter 4)

Conference papers (see appendices):

- 1- Examining the assumption of homogeneous horizontal layers within seismic site response analysis, Carolina Volpini & John Douglas (2017), *Performance Based Design III (PBD)*, *Earthquake Geotechnical Engineering*, Vancouver.
- 2- Assessing earthquake site amplification for deep soil sites with uncertain bedrock conditions, Carolina Volpini & John Douglas, (2019), *7th International Conference on Earthquake Geotechnical Engineering*, Rome.

Contents

Introduction	1
1.1 Seismic Hazard.....	2
1.2 Site effects	5
1.3 Uncertainties connected to site response analysis.....	8
1.4 Thesis outline	15
References	15
Chapter 2.	19
2.1 Introduction	19
2.2 Guidance on conducting 2D linear viscoelastic site response analysis using a finite element code.....	24
Abstract	24
Keywords.....	25
2.2.1.Introduction	25
2.2.2.One-Dimensional Approach.....	26
2.2.3.Two-Dimensional Approach	29
2.2.3.1 Limitations of the 2D approach.....	29
2.2.3.2 Boundary conditions.....	30
2.2.3.3 Mesh Dimension.....	33
2.2.3.4 Input Motion.....	34

2.2.3.5 Damping	34
2.2.4. Testing Abaqus	37
2.2.5. Testing FLAC3D	48
2.2.5.1 Comparing Abaqus and FLAC3D	50
2.2.6. Conclusions	52
Acknowledgements	54
Bibliography	54
3.1 Introduction	59
References	65
3.2 An accessible approach for the site response analysis of quasi-horizontal layered deposits	67
Abstract	67
Keywords.....	68
3.2.1 Introduction	69
3.2.2 Previous studies on the limits of 1D SRA.....	70
3.2.3 Comparing 1d and 2d sra.....	77
3.2.3.1 Defining the tools	78
3.2.3.2 Results	82
3.2.4 Investigating numerically the boundary between 1d/2d for quasi-horizontal layers	84
3.2.5 Development of the chart	92
3.2.6 Probing the guidelines	94
3.2.7 Conclusions	98

Acknowledgements	98
Bibliography	99
Chapter. 4	104
4.1 Introduction	104
4.2. The influence of limited knowledge of deep (>100m) shear-wave velocities on estimated site amplifications.....	108
Abstract	108
4.2.1 Introduction	109
4.2.2 Literature review	111
4.2.2.1 Quarter-wavelength method	114
4.2.2.2 Site response analysis.....	116
4.2.3 Database	119
4.2.4 Method.....	120
4.2.5. Results	127
4.2.5.1 First profile with $50\text{m} < D \leq 100\text{m}$	127
4.2.5.2 Second profile with $50\text{m} < D \leq 100\text{m}$	129
4.2.5.3 Memphis profile with $D > 100\text{m}$	130
4.2.5.4 $D \leq 50\text{m}$ profile	132
4.2.5.5 Influence of thickness and velocity step on the inversion.....	133
4.2.6 NALS station.....	136
4.2.7. Conclusions	137
Bibliography	139

5. Conclusions and future works	145
Appendices	149
Appendix 1: Conference Paper “Examining the assumption of homogeneous horizontal layers within seismic site response analysis	149
Appendix 2: Conference paper “Assessing earthquake site amplification for deep soil sites with uncertain bedrock conditions”	168
Appendix 3: Results of Abaqus simulations:	182
Appendix 4: Validation of the software used in Chapter 4	192

List of Figures

Figure 1.1. Components of seismic risk. Seismic hazard map is from INGV. 3

Figure 1.2. The five steps of PSHA [taken from Baker (2008)]. 5

Figure 1.3. Seismic hazard calculation: source, path and site 6

Figure 1.5. Comparison between the site amplification from QWM and SRA for the actual Columbia profile 1..... 13

Figure 2.1: Soil column in Speed 21

Figure 2.2. Comparison between Speed and Deepsoil transfer functions for the considered soil column (see Figure 2.1)..... 22

Figure 2.2.1. Example showing how both FLAC3D and Abaqus display free-field boundaries. 33

Figure 2.2.2. Example of input motion chosen from the ITACA database, PGA=0.09g (Luzi et al., 2017)..... 34

Figure 2.2.3. Critical damping ratio as a function of angular frequency 37

Figure 2.2.4. Comparison between Strata and Abaqus using tied boundaries and the free-field option. Left: for 1%, STRATA, Free-field and Tied boundaries PGA=0.15g. Right: for 10%, STRATA, Free-field and Tied boundaries PGA=0.13g..... 39

Figure 2.2.5. Comparison between STRATA and Abaqus using the free-field option. Left: Vs= 200m/s. STRATA , D=1%, PGA=0.16g Abaqus PGA=0.15g. STRATA , D=10%, PGA=0.05g, Abaqus , D=10%, PGA=0.04g, Right: Vs=300 m/s. STRATA D=1% PGA=0.18g, Abaqus PGA=0.17g, STRATA D=10% PGA=0.08g, Abaqus D=10% PGA=0.09g, Top: 1% damping. Bottom: 10% damping..... 41

Figure 2.2.6. Comparison of the transfer function for different mesh dimensions, STRATA PGA=0.18g, Abaqus 2m PGA=0.13g, Abaqus 1m PGA=0.17g..... 42

Figure 2.2.7. $V_s = 600\text{m/s}$ model. On the left: comparison between symmetric matrix and asymmetric matrix; on the right: study on the influence of the width in asymmetric system, $w_{ff}=1$ and $w_{ff}=100$, STRATA, symmetric, asymmetric $\text{PGA}=0.15\text{g}$	42
Figure 2.2.8. Comparison between transfer functions for different choices of α and β depending on the frequencies targeted: 10% above, 1% below on the left (STRATA, $3f_0$, $5f_0$, $7f_0$ $\text{PGA}=0.15\text{g}$), 0.1% below on the right.	44
Figure 2.2.9. The domains and output locations considered for the buffer zone comparisons. ...	46
Figure 2.2.10. Comparisons in transfer functions for different buffer zone widths and damping ratios. Top: 1%. Middle: 3%. Bottom: 10%. Left: Centre. STRATA $d=1\%$: $\text{PGA}=0.34\text{g}$, Abaqus 50m $\text{PGA}=0.40\text{g}$, Abaqus 10m $\text{PGA}=0.37\text{g}$. Right: Right-hand buffer zone. STRATA= 0.35g Abaqus 50m $\text{PGA}=0.34\text{g}$, Abaqus 10m= 0.41g , Left: Centre. STRATA $d=3\%$: $\text{PGA}=0.32\text{g}$, Abaqus 50m $\text{PGA}=0.34\text{g}$ Abaqus 10m	47
Figure 2.2.11. The influence of the control frequency in FLAC3D on the transfer function. STRATA, f_0 , f_a $\text{PGA}=0.52\text{g}$, f_l $\text{PGA}=0.51\text{g}$	49
Figure 2.2.12. Abaqus and FLAC3D transfer functions for the three dipping layers model, Abaqus centre $\text{PGA}=0.045\text{g}$, FLAC $\text{PGA}=0.05\text{g}$	52
Figure 3.1. Geometry of the considered site (Modified from Appendix 1)	60
Figure 3.2. Comparison among the standard deviations of the logarithms of the velocity profiles with only geometric effects (blue), with geometric and.....	63
randomization effects (red) and the difference between the two (green) [from Volpini & Douglas (2017) – see appendix 1]	63
Figure 3.3. First criterion considered. Top: Geometry of the model, with the soil column and the control point chosen for the comparison; Bottom: comparison of 1D and 2D transfer functions, plus the 1D transfer function increased by 200%.....	64
Figure 3.4. Turkey Flat valley scheme.	65

Figure 3.2.1. 1-D SRA transfer function.	71
Figure 3.2.2. Example 1D and 2D transfer functions in a valley (Delépine and Semblat 2012).	72
Figure 3.2.3. The critical shape ratio equation of Bard and Bouchon (1985) and the parametric analyses conducted by Chavez-García and Faccioli (2000) to validate this equation.	74
Figure 3.2.4 The threshold between 1D and 2D SRA at the edge of the Duzce basin proposed by Emre et al. (2017).	75
Figure 3.2.5 Geometry of the model considered.	79
Figure 3.2.6 Examples of input motion chosen from the ITACA database.	81
Figure 3.2.7 Comparison between 1D SRA and 2D SRA. 1a-b 2° good and poor match, 2a-b 3° good and poor match, 3a-b 4° good and poor match, 4a-b 5° good and poor match.	84
Figure 3.2.8 Comparison of the 1D and 2D transfer functions for the 2° model and $V_s=400\text{m/s}$ at control point 250m as well as the graph for computing the goodness of fit parameter r	85
Figure 3.2.9 Summary of the Pearson's sample correlation coefficient, r , for all analyses. The colours and symbols identify different impedance contrasts. Each subplot is for a different slope angle and on each the results for every control point are plotted.	86
Figure 3.2.10 Summary of the Pearson's sample correlation coefficient, r , for the 200 m/s and 700 m/s analyses.	87
Figure 3.2.11 Summary of when the Pearson's sample correlation coefficient, r is above or below the 0.6 threshold. Each subplot is for a given control point: 250, 500, 750 and 1000m. The red dots indicates $r<0.6$ and black dots $r>0.6$	88
Figure 3.2.12 Examples of irregularities that can be encountered on real sites (a-b) and its simplification (c).	91
Figure 3.2.13 Summary of when the Pearson's sample correlation coefficient, r is above or below the 0.6 threshold for a control point of 750m, which is used as the basis of the guidelines. The threshold indicates the boundary between 1D being acceptable and 2D being required.	93

Figure 3.2.14 Comparison between the guidance proposed in this study and previous studies. .	98
Figure 4.1. Investigated volumes of invasive and non-invasive test. In particular a suspension logging test (PSSL), down-hole test (DH), cross-hole test (CH) and a general volume referred to as non-invasive test	105
Figure 4.2. Example of a deep shear wave velocity profile (Charleston) from Chapman et al. (2006) showing a comparison between it and the general USGS assumption.....	106
Figure 4.2.1: Memphis profile from Gomberg et al. (2003) and Cramer et al. (2004). Figure modified from Volpini and Douglas (2019)(see Appendix 2)	114
Figure 4.2.3: Procedure of Douglas et al. (2009) to generate V_s profiles. They identify the most uncertain zone by a dashed line [from Douglas et al. (2009)]	119
Figure 4.2.6: Description of the steps to come up with the final database.....	120
Figure 4.2.7: Scheme of the information taken from database needed to build randomized profiles.....	121
Figure 4.2.8a: Cumulative relative frequency plots of length after D and thickness of the layers. Top: $D \leq 50m$ profiles, center: $50m < D \leq 100m$, bottom: $D > 100m$	123
Figure 4.2.8b. Example for $D > 100m$. Top left: Thickness of velocity inversion; top right: Thickness of the top layer; bottom: velocity step in the inversion.....	124
Figure 4.2.9. V_s profiles for considered sites. Top: $D \leq 50m$, profiles 254 and 352 from the database. Bottom: $50m < D \leq 100m$, profiles 996 and 981 from the database.	126
Figure 4.2.10a. Randomized profiles assuming an inversion of type 1 and the resulting amplifications.	128
Figure 4.2.10b. Randomized profiles assuming an inversion of type 2 and the resulting amplifications.	128
Figure 4.2.10c. Randomized profiles assuming an inversion of type 3 and the resulting amplifications.	128

Figure 4.2.11a. Randomized profiles assuming an inversion of type 1 and the resulting amplifications.	129
Figure 4.2.11b. Randomized profiles assuming an inversion of type 3 and the resulting amplifications.	130
Figure 4.2.12a. Amplification function assuming inversions of type 1 (left) and type 3 (right).	131
Figure 4.2.12b. Comparison of the results of the two methods, where the dashed lines indicate the 95% confidence limits.	131
Figure 4.2.12c. Left: Profiles with no inversion of velocity; Right: Amplification functions of the original profile and the mean +/- confidence limits of the randomized profiles.	132
Figure 4.2.13. Amplification function assuming an inversion of type 3 for both profiles.....	133
Figure 4.2.14. Left: Original Vs profile and inversions of different thicknesses; Right: Original Vs profile and inversions with different velocity steps.	134
Figure 4.2.15a. Left: Comparison between results of QWM and SRA for different thicknesses. Right: Comparison between the results of QWM and SRA for different velocity steps. In both cases, the profiles refer to figure 4.2.14	135
Figure 4.2.15b. Left: Results of QWM for different velocity steps; Right: Results of QWM for different inversion thicknesses. In both cases, QWM is performed using the Vs profiles from figure 4.2.14, whereas the red curves are the results of the randomized procedure proposed here.	135
Figure 4.2.16a. Randomized shear-wave profiles and the related transfer functions (Inversion Type 1)	137
Figure 4.2.16b. Randomized shear-wave profiles and the related transfer functions (Inversion Type 3)	137
Figure D-1. Vs profiles used to validate Seismo-soil.....	192

Figure D-2. Comparison between Seismo-soil and Deepsoil transfer functions of the two Vs profiles (A and B). The blue curve indicates the ratio between the results of the two programs.

..... 193

List of Tables

Table 2.2.1. Characteristics of the soil column used for the tests	38
Table 2.2.2. Characteristics of the two soil columns used for the tests on the mesh size	40
Table 2.2.3. α and β for different values of f_1	44
Table 2.2.4. Characteristics of the model in FLAC3D.....	49
Table 2.2.5. Geometries of the three dipping layers considered	50
Table 2.2.6. Properties of the model with three dipping layers.....	51
Table 3.1: V_s profile	60
Table 3.2. Parameters of the Toro (1995) model for $V_s=180-360$ m/s, where $\rho_0, \rho_{200}, \Delta, d_0$ are respectively the initial correlation, correlation coefficient at 200m, model fitting parameter, initial depth parameter.....	62
Table 3.2.2 Pearson's sample correlation coefficient for geometries a, b and c.	91
Table 3.2.2 Summary of the real cases added to the guideline.	98
Table 4.2.1. Parameters defining the characteristics of the V_s profiles for the considered sites.	125

Introduction

An earthquake can be defined as the shaking of the Earth's surface due to the sudden release of energy in the lithosphere. The earthquake rupture creates seismic waves that radiate away from the source and travel through the crust until they reach the surface. Once the waves reach the end of this path they produce shaking on the ground surface with variable amplitude, duration and frequency content.

The strength, frequency content and duration at a particular site is a function of the size (i.e. how large the rupture is), location (e.g. distance from the site) and other source characteristics (e.g. focal mechanism) of the earthquake and on the characteristics of the site. This last factor is the core of this work. In fact, despite seismic waves travelling for the majority of their path through hard rock, at the very end of their journey, they generally encounter soil deposits. As can be realized, the characteristics of soil differ from those of the rock and these differing characteristics can greatly influence the nature of the shaking at the ground surface. Seismic waves invariably pass from harder (at the earthquake source) to softer rocks and sediments (near the surface). Passing from a stiffer material to a softer one means the waves slow down. This slowing down is translated into a bigger amplitude in order for the waves to carry the same amount of energy.

We can call soil deposits "filters" to seismic waves because they have the power to attenuate (or de-amplify) the ground motion at certain frequencies and amplifying it at others. The main issue associated with site effects is the fact that soil conditions often vary dramatically over short distances (<100m) and this causes a variation also in the

shaking of the ground within a small geographical area (e.g. the footprint of a large structure, such as a nuclear power plant).

“One of the most important aspects of geotechnical earthquake engineering practice involves evaluation of the effects of local soil conditions on strong ground motion.”
(Kramer, 1996).

This quotation, taken from the well-known book entitled “Geotechnical Earthquake Engineering”, demonstrates the importance of studying site effects and the influence of soil deposits on earthquake ground motions.

In the following sections, the principal aspects of seismic hazard assessment are discussed and the scope of this thesis defined.

1.1 Seismic Hazard

From an engineering point of view, during the design of a project, it is fundamental to make a trade-off between the costs of the structure and the risk to which it is subjected. The prediction and assessment of the effects of a seismic event is a multidisciplinary process, involving many experts, such as seismologists, geotechnical and structural engineers, and risk managers. The risk (Figure 1.1) associated to earthquakes can be split into three main components, which are:

- Seismic hazard assessment (Hazard), which is the probability an earthquake will occur in a certain area, within a certain window of time and with ground motion intensity exceeding a certain threshold;
- Structural response and damage to components (Vulnerability), which is predictable as function of the prescribed intensity measures adopting full probability distribution functions; and

- Repair costs and loss analysis (Exposure). In this context, we talk about “elements at risk”, which can be buildings, population, lifeline systems or socioeconomic activities. Exposure data can vary, depending on the scale of the analysis, from the detailed descriptions of characteristics of structural elements to larger geographical entities, such as administrative units, cities or countries.

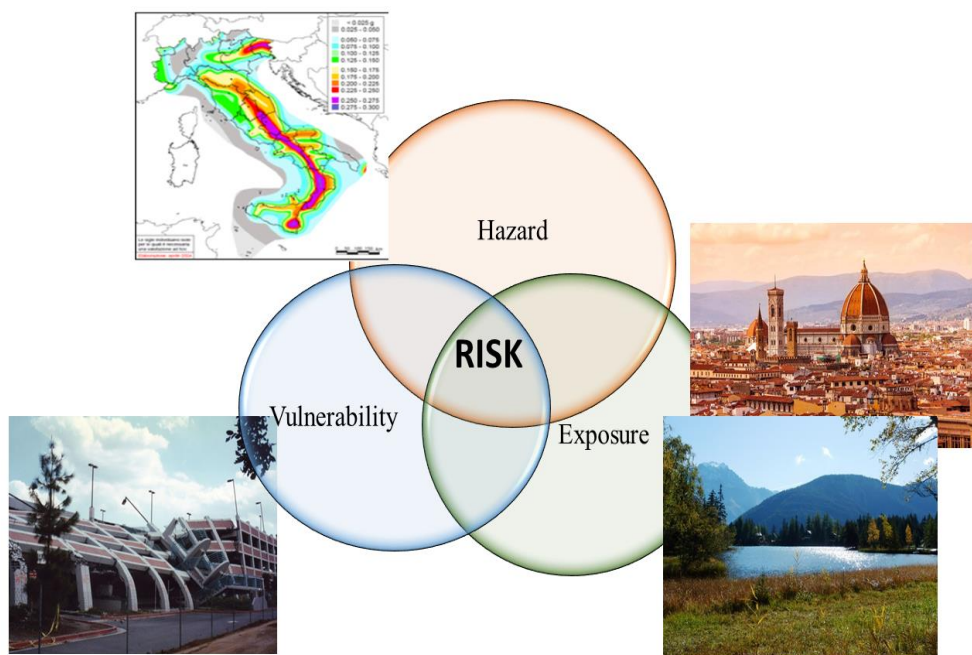


Figure 1.1. Components of seismic risk. Seismic hazard map is from INGV.

All of these components are affected by uncertainties. In this work, I concentrate on the seismic hazard component only. In particular, as it is impossible given the time available for this thesis to account for all the complex factors that control ground motion at a site (source, path and site effects), I focus on just in the third one: the evaluation of site effects through site response analysis (SRA). The importance of this contribution to the assessed seismic hazard is discussed, for example, in Bazzurro and Cornell (2004), where they performed a statistical study on the effect of soil layers with uncertain properties on ground-motion intensity at

the surface. They study the effect of the soil in terms of a site-specific, frequency-dependant amplification function, $AF(f)$, where f is a generic frequency, with the aim to identify parameters [magnitude, M , source-to-distance, R , peak ground acceleration, PGA , spectral acceleration values, $Sa(f)$] to give an efficient prediction.

When discussing seismic hazard assessment it is important to highlight the concept of probabilistic seismic hazard analysis (PSHA), described for the first time by Cornell (1968). PSHA estimates the probability of exceeding various ground-motion levels at a given site or area in a given future window of time. We can divide this procedure into five main steps (Figure 1.2):

- 1- Identification of all earthquake sources capable of producing damaging ground motions;
- 2- Definition of the rates at which earthquake of various magnitudes are expected to occur;
- 3- Characterization of the distribution of source-to-site distances associated with potential earthquakes;
- 4- Prediction of the distribution of ground-motion intensity as a function of magnitude, distance and so forth;
- 5- Combine uncertainties in earthquake size, location and ground-motion intensity, using a calculation known as the total probability theorem.

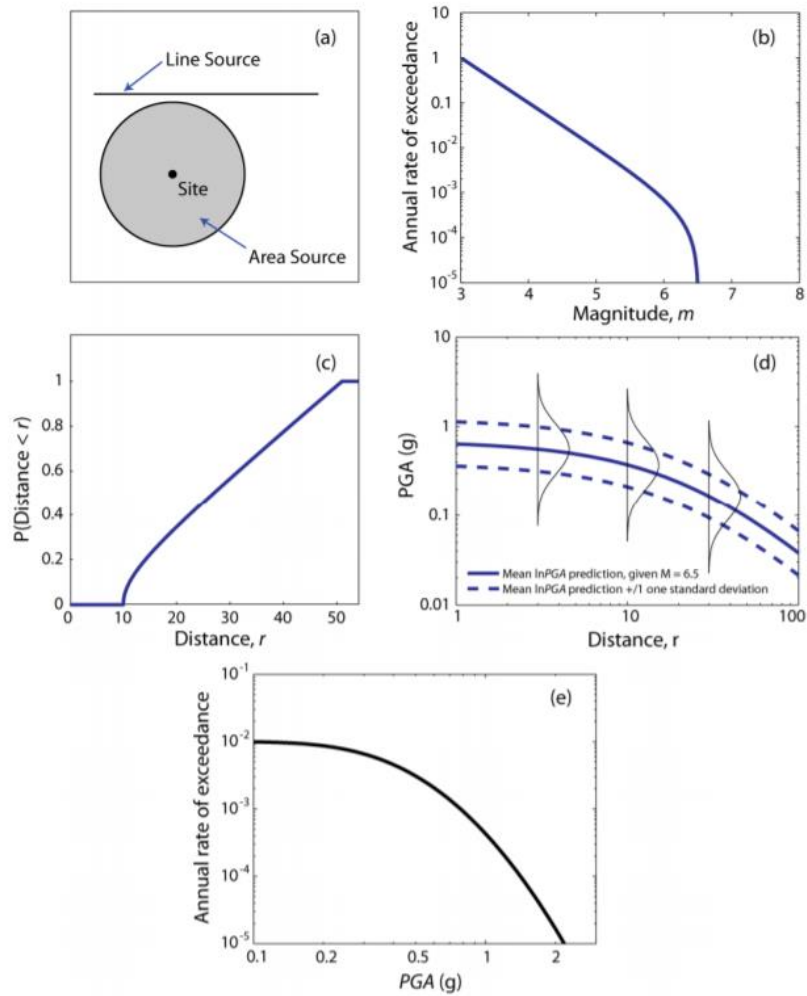


Figure 1.2. The five steps of PSHA [taken from Baker (2008)].

Previously, it was common to use deterministic seismic hazard analysis, where a single deterministic design earthquake resulted from the analysis. The analyses presented in this thesis are still relevant in this case as site effects can be seen as an extension of step 4 of PSHA (which is required both for probabilistic and deterministic analyses) for the case of non-rock sites.

1.2 Site effects

Once the PSHA has determined the prescribed ground motion at a reference condition, the site effects need to be assessed. They can be quantified by the

difference between the ground motion for the true site conditions at the surface at a location of interest and the results of the PSHA for the reference conditions.

In fact, going beyond the source and path, the site response should be addressed to evaluate the complete seismic hazard. Figure 1.3 displays a sketch of these steps.

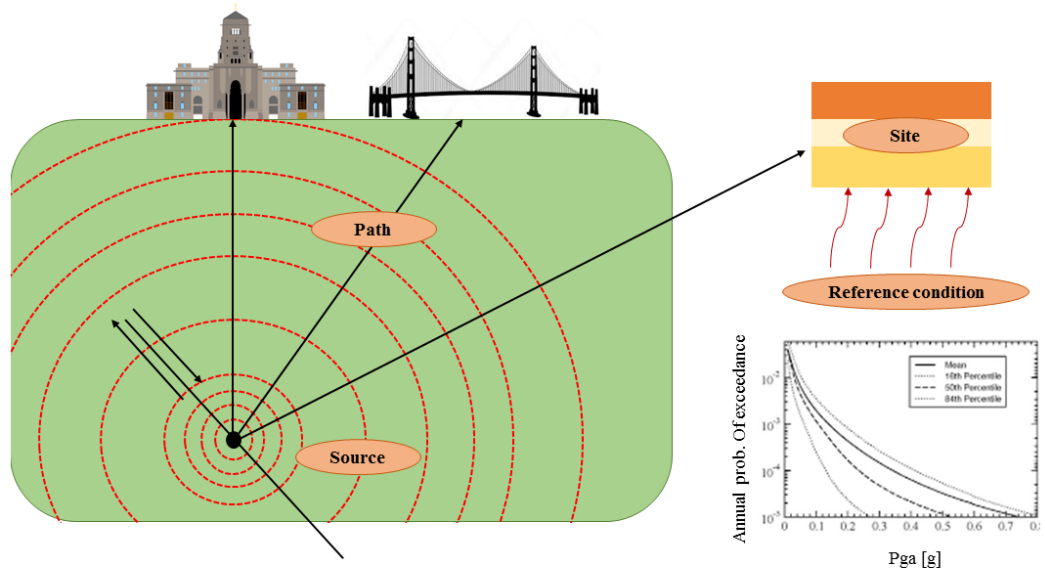


Figure 1.3. Seismic hazard calculation: source, path and site

Site response analysis (SRA) is generally represented in the frequency domain. The response spectral acceleration (SA) of an oscillator with period T_0 , is the maximum acceleration of a single degree of freedom (SDOF) system with a natural period T_0 , subjected to an input motion:

$$SA(T_0) = \max[a(t)]_{T=T_0} \quad [1]$$

The curve obtained by plotting SA as a function of T_0 is called the response spectrum (RS).

The spectral acceleration computed at $T_0=0s$ equals the peak ground acceleration (PGA). The amplification function of the system is defined as the ratio between the surface spectral acceleration and the input spectral acceleration (Equation 2):

$$\overline{AF(T)} = \frac{SA(T)_{surface}}{SA(T)_{input}} \quad [2]$$

It is essential to include $\overline{AF(T)}$ in the PSHA to obtain a more rigorous and site-specific evaluation of the hazard (Pehlivan et al., 2016). The mean amplification function should be calculated along with its standard deviation. Performing this calculation within a rigorous probabilistic approach to account for site effects allows for a consistent probabilistic evaluation of the hazard at the specific site. Figure 1.4 displays this approach to incorporate SRA into PSHA. Further details about the steps of SRA are given in the main chapters of this thesis.

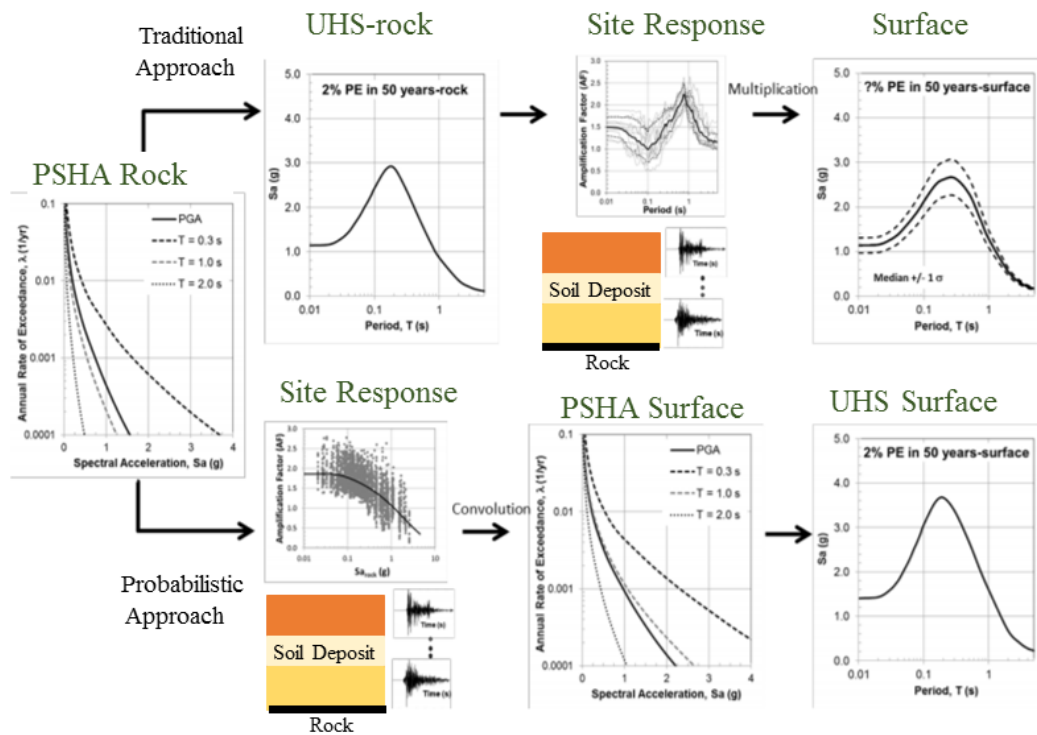


Figure 1.4. Scheme to incorporate site response into PSHA. UHS is the uniform hazard spectrum. Modified from Pehlivan et al. (2016).

1.3 Uncertainties connected to site response analysis

One of the aspect that should be addressed here is the concept of uncertainties when talking about SRA. In fact, as stated in the sentence of Kramer (1996) quoted above, soil conditions can vary dramatically within a small area, so in an ideal case we would know these conditions in detail. Such a situation appears to be impossible using present technology and particularly for the vast majority of sites.

The first limitation comes from the knowledge of the geology of the site, which is directly connected to its stratigraphy and topography. In this work, we will specifically address the uncertainty connected to quasi-horizontal layers (i.e. the problem of stratigraphy and spatial variability). The second main problem is connected to the *in-situ* measurements, which are affected (for their intrinsic definition) by error. Hence, the geomechanical parameters of the soil deposit are affected by uncertainties.

Consequently, a model for the soil behaviour should be taken into consideration, according to the level of knowledge of the soil parameters. Despite the fact that soils clearly behave non-linearly (Aki, 1988; Vucetic, 1994; Ordaz and Faccioli, 1994) under strong input motions, the parameters necessary to describe a non-linear constitutive model are often difficult to define and there is the risk of introducing more uncertainties. That is why simpler models of soil behaviour are useful. The easiest one is the linear elastic model, whose use should be restricted to small shear strain amplitudes (small to moderate ground motion), e.g. up to a shear strain of 10^{-5} (Vucetic, 1994). Here the material does not present dissipative characteristics, which is, conversely, a property of linear viscoelastic models. These will be the main models used within this work. Further details of these models are explained in Chapters 2 and 3.

At the boundary between linear and non-linear model behaviours, there is the equivalent-linear approach, originally proposed by Schnabel et al. (1972). Herein, the effects of non-linearity are approximated by performing a series of linear analyses in which the average, or secant shear modulus and the damping ratio are varied until their values are consistent with the level of the strain induced in the soil.

Concentrating our attention on linear models, we can clearly define the main parameters needed as the stiffness (G), damping (D), density and Poisson's ratio. This last one is particularly important when it comes to P-waves. Among them, the most important are G and D . G is directly connected to the shear wave velocity (V_s) and the density (ρ) of the soil, in this way:

$$G_{max} = \rho V_s^2 \quad [3]$$

where G is denoted as G_{max} because it is the value of stiffness at low strains.

D can be associated with the capacity of the soil to dissipate energy. In fact, part of the elastic energy of a travelling wave is always converted to heat, which means a decrease in the amplitude of the wave. For simplicity, we use viscous damping to represent this dissipation of elastic energy. In this approach, the soil is modelled as a Kelvin-Voigt solid where the stress-strain relationship can be expressed as:

$$\tau = G\gamma + \eta \frac{\partial \gamma}{\partial t} \quad [4]$$

Where τ is the shear stress, γ is the shear strain and η is the viscosity of the material. According to this formula, τ is the sum of an elastic part and a viscous part. For a harmonic shear strain:

$$\gamma = \gamma_0 \sin \omega t \quad [5]$$

Combining equations [4] and [5], the stress-strain loop of a Kelvin-Voigt solid is elliptical. The elastic energy dissipated in a single cycle is given by the area of the ellipse. Equation [6], which gives the amount of dissipated energy, tells also that this last one is proportional to the frequency of loading:

$$\Delta W = \int_{t_0}^{t_0+2\pi/\omega} \tau \frac{\partial \gamma}{\partial t} dt = \pi \eta \omega \gamma_0^2 \quad [6]$$

In reality, the dissipated energy is insensitive to frequency. Connected to this, there is the concept of damping ratio, which can be computed as:

$$\xi = \frac{1}{4\pi} \frac{\Delta W}{W} = \frac{1}{4\pi} \frac{\pi \eta \omega \gamma_0^2}{\frac{1}{2} G \gamma_0^2} = \frac{\eta \omega}{2G} \quad [7]$$

To eliminate the dependence on frequency, equation [7] is rewritten to produce an equivalent viscosity, so that the damping ratio is independent of frequency:

$$\eta = \frac{2G}{\omega} \xi \quad [8]$$

Further details on the damping formulation are given in Chapters 2 and 3.

Kramer (1996) pointed out the influence of the soil deposit as the major reason for variations in ground motion over a small area. This variation is mainly due to differences in the stiffness of the soil near the surface. Seismic waves generally travel through tens of kilometres of rock until they reach the soil deposit, which is often not deeper than 150m. At the interface between two materials with different stiffnesses, the body waves are reflected and refracted. Due to the fact that wave propagation

velocities of shallower materials are generally lower than the ones beneath them, inclined rays, when reaching horizontal layers are usually refracted to a more vertical direction. This is the main assumption that one-dimensional SRA uses, combined with the concept that the response of a soil deposit is predominantly caused by SH-waves, which propagate vertically from the underlying bedrock.

This common assumption leads to the first question I will try to answer in this thesis: is it always possible to use one-dimensional SRA to study a soil deposit? The answer is clearly no because there are several situations where the complex geometry of the site prevents SRA from returning a correct answer. Indeed, despite its simplicity and the fact that good results are obtained for flat soil deposits, there are many cases, such as sloping or irregular ground surfaces or valleys or even the presence of an embedded structure, like a wall or a tunnel, where the one-dimensional approach is no longer applicable. These particular conditions require the use of more complex analyses, such as two-dimensional (2D) or three-dimensional (3D) approaches. The main advantage of 2D or 3D analysis is the possibility of simulating the complete wavefield within the model. Moreover, both surface waves (e.g. Rayleigh and Love), compressional waves (i.e. P) and vertically polarized shear waves (i.e. SV) can propagate within the model. The problems associated with these analyses are: the difficulty in assigning boundary conditions to the model, what input motion should be applied, the discretization of the model (mesh), the damping formulation, the constitutive models and the computational cost. For all these reasons, such kind of analyses are used just for particular conditions and for projects that can afford the resources in terms of time and effort to conduct the analyses and interpret the results.

Pehlivan et al. (2012) investigated the different results obtained with 1D and 2D SRA to spatial variability in the shear-wave velocity via a Monte Carlo simulation

technique. The results showed that multiple 1D analyses could generate similar median response spectra across a region of interest to 2D analyses. The largest observed difference was about 10%. In contrast, the differences in the variability in the computed responses was more significant.

In this work, I focus my attention on site deposits that are at the boundaries between these two worlds: perfectly 1D and obviously 2D. Further details on these analyses will be explained in Chapters 2 and 3.

Connected to the in-situ measurements (V_s) of the soil stiffness (G) there is another aspect that should be addressed. These tests have a limited capacity to sample V_s in the deep portion of a soil deposit. The reasons for this are:

- Loss of resolution of the tests. For instance, non-invasive tests, which do not require a borehole present this kind of problem;
- High costs, especially connected to invasive tests (those which require at least one borehole to the depth where V_s is required); and
- Difficulty in the interpretation of the results from great depths, especially for non-invasive tests.

One of the potential solutions to overcome this problem is the quarter wavelength method (QWM), proposed by Joyner et al. (1981) and then optimized by Boore (2013). The power of this method compared to using the single V_s profile obtained with an in-situ measurement is because the QWM uses the *average* velocity up to a depth that corresponds to one quarter of the wavelength of interest and hence the results are less sensitive to uncertainties in the details of the profile. The main difference between QWM and SRA is the fact that, because it uses an average velocity, it is insensitive to details of the profile. Conversely, SRA uses the V_s profile provided by the in-situ

measurements. This results in the site amplification, where QWM is able to reproduce the shape of SRA, but it generally underestimates the amplitude of the first peak of frequency. Figure 1.5 compares the results of QWM and SRA for the Columbia soil profile.

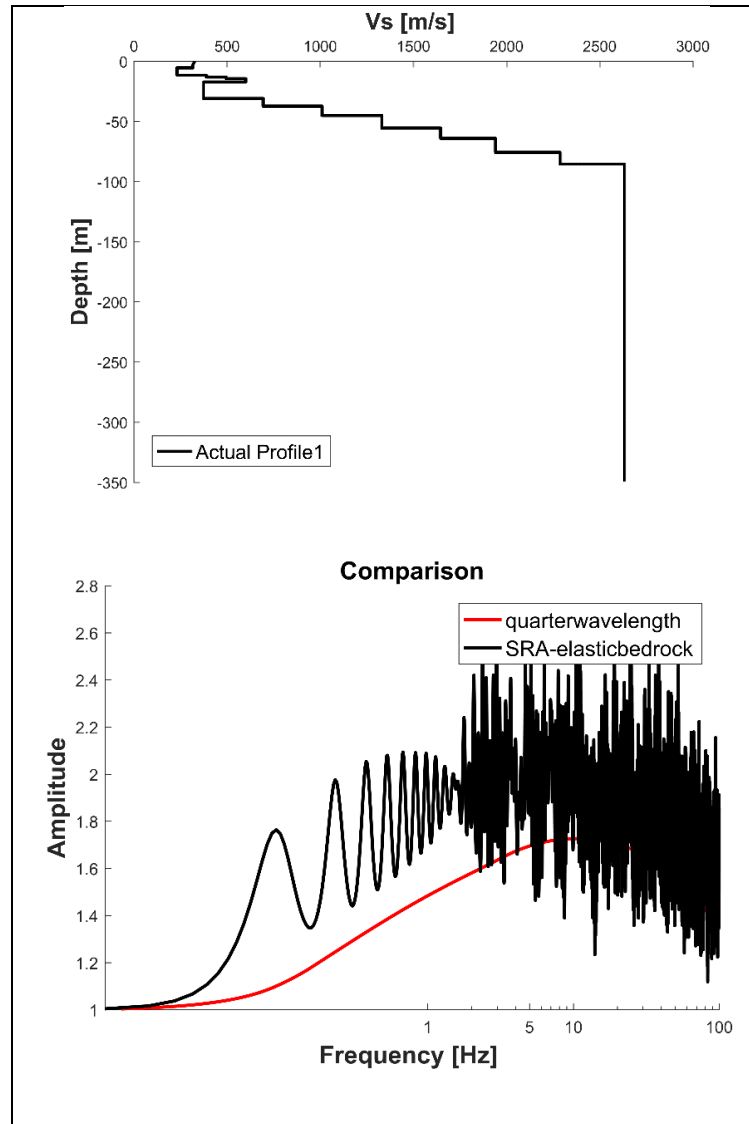


Figure 1.5. Comparison between the site amplification from QWM and SRA for the actual Columbia profile 1

The method was first used to compute amplification factors for generic rock profiles (Boore and Joyner, 1997) but the concept of averaged velocity is also applied to define the well-known V_{s30} , i.e. the average velocity over the upper 30m of the crust (Borcherdt, 1994). V_{s30} has a number of applications. The principal two being:

- Explanatory variable for site effects in a number of recent ground motion prediction equations (e.g. Abrahamson et al., 2008); and
- Basis for the site classification in various building codes in Europe and the US (Dobry et al., 2000; Building Safety Council, 2003; Eurocode 8, 2004; American Society of Civil Engineers, 2010; NTC, 2018).

For instance, a rock deposit in Eurocode 8 is defined as having a $V_{s30} > 800$ m/s. However, this definition is intrinsically “relative”. There are situations in seismic site characterization where it is impossible to define and clearly identify a stiff material. In such cases of deep bedrock or lack of resolution of the in-situ test, the V_s profile ends with a soil half-space, instead of the classic bedrock (Foti et al, 2009). The seismic bedrock represents the conjunction between the seismic hazard assessment for the reference condition and the site response. This means that below this value, site response tends to consider everything as a stiff material (rock).

Despite this consideration, there are situations in which further analyses should be undertaken and the portion immediately after the seismic bedrock should be considered as an integral part of the analysis. Considerations on this topic can be found in Douglas et al. (2009) and in Volpini and Douglas (2019), where the central portion (between seismic bedrock and crustal velocity) is defined as the “dark zone”, because little information is available. Further details will be given in Chapter 4.

1.4 Thesis outline

After this overview of the research background (**Chapter 1**), the thesis is structured as follows:

Chapter 2 presents a journal article (reproduced from the *Journal of Earthquake Engineering*) on the use of the finite element software Abaqus to perform dynamic site response analyses. In this chapter the results of this software are compared to a well-known one-dimensional SRA software and a finite difference software, FLAC3D.

Chapter 3 presents a journal article (reproduced from the *Bulletin of Earthquake Engineering*) on an accessible approach to the modelling of a particular type of sites, namely those with quasi-horizontal layered soil deposits. The aim is to identify whether and when these deposits can be studied with one-dimensional SRA without committing large errors.

Chapter 4 presents a planned journal article (as yet not submitted) on the impact on SRA of a lack of knowledge of geomechanical characteristics of soil deposits. In particular, I focus on the final effect on SRA of the deep portion of a site, i.e. the part below the seismic bedrock ($V_s \geq 800\text{m/s}$).

References

- Abrahamson, N. A., and W. J. Silva, (2008). Summary of the Abrahamson & Silva NGA ground-motion relations, *Earthquake Spectra*, 24(1): 67-97.
- Aki, K. (1988). Local site effect on ground motion, in *Earthquake Engineering and Soil Dynamics. II: Recent Advances in Ground-Motion Evaluation*, J. Lawrence Von Thun (Editor), *Am. Soc. Civil Eng. Geotechnical Special Publication*, 20:103-155.

- American Society of Civil Engineers (ASCE) (2010). Minimum Design Loads for Buildings and Other Structures, Standards ASCE/SEI 7-10, ISBN 9780784410851, 650 pp.; <http://www.asce.org/Product.aspx?id=2147487569>,
- Baker J. W., (2008). An introduction to probabilistic seismic hazard analysis (PSHA), *Version 1.3, Stanford University*
- Bazzurro, P., and C. A. Cornell (2004). Ground-motion amplification in nonlinear soil sites with uncertain properties, *Bulletin of the Seismological Society of America*, 94: 2090-2109.
- Boore, D. M., and W. B. Joyner (1997). Site amplification for generic rock sites, *Bulletin of the Seismological Society of America*, 87(2):327-341.
- Boore, D. M., (2013). The uses and limitation of the square-root-impedance method for computing site amplification, *Bulletin of the Seismological Society of America*, 103(4):2356-2368.
- Borchardt R. D. (1994). Estimates of Site-Dependent Response Spectra for Design (Methodology and Justification). *Earthquake Spectra*, 10(4):617-653.
- Building Seismic Safety Council (2003). Recommended Provisions for Seismic Regulations for New Buildings and Other Structures, Part 1: Provisions. *Report No. FEMA-450, Federal Emergency Management Agency*, Washington, D.C., 303 pp
- Cornell, C. A. (1968). Engineering seismic risk analysis. *Bulletin of the Seismological Society of America*, 58:1583-1606.
- Dobry, R., R. D. Borchardt, C. B. Crouse, I. M. Idriss, W. B. Joyner, G. R. Martin, M. S. Power, E. E. Rinne, and R. B. Seed (2000). New site coefficients

and site classification system used in recent building seismic code provisions, *Earthquake Spectra*, 16(1):41-67.

- Douglas, J., P. Gehl, L. F. Bonilla, O. Scotti, J. Régnier, A-M. Duval and E. Bertrand, (2009). Making the most available site information for empirical ground-motion prediction, *Bulletin of the seismological society of America*, 99(3):1502-1520, doi: 10.1785/0120080075
- Eurocode 8 (2004). Design of structures for earthquake resistance, part 1: General rules, seismic actions and rules for buildings, EN 1998-1, European Committee for Standardization (CEN), <http://www.cen.eu/cenorm/homepage.htm> (last accessed July 2011).
- Foti, S., C. Comina, D. Boiero, and L. Socco, (2009). Non-uniqueness in surface-wave inversion and consequences on seismic site response analyses. *Soil Dynamics and Earthquake Engineering*, 29:982-993.
- Joyner, W. B., R. E. Warrick, and Fumal, T. E. (1981). The effect of Quaternary alluvium on strong ground motion in the Coyote Lake, California, earthquake of 1979, *Bulletin of the Seismological Society of America*, 71:1333-1349.
- Kramer S., (1996). *Geotechnical Earthquake Engineering*”, 1st edition, New Jersey, Prentice-Hall;
- Ntc 2018. *Norme Tecniche per le Costruzioni Consiglio Superiore dei Lavori Pubblici, Ministero per le Infrastrutture e dei Trasporti.*
- Ordaz M. and E. Faccioli, (1994). Site response analysis in the valley of Mexico: Selection of input motion and extent of non-linear soil behaviour,

Earthquake Engineering and Structural Dynamics, 23(8):895-908,
DOI:10.1002/eqe.4290230806

- Pehlivan, M., E. M. Rathje, and R. B. Gilbert, (2012). Influence of 1D and 2D spatial variability on site response analysis, *15th World conference of Earthquake Engineering*, Lisboa.
- Pehlivan, M., E. M. Rathje, and R. B. Gilbert, (2016). Factors influencing soil surface seismic hazard curves, *Soil Dynamics and Earthquake Engineering*, 83: 180-190.
- Schnabel P.B., J. Lysmer and H. B. Seed, (1972). SHAKE: a computer program for earthquake response analysis of horizontally layered sites, *Report No. EEC72-12*, University of California, Berkeley
- Volpini C. and J. Douglas, (2019). Assessing earthquake site amplification for deep soil sites with uncertain bedrock conditions, *7th International conference on earthquake geotechnical engineering*, Roma (Italy)
- Vucetic, M., (1994). Cyclic threshold shear strains in soils, *Journal of Geotechnical Engineering*, ASCE, 120(12):2208-2228

Chapter 2

2.1 Introduction

The objective of this chapter is to introduce the numerical simulation tools used during subsequent analyses and to validate them. In particular, a journal article is presented about the use of the finite element software Abaqus (Dassault Systèmes, 2013) to reproduce the viscoelastic site response analysis of a two-dimensional (2D) model. The output of the model is then compared with another software, FLAC3D (Itasca group, 2009), which uses the finite difference method.

This piece of work was undertaken because the software used for the site response analysis in Chapter 3, Abaqus, is a multi-physics tool, so it was not specifically developed for geotechnical purposes and, in particular, it does not have the boundary conditions needed for dynamic analyses. Hence, for this thesis I have implemented these boundary condition using an external code. FLAC3D, a software developed specifically for geotechnical purposes, was then used to validate the results obtained. FLAC3D includes the boundary conditions required for these analyses.

Several software packages were tested to study the concept of spatial variability within site response analyses. At the beginning, I studied the influence of dipping layers on amplification with one-dimensional (1D) software, such as Deepsoil (Hashash et al., 2016), Strata (Kottke and Rathje, 2008) and EERA (Bardet et al., 2000). The main issue of using them was the fact that we were trying to study a 2D problem using 1D software. In particular, since I focused on wave propagation through a layered

medium, using these software packages neglected the lateral propagation of the waves, altering their real paths.

By using a simple 2D/3D model I am evidently simplifying the reality because I consider a limited space instead of a soil deposit with no boundaries. Despite this, a 2D/3D model is certainly more appropriate for such a kind of study. Therefore, Abaqus was chosen as the main software. Before finally deciding on this one, I tried many other options, such as Quake/w (Geoslope, 2007), Plaxis (Brinkgreve et al., 2010) and Speed (Spectral Elements in Elastodynamics with Discontinuous Galerkin) (Mazzieri et al., 2013), an open source code developed by Politecnico di Milano.

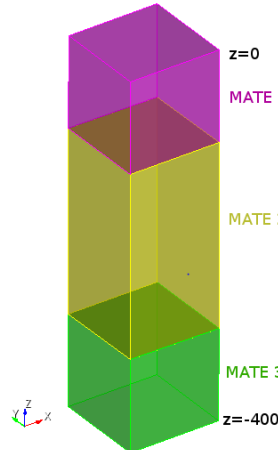
Quake/w is a finite element code, which is part of the Geoslope package. It is able to reproduce dynamic earthquake analyses. However, I found it inappropriate for my purposes so I looked for other possibilities.

Plaxis (Brinkgreve et al., 2010) could have been another effective option for my analyses because it includes a “2D Dynamic” module, which allows analysis of the effects of vibrations in the soil. Moreover, this software includes also the boundary conditions needed for our analyses. In fact, to reduce spurious reflections of waves reaching the model boundaries, free-field and compliant base boundaries can be selected. The theory behind them will be explained below. Due to a lack of a valid licence at the University of Strathclyde for this software it was not considered further.

One last software package was considered: Speed (Mazzieri et al., 2013), an open-source code from Politecnico di Milano. This software has been designed with the aim of simulating large earthquakes in 3D complex media: from far-field to near-field including soil-structure interaction effects. It combines the flexibility of the

discontinuous Galerkin methods to connect together, through a domain, decomposition paradigm, Spectral Element blocks, using high-order polynomials.

An example of calculations using Speed for SRA are shown here. Consider a simple three-layered column (Figure 2.1):



LAYER	V_s [m/s]	Density [Kg/m ³]	Q_s	Thickness [m]
1	300	1800	50	100
2	2000	2200	50	200
3	2000	2200	50	100

Figure 2.1: Soil column in Speed

A viscoelastic analysis is performed, where Q_s represents the quality factor, which is the inverse of attenuation:

$$Q_s = \frac{1}{2\zeta} \quad [9]$$

where ζ is the damping ratio. The result, in terms of its transfer function, is then compared to the results from a purely 1D SRA software, Deepsoil (Hashash et al.,

2016). Figure 2.2 compares the results, demonstrating that Speed produces an appropriate result. In fact, the two curves present an almost perfect alignment in terms of natural frequencies, except for the second one. Despite the good result, I decided to abandon this code, before considering any more complex soil columns, in favour of Abaqus (Dassault Systèmes, 2013), because Speed was too slow in achieving effective results for my purposes.

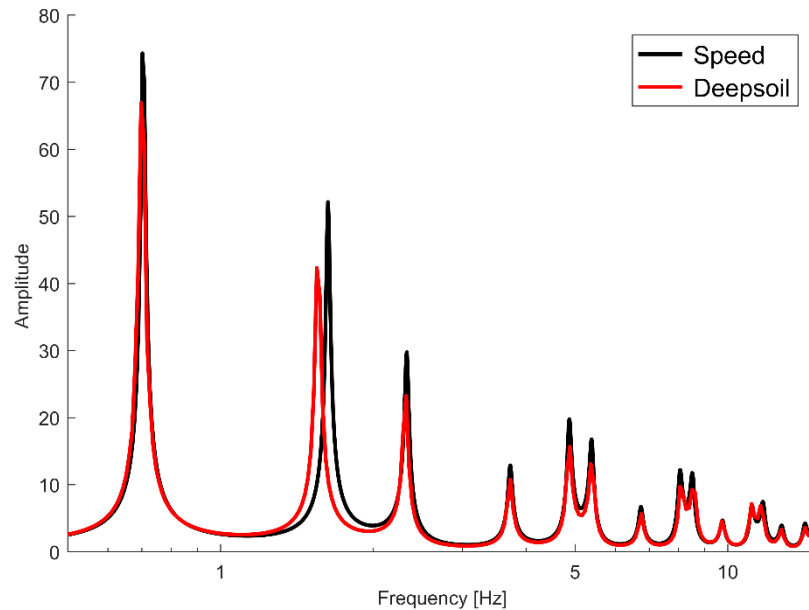


Figure 2.2. Comparison between Speed and Deepsoil transfer functions for the considered soil column (see Figure 2.1)

References

- Bardet, J. P., K. Ichii and C. H. Lin, (2000). EERA: A computer program for equivalent-linear earthquake site response analysis of layered soil deposits, department of civil Engineering, University of Southern California.

- Brinkgreve, R., Engin, E., Swolfs, W., Waterman, D., Chesaru, A., Bonnier, P., and Galavi V., (2010). PLAXIS 2D 2010, Tech. rep., PLAXIS B. V., The Netherlands.
- Dassault Systèmes – SIMULIA (2013). Abaqus Analysis User’s Guide, v6.13.
- GEOSLOPE International Ltd (2007). SLOPE/W User’s manual. Calgary, Alberta, Canada.
- Hashash, Y.M.A., M. I. Musgrove, J. A. Harmon, Groholski, D.R., Phillips, C.A., and Park, D. (2016). DEEPSOIL 6.1, User Manual”. Urbana, IL, Board of Trustees of University of Illinois at Urbana-Champaign
- Itasca Consulting Group, Inc., (2009). Fast Lagrangian Analysis of Continua in 3 Dimensions User's Manual, Minneapolis, Minnesota, U.S.A.
- Mazzieri I., M. Stupazzini, R. Guidotti and C. Smerzini, (2013). SPEED: Spectral Elements in Elastodynamics with Discontinuous Galerkin: a non conforming approach for 3D multi-scale problems, *International Journal for Numerical Methods in Engineering*, 12:991-1010.

2.2 Guidance on conducting 2D linear viscoelastic site response analysis using a finite element code

Carolina Volpini¹, John Douglas¹ and Andreas Hvidtfelt Nielsen²

1- Department of Civil and Environmental Engineering, University of Strathclyde, Glasgow (UK)

2- Atkins (member of the SNC-Lavalin Group), Glasgow (UK)

Corresponding author e-mail: carolina.volpini@strath.ac.uk

Abstract

Various software packages are available to conduct one-dimensional (1D) and two-dimensional (2D) site response analyses (SRAs). In this article, a finite element program is tested with the purpose of assessing the importance of several aspects on the obtained results and verifying the software. Abaqus (Dassault Systèmes) is compared with the 1D SRA software STRATA (Kottke & Rathje, 2008) for simple 1D models to understand the influence of the boundary conditions; as being a 1D SRA program, STRATA does not require vertical boundary conditions. For Abaqus the subroutine by Nielsen (2006, 2014) is used to implement free-field boundary conditions.

In addition, we test the influence of mesh dimension and Rayleigh damping as well as the importance of buffer-zone width. 2D SRAs with Abaqus and FLAC3D (Itasca Consulting Group, 2012), which is commonly used for geotechnical analyses, are compared as part of the assessment. Similar results are obtained from the two programs but Abaqus is preferred as it is more efficient for linear elastic analyses than FLAC3D, which, on the contrary, performs well for soil presenting strongly non-linear behaviour and effective stress. We demonstrate that reliable results can be achieved, not only for simple uniform sites but also for complex sites with multiple layers and dipping stratigraphy.

Keywords

One-dimensional, two-dimensional, site response analysis, free-field boundary conditions, damping

2.2.1.Introduction

An important part of geotechnical earthquake engineering is the study of the response of the ground under earthquake excitation by means of site response analysis (SRA). Based on the characteristics of the problem studied, several approaches can be used: from one-dimensional (1D) to three-dimensional (3D) analyses and from linear-elastic to fully non-linear soil behaviour. 1D linear-elastic SRA is often a good starting point for all such studies, even though it is unrealistic in many cases (e.g. when the site is subject to high-amplitude shaking, for which a non-linear analysis would provide more accurate results, and in the case of sedimentary valleys and basins, where 3D effects are pronounced). A complete SRA should include a consideration of the 3D geometry and non-linear soil behaviour and the consideration of effective stress, which is

important, for example, for the study of soil liquefaction. The seismic waves, under these conditions, can generate an increase in the pore water pressure producing a reduction of stiffness and strength of the soil. However, it is not common to perform such analyses, because the more complex a model is, the more input parameters are needed, which means that a full characterization of the site must be available to the engineer. In addition, 3D and non-linear analyses require long computational times, sophisticated software and much experience in conducting the analyses and in interpreting the results.

In this work, we test several approaches, but we will limit ourselves to 1D and 2D SRA and to linear-elastic behaviour with viscous damping. A recent example of a comparison between 1D and 2D SRA can be found in Volpini and Douglas (2018). We make several comparisons between different software packages and test their capabilities to treat irregular geometries, such as gently dipping layers. We use a finite element (FE) code, Abaqus (Dassault Systèmes), and a finite difference code, FLAC3D (Itasca Consulting Group, 2012), for the 2D analyses, and the code STRATA (Kottke and Rathje, 2008) for the 1D simulations. We then examine the shape of the amplification functions obtained from different software packages as they yield valuable physical insight into the frequency dependence of the response.

2.2.2. One-Dimensional Approach

The easiest way to conduct a SRA is to use a 1D approach, where the soil deposits are modelled as a layered column. The first popular program developed for such analyses was SHAKE (Schnabel et al, 1972). Following SHAKE, several other software packages have been published using the same basic approach including STRATA. In this section, some of the basic analytical results for 1D SRA are presented as they are

useful for the rest of the article.

The 1D approach is underpinned by two fundamental assumptions: (1) the ground is composed of one or more parallel layers, extending to infinity in the horizontal plane; and (2) incoming seismic waves follow vertical ray paths. This final assumption is normally justified through Snell's law, which informs us that inclined waves propagating through horizontal layers of soil layers with successively lower impedances will be refracted closer to a vertical path (Kramer, 1996).

The simplest case is a single layer of soil overlying an infinite nearly-rigid half-space. Assuming linear-elastic material properties, the amplification function $A_r(\omega)$, which is defined as the ratio between the displacement amplitude recorded at the surface and the amplitude of the input motion entering at the base of the layer, can be computed as (Kramer, 1996):

$$A_r(\omega) = |H_r(\omega)| = \left| \frac{U(0, \omega)}{U(H, \omega)} \right| = \frac{1}{\left| \cos\left(\frac{\omega H}{V_s}\right) \right|} \geq 1 \quad [10]$$

where $H_r(\omega)$ is the complex transfer function, $U(z, \omega)$ is the magnitude of horizontal displacement at depth z , ω is angular frequency, and H and V_s are the depth and shear-wave velocity of the soil layer, respectively. For $\frac{\omega H}{V_s} = \frac{\pi}{2} + n\pi$, with $n = 1, 2, \dots$, the amplification function tends to infinity, which signifies resonance. For $n = 1$, ω is equal to the natural or fundamental frequency of the layer, which is given by:

$$\omega_r = \frac{\pi V_s}{2H} \quad , \quad f_r = \frac{V_s}{4H} \quad [11]$$

The amplification function can be modified to consider the effect of energy dissipation

(damping) within the soil. The simplest approach is to assume that the material damping is of the viscous type. Incorporating damping means the displacement amplitudes associated with the resonant frequencies are no longer infinite, and equation [10] is modified to (Kramer, 1996):

$$A_r^*(\omega) = |H_r^*(\omega)| = \frac{1}{\sqrt{\cos^2(kH) + (DkH)^2}} \quad [12-a]$$

$$(A_r^*)_{max} \cong \frac{2}{(2n-1)\pi D} \quad n = 1, \dots, \infty \quad [12-b]$$

where k is the wave number and D is the damping ratio.

In this article, only linear-elastic models with viscous damping are considered. It is possible to model the non-linear behaviour of the soil, which is more realistic especially for high-amplitude shaking. In practice, the equivalent linear approach (for low to moderate levels of soil nonlinearity) is often used (Schnabel et al, 1991), in which the shear modulus and damping ratio of each layer are adjusted after each analysis, based on the peak shear strain observed during the analysis. The analysis is then repeated until the properties converge to a stable set of values. The other option is a fully non-linear approach (Bonilla, 2000). Comparisons between equivalent linear analysis and fully non-linear analysis are presented by Kaklamanos et al. (2013, 2015). Kaklamanos et al. (2013) suggest limits, in terms of maximum shear strain and peak ground acceleration (PGA), of when linear and equivalent-linear analyses are valid.

The 1D approach is no longer valid for sites characterised by irregular subsurface stratigraphy, irregular surface topography or incident body waves with non-vertical ray paths (or incident surface waves). A typical example is a sedimentary valley, where

the soil deposit is much softer than the bedrock; in such conditions, a complex wave field can be generated due to multiple refractions and reflections in the interfaces, which can lead to long duration ground motions and high amplification. Indeed, the soil deposits overlying the curvature of a basin can trap body waves and convert body waves into standing surface waves (Vidale et al, 1988; Bard and Bouchon, 1980a, 1980b; Bard and Bouchon, 1985; Chávez-García and Faccioli, 2000). This kind of situation requires 2D or ideally 3D SRA. Useful studies on the applicability of 1D SRA for different situations are by Thompson et al. (2012), Stewart et al. (2014) and Stewart et al. (2017).

2.2.3. Two-Dimensional Approach

2.2.3.1 Limitations of the 2D approach

As previously mentioned, when a real site is characterised by irregular subsurface stratigraphy and/or surface topography, it is necessary to use 2D or 3D SRA. The jump from one dimension to multiple dimensions involves additional challenges. First, it must be noted that it is impossible to construct an equivalent 2D slice that matches the dynamic behaviour of a true 3D site. A 2D model with the same dimensions and material properties will generally overestimate the soil's dynamic stiffness and radiation damping due to geometric spreading of waves (Wolf, 1994). Nevertheless, the study of 2D models is instructive as they pose many of the same practical challenges as 3D models. In this section we outline some of the key considerations.

2.2.3.2 Boundary conditions

An earthquake affects a large area of the Earth's surface. However, engineers are usually concerned with the response of a relatively small site and a single structure. Instead of modelling the entire region affected by an earthquake, which is generally not feasible and almost never desirable, it is common practice to truncate the model at a certain distance from the region of interest. This truncation introduces artificial borders around the model. The geological media outside these artificial borders are assumed to be unbounded (semi-infinite), and their presence is simulated by enforcement of appropriate boundary conditions. The literature on this subject is vast. However, it is possible to distinguish between two fundamental types of boundary conditions: elementary boundary conditions (EBCs) and absorbing boundary conditions (ABCs).

The EBCs are either fixed or free. With EBCs, the numerical model should be so large that any waves reflected at the boundaries do not have time to return to the central region of the model. Much smaller models are feasible with ABCs, which therefore have gained much interest.

ABCs can be either global or local. In a global scheme, each boundary node is fully coupled to all other boundary nodes in both space and time. In a local scheme, the solution at any time step depends only on the current node and the current time step, and perhaps a few neighbouring points in time and space. Theoretically speaking, global boundaries are exact (although exact solutions are rarely attained in practice). Local boundaries are approximate, but appear much more attractive for numerical implementation than global boundaries.

The first local ABC was proposed by Lysmer and Kuhlemeyer (1969), who used

viscous boundary tractions (dashpots) to absorb outgoing waves. For a vertical boundary parallel with the y -axis, the tractions can be written as [13]:

$$f_x = -\rho V_p \frac{\partial u}{\partial t}$$

$$f_y = -\rho V_s \frac{\partial v}{\partial t}$$
[13]

where ρ is the material density, V_p is the P-wave speed, V_s is the S-wave speed, and (u, v) are displacements in the (x, y) directions, respectively. This boundary condition is completely effective at absorbing body waves approaching the boundary at normal incidence. For oblique angles of incidence and for surface waves there is still energy absorption, but it is not perfect. The viscous boundary is currently the only type of ABC available in Abaqus.

The viscous boundary works well when the seismic source is within the model, but when the seismic waves enter through the base of the model, an extension is required. The problem is that the viscous boundary defined on the vertical boundaries of the model will attenuate the incoming seismic waves as they travel up through the model. A solution is to define the dashpots such that they act on the scattered waves propagating outwards from the centre of the model. The scattered wave field may be computed as the difference between the wave field that would exist in the absence of any irregularities within the main model (also called the free-field motion) and the total motion at the boundaries of the model. This solution is often called free-field boundary conditions. The free-field boundary conditions were first introduced by Wolf (1988) and Zienkiewicz et al. (1989). The solution requires an independent free-field model as an extension to the main model (Figure 2.2.1). In the 2D case, the free-field model

comprises two soil columns placed at the edges of the main model, with each column acting as a 1D model. In practice, this extension requires the analysis of free-field motions either prior to, or in parallel with, the analysis of the main model. The main model and the free-field columns are coupled through the normal and shear tractions, f_x and f_y , defined as [14]:

$$f_x = \rho V_p \left(\frac{\partial u'}{\partial t} - \frac{\partial u}{\partial t} \right) + \ell_x \sigma'_x$$

$$f_y = \rho V_s \left(\frac{\partial v'}{\partial t} - \frac{\partial v}{\partial t} \right) + \ell_x \tau'_{xy}$$
[14]

where prime indicates a quantity evaluated in the free-field, ℓ_x equals +1 if an outward normal points in the positive x direction and equals -1 if it points in the negative x direction. The first part of the equation is the viscous boundary as per equation [13]. The second term of the equation is the surface stress required to maintain free-field wave propagation plus any static reactions. In this manner, the viscous boundary absorbs only scattered waves due to irregularities within the main model, but leaves the input motion unaffected.

We use the free-field boundary conditions in this work, both in Abaqus and in FLAC3D. The procedure is not directly available in Abaqus; however, Nielsen (2006, 2014) has shown how it may be implemented, and we follow this procedure.

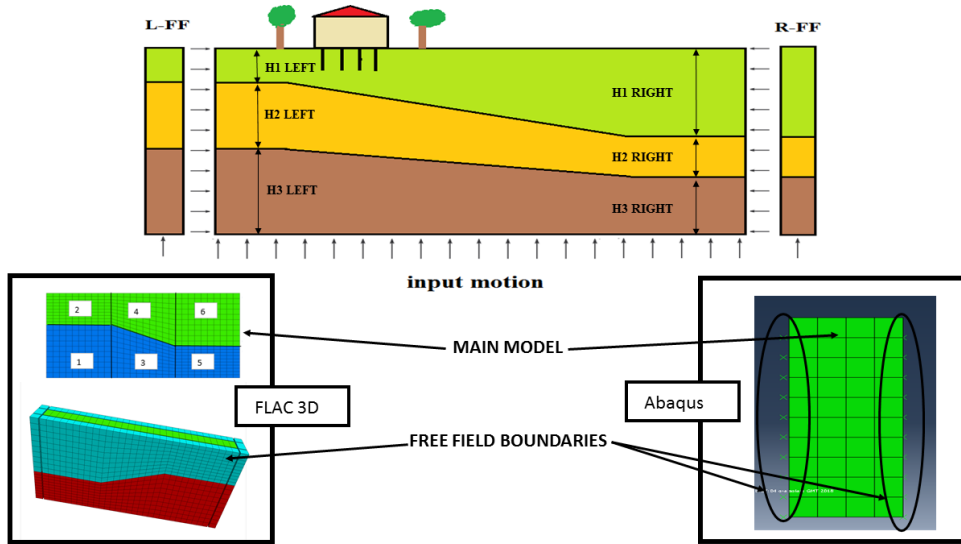


Figure 2.2.1. Example showing how both FLAC3D and Abaqus display free-field boundaries

2.2.3.3 Mesh Dimension

When modelling wave propagation within a continuum in 2D or 3D, it is important how the space is discretized. In contrast to the 1D approach, where no dimensions except for the height of the column are considered, there is also a width in 2D (and breadth for 3D domains). According to Kuhlemeyer and Lysmer (1973), the maximum frequency transmitted by a model can be estimated based on the largest elements or zones within the slowest material as follows [15]:

$$\Delta l_{max} \leq \frac{\lambda_{min}}{10} \leq \frac{V_{s,min}}{10f_{max}} \quad \text{or} \quad f_{max} \leq \frac{V_{s,min}}{10\Delta l_{max}} \quad [15]$$

where Δl_{max} is the maximum dimension of the element, λ the wavelength of the passing wave, V_s is the layer's shear-wave velocity and f_{max} is the maximum frequency of interest, which is typically around 10-15 Hz.

2.2.3.4 Input Motion

The input motion can be an external or internal dynamic action. In this work, we consider just the external option, defined as an input motion applied to the base of the model, which can be flexible or rigid. If the base is flexible, the input motion can be applied by imposing a traction at the base of the model (option *DLOAD in Abaqus), which is the same as the approach of FLAC; whereas, if it is rigid, the motion is imposed as an acceleration or displacement time history. In this article we assume a rigid base, and we restrict our investigations to the case of horizontal base excitation. The input we are using is a within motion, which has been applied as an acceleration time-history in all three software packages (Abaqus, FLAC3D and STRATA). An example of the type of motion used is displayed in Figure 2.2.2.

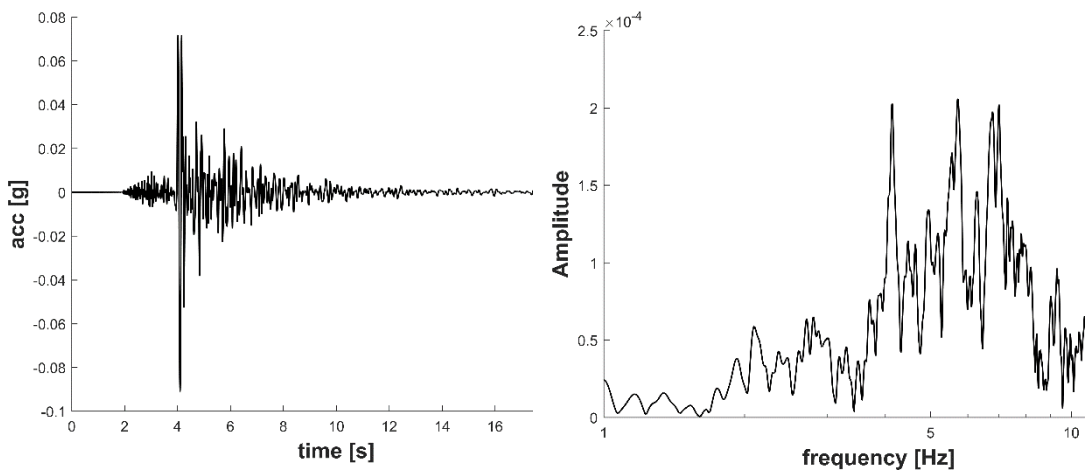


Figure 2.2.2. Example of input motion chosen from the ITACA database,

$PGA=0.09g$ (Luzi et al., 2017)

2.2.3.5 Damping

Damping, introduced in equation 16, 17 and 18, is a measure of the dissipative characteristics of the material and it has been found experimentally to be independent of frequency (Kimball and Lowell, 1927). For this reason, linear viscoelastic

frequency-domain analysis (e.g. via STRATA) may be preferred over time-domain analysis (e.g. via Abaqus or FLAC3D) as it is easier to model frequency-independent damping in the former. In this study we are using and comparing the two approaches so an approximation must be found to simulate “constant” damping over the frequency range of interest.

Both Abaqus and FLAC3D allow the use of Rayleigh damping (Rayleigh and Lindsay, 1945), where the damping matrix is a linear combination of the mass and stiffness matrices using the coefficients α and β :

$$[C] = \alpha[M] + \beta[K] \quad [16]$$

The damping ratio at frequency ω_i for a multiple degree-of-freedom system can be found using (Bathe and Wilson, 1976):

$$\xi_i = \frac{1}{2} \left(\frac{\alpha}{\omega_i} + \beta \omega_i \right) \quad [17]$$

A system of two equations is needed to determine α and β from any two known frequencies, ω_0 and ω_1 :

$$\alpha = \xi \frac{2\omega_0\omega_1}{\omega_0 + \omega_1} \quad \text{and} \quad \beta = \xi \frac{2}{\omega_0 + \omega_1} \quad [18]$$

The literature contains various suggestions about how to choose these frequencies. Chopra (1995) affirms the most common position that modes n and m should be specified to ensure reasonable damping values for all frequencies contributing to the response. Hashash and Park (2002) pointed out that for 1D linear SRA the two frequencies should represent the soil column’s fundamental mode (f_0) and one of its

higher modes with a frequency given by multiplying f_0 by an odd integer (e.g. 3, 5 or 7).

Abaqus uses the complete equation [17], but FLAC3D uses a simplified method, where only a single frequency can be specified. This appears to be the frequency where the damping is lowest, which occurs when the derivative of the equation becomes zero, i.e.:

$$\frac{d\xi}{d\omega} = 0 \quad \Rightarrow \quad \omega_{min} = \sqrt{\frac{\alpha}{\beta}} \quad \text{or} \quad f_{min} = \frac{1}{2\pi} \sqrt{\frac{\alpha}{\beta}} \quad [19]$$

The choice of ω_{min} is not obvious. As the authors of FLAC suggest, once ω_{min} is chosen, the damping ratio should be almost constant over a range between $\omega_{min}/1.5$ and $2\omega_{min}$. Thus, ω_{min} should be chosen as a value lying in the centre of the range of frequencies present in the model or the predominant input frequencies. Figure 2.2.3 displays the critical damping ratio as a function of angular frequency

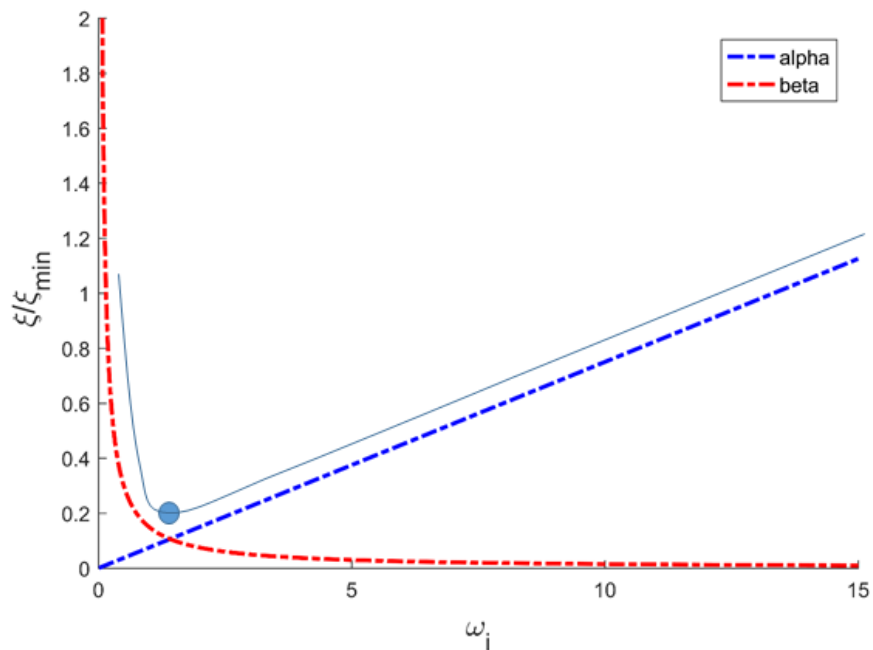


Figure 2.2.3. Critical damping ratio as a function of angular frequency

2.2.4. Testing Abaqus

Abaqus is a multi-physics FE software package. Certain types of boundary conditions, such as free-field boundary conditions, are not standard options. When performing a 1D analysis (single column with flat layers), it is possible to use tied boundaries, where we constrain the motion of each node on the right boundary to the corresponding node on the left boundary or vice versa. Any pair of two nodes must be at the same level and must present the same stiffness, so this simplification is useful only for flat layers and not irregular models. To use free-field boundary conditions, it is necessary to extend Abaqus by means of the UEL (user subroutine to define an element) code written by Nielsen (2006, 2014) for implicit dynamic analysis.

As Abaqus is the focus of our study, it is useful to conduct several analyses to understand its capabilities. These tests aim to evaluate the:

- ability of the free-field subroutine to model the simple case of 1D wave propagation and a comparison to the solution with tied boundaries;
- influence of the mesh dimension;
- difference between symmetric and asymmetric matrices for the free-field boundary option;
- influence of the choice of frequency for the damping formulation; and
- influence of the width of the buffer zones, which is a portion of the main model that is important when using free-field boundary conditions.

The Abaqus analysis is conducted as a time-history analysis with a base motion

defined by an accelerogram of 20 seconds' duration. We compute the Fourier amplitudes of the base motion, $U_H(\omega)$, and the Fourier amplitudes of the motion at the surface, $U_0(\omega)$, and then we evaluate the amplification function as the ratio of the two amplitudes, $A_r(\omega) = U_0(\omega)/U_H(\omega)$.

We use STRATA to obtain a benchmark solution for simple soil columns, and we compare the results from STRATA to those obtained from Abaqus. For simple soil columns with one layer, the STRATA solution is in fact identical to the theoretical solution represented by equation [12]. The soil column specified in table 2.2.1 is used for the following calculations. The natural frequency of this soil column equals 3Hz (from equation 11).

Height, H [m]	50
Bulk modulus, K [MPa]	1170
Shear modulus, G [MPa]	540
Density, ρ [kg/m³]	1500
S-wave velocity, V_s [m/s]	600
P-wave velocity, V_p [m/s]	1122

Table 2.2.1. Characteristics of the soil column used for the tests

Two damping levels are considered: 1% and 10%. According to equation (12-b), the amplitudes should be:

$$(A_{1\%}^*)_{max} \cong \frac{2}{(2-1)\pi \cdot 0.01} = 63.66 \quad [20]$$

$$(A_{10\%}^*)_{max} \cong \frac{2}{(2-1)\pi \cdot 0.1} = 6.366$$

The results obtained from STRATA and from Abaqus using tied boundaries and the free-field option are shown in Figure 2.2.4. The results indicate a good match between the STRATA solution and both the options of Abaqus. We note that the free-field boundary behaves as well as the tied boundary and that it agrees with the STRATA solution up to about 13 Hz. Here we focus on frequencies up to 15Hz because this is generally the range of engineering interest.

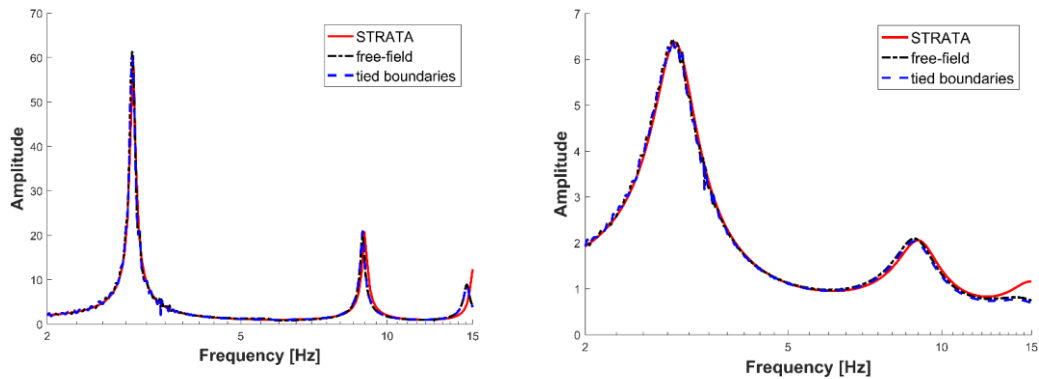


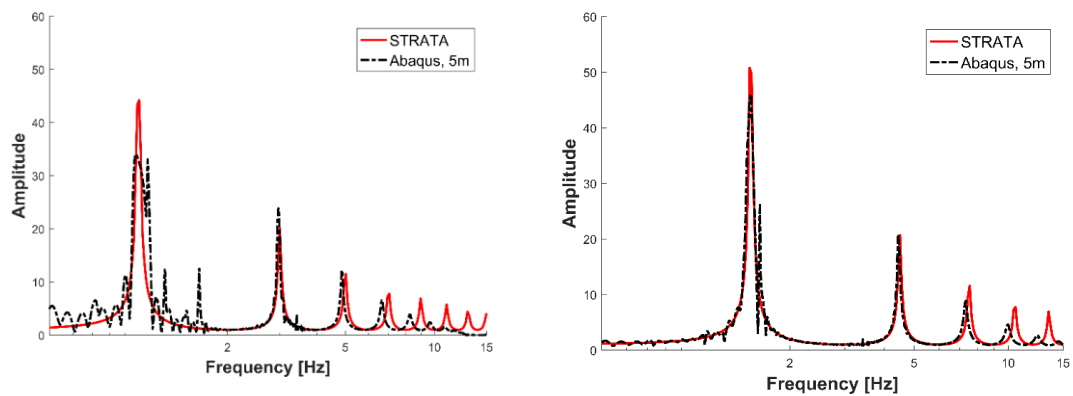
Figure 2.2.4. Comparison between Strata and Abaqus using tied boundaries and the free-field option. Left: for 1%, STRATA, Free-field and Tied boundaries PGA=0.15g. Right: for 10%, STRATA, Free-field and Tied boundaries PGA=0.13g

Because of its importance, we next study the influence of the mesh dimension in detail. The previous good results were obtained for a model with $V_s = 600\text{m/s}$ and an element size of 5m. Now we will use the same mesh with a lower wave velocity. In this way, the consequences of violating inequality (6) will be seen. The two models listed in Table 2.2.2 are studied.

H [m]	50	50
K [MPa]	130	293
G [MPa]	60	135
ρ [kg/m ³]	1500	1500
V_s [m/s]	200	300
V_p [m/s]	374	561

Table 2.2.2. Characteristics of the two soil columns used for the tests on the mesh size

As before, the STRATA solution is compared with the results obtained using the free-field option (from Abaqus) for damping ratios of 1% and 10% in Figure 2.2.4. From the graphs, we conclude that the mesh dimension is, as expected, not adequate for the lower stiffness of the model. We also note that the level of damping has a marked influence on the result. The Abaqus solution displays considerable numerical noise for a damping ratio of 1%, but this noise appears to be reduced when the damping ratio is increased to 10%. However, the Abaqus solutions remain useful in terms of identifying the first two or three natural frequencies.



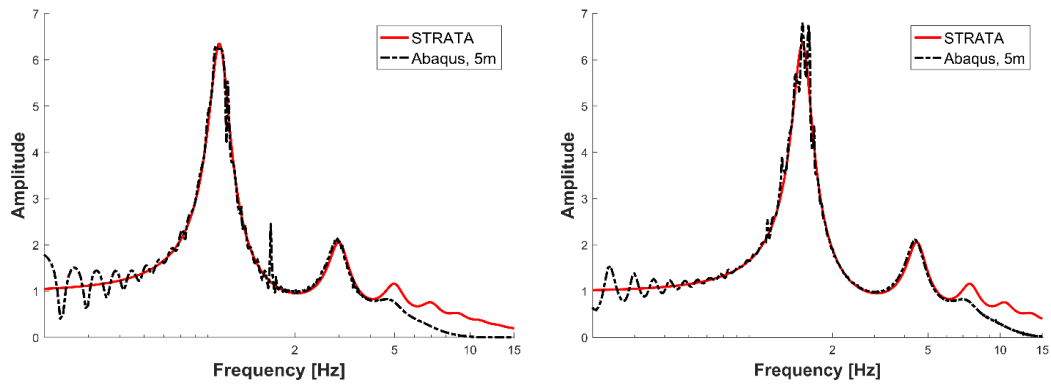


Figure 2.2.5. Comparison between STRATA and Abaqus using the free-field option.

Left: $V_s = 200\text{m/s}$. STRATA, $D=1\%$, $\text{PGA}=0.16\text{g}$ Abaqus $\text{PGA}=0.15\text{g}$. STRATA, $D=10\%$, $\text{PGA}=0.05\text{g}$, Abaqus, $D=10\%$, $\text{PGA}=0.04\text{g}$, Right: $V_s=300\text{ m/s}$. STRATA $D=1\%$ $\text{PGA}=0.18\text{g}$, Abaqus $\text{PGA}=0.17\text{g}$, STRATA $D=10\%$ $\text{PGA}=0.08\text{g}$, Abaqus $D=10\%$ $\text{PGA}=0.09\text{g}$, Top: 1% damping. Bottom: 10% damping.

We consider the model with $V_s = 300\text{m/s}$ and 1% damping in more detail. According to inequality [15] the dimensions of the elements should be smaller than 2m for accurate results. Figure 2.2.6 compares the results obtained using a 2m and a 1m mesh. This comparison indicates that the denser the mesh, the better the match with the peak magnitude predicted by STRATA at the first natural frequency, whereas at higher frequencies a less dense mesh gives a better match to the STRATA solution.

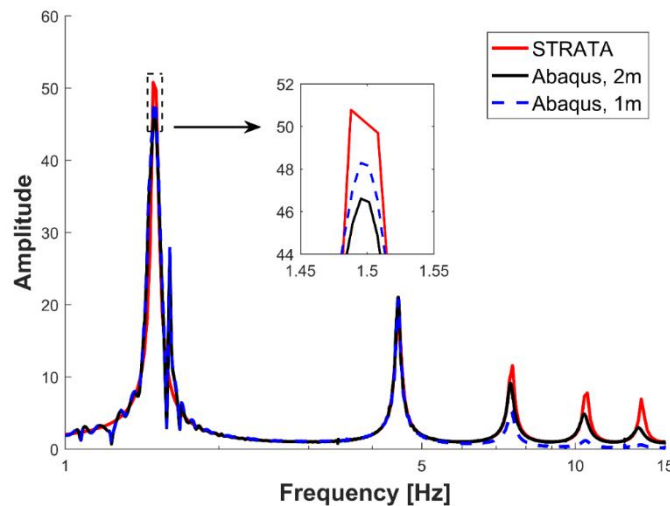


Figure 2.2.6. Comparison of the transfer function for different mesh dimensions, STRATA PGA=0.18g, Abaqus 2m PGA=0.13g, Abaqus 1m PGA=0.17g

Another important comparison to make is between results obtained using symmetric or asymmetric matrices within the free-field subroutine. Using symmetric matrices is more time efficient, but it approximates the more rigorous technique based on asymmetric matrices. Figure 2.2.7, which compares results for symmetric and asymmetric matrices, shows no differences for a soil column. Nielsen (2014) suggests that the free-field column width can be taken equal to unity for an asymmetric system as the width does not affect the results. We conducted one further test to verify this, as the right-hand figure shows.

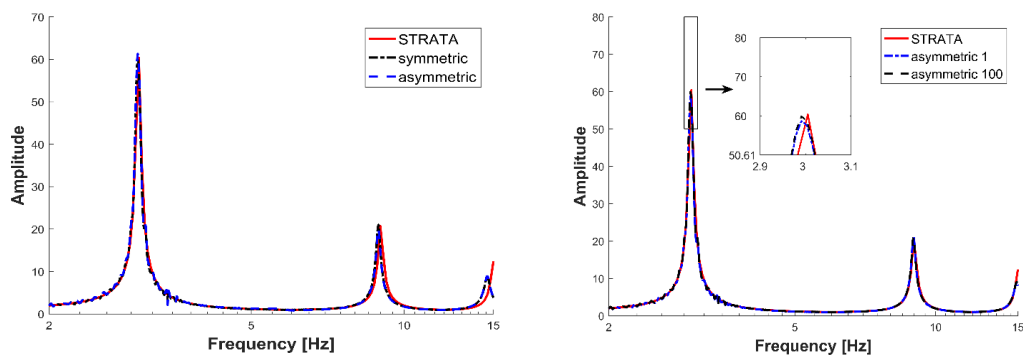


Figure 2.2.7. $V_s = 600\text{m/s}$ model. On the left: comparison between symmetric matrix and asymmetric matrix; on the right: study on the influence of the width in asymmetric system, $wff=1$ and $wff=100$, STRATA, symmetric, asymmetric PGA=0.15g.

Another interesting point to investigate is the Rayleigh damping and its proper use, in particular to check the recommendations of Hashash and Park (2002) stated above. The model chosen for this test is the $V_s = 600\text{m/s}$ column because, owing to its stiffness, the element dimensions can be large enough for relatively rapid analyses.

The fundamental frequency is equal to 3Hz. Several values of damping have been considered, from 0.1% (approximating an undamped model) to 10%. Table 2.2.3 indicates α and β for all considered frequencies and damping ratios. Examining Figure 2.2.8 leads to the following conclusions: all analyses show a good match between Abaqus results and the STRATA solutions for the first amplitude; solutions with $f_1 = 5f_0$ and $f_1 = 7f_0$ tend to overestimate the second peak as this is under-damped; solutions with $f_1 = 3f_0$ present a good match for the second peak as well as the first one, whereas higher frequency peaks are over-damped.

f_1 [Hz]	9			15			21		
ξ [%]	10	1	0.1	10	1	0.1	10	1	0.1
α	2.8	0.28	0.028	3.1	0.31	0.031	3.3	0.33	0.03
$\beta \times 1000$	2.7	0.27	0.027	1.7	0.17	0.017	1.3	0.13	0.013

Table 2.2.3. α and β for different values of f_1

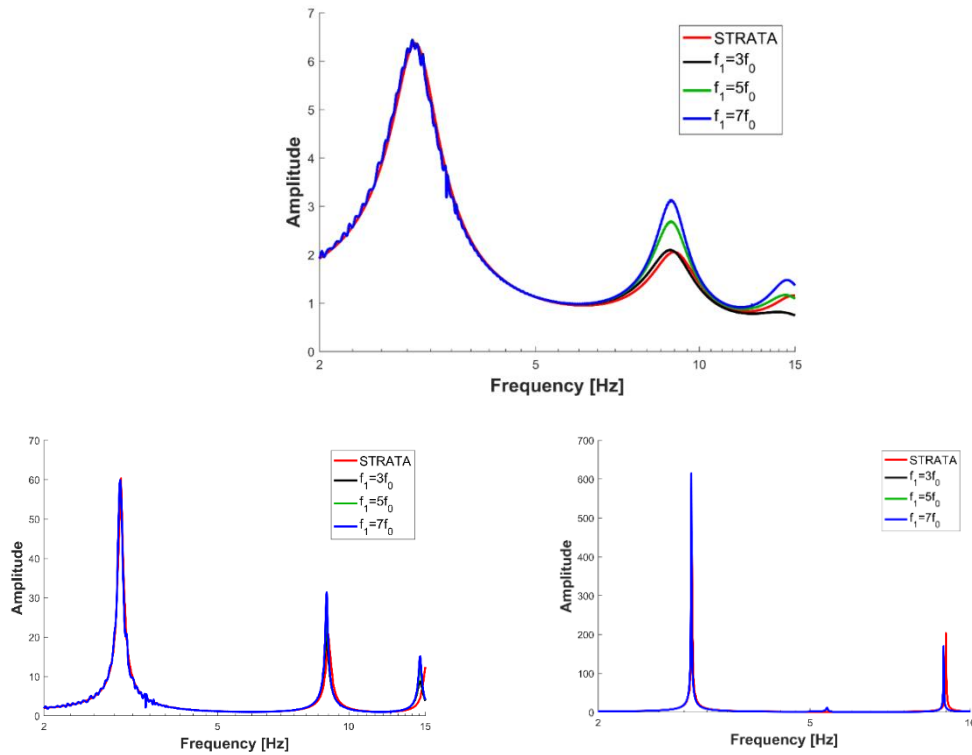


Figure 2.2.8. Comparison between transfer functions for different choices of α and β depending on the frequencies targeted: 10% above, 1% below on the left (STRATA, $3f_0$, $5f_0$, $7f_0$ PGA=0.15g), 0.1% below on the right.

Finally, the influence of the width of the buffer zones width is investigated. The buffer zone must have a regular shape (i.e. flat, parallel layers). We consider that the width of the buffer zone should be about the same as the width of the central region of the main model, although we would recommend that the adopted buffer zone width be validated for each case. To demonstrate this, a simple example is studied here: a two-layer geometry, with an irregularity. The central region of the main model measures $50\text{m} \times 50\text{m}$. Two different options will be analysed (Figure 2.2.9): in the first one the buffer zone width is 10m, while in the second it is 50m. Results at three location points, one in the middle of each region, are studied. We will also analyse the influence of the damping ratio (1%, 3% and 10%) on the results from different widths of buffer zone.

Figure 2.2.10 reports the results obtained for the central region and one of the two buffer zones. The STRATA solution for a regular site corresponding to the right-hand buffer zone is also shown for comparison. According to Seed et al. (1975), when the damping is increased the influence of geometrical irregularities on the results tends to decrease. As we expected, the influence of buffer zone width is larger for lower levels of damping. Moreover, it would seem that the model with 10m width of buffer zone does not capture the correct peak associated with the first natural frequency in the buffer zone. This difference becomes less important as the damping level increases.

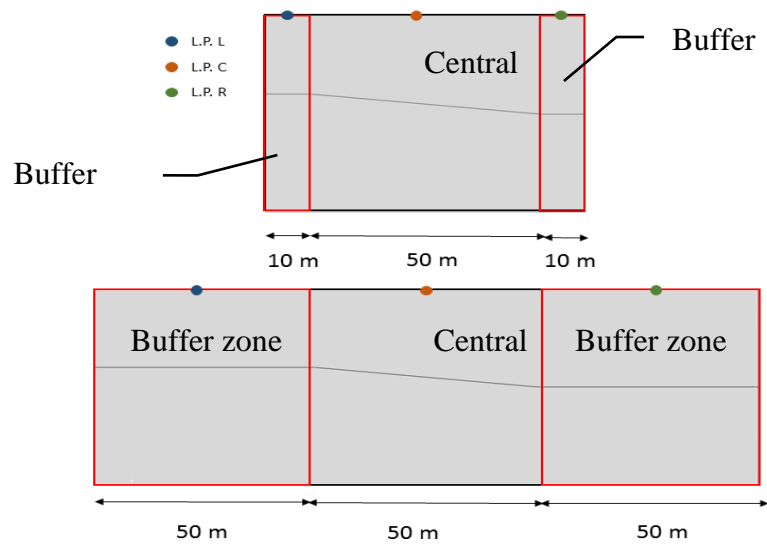


Figure 2.2.9. The domains and output locations considered for the buffer zone comparisons.

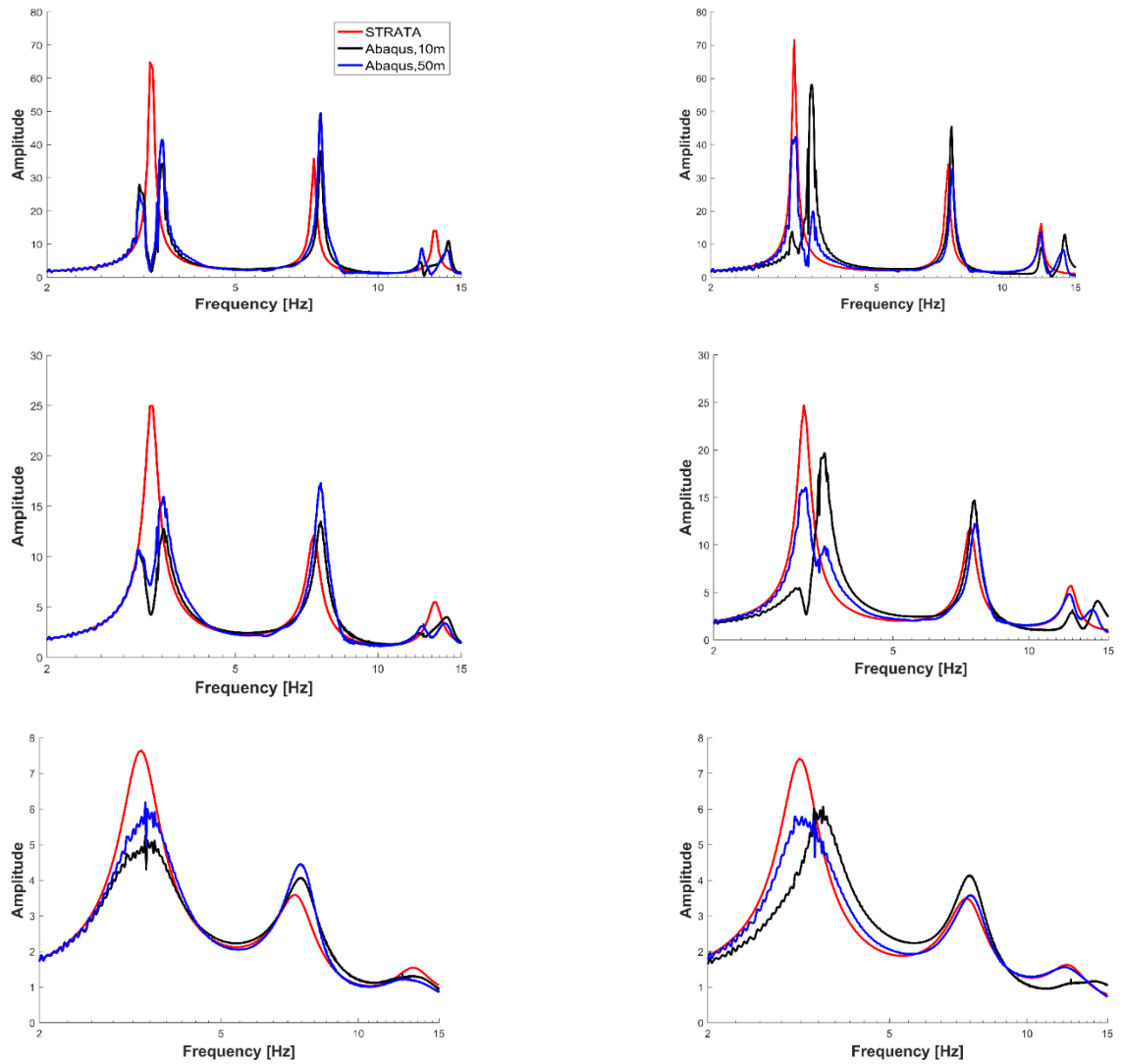


Figure 2.2.10. Comparisons in transfer functions for different buffer zone widths and damping ratios. Top: 1%. Middle: 3%. Bottom: 10%. Left: Centre. STRATA $d=1\%$:PGA=0.34g, Abaqus 50m PGA=0.40g, Abaqus 10m PGA=0.37g. Right: Right-hand buffer zone. STRATA=0.35g Abaqus 50m PGA=0.34g, Abaqus 10m=0.41g, Left: Centre. STRATA $d=3\%$:PGA=0.32g, Abaqus 50m PGA=0.34g Abaqus 10m PGA=0.34g Right: Right-hand buffer zone. STRATA=0.30g Abaqus 50m PGA=0.31g Abaqus 10m=0.34g, STRATA $d=10\%$:PGA=0.25g, Abaqus 50m PGA=0.25g, Abaqus 10m PGA=0.26g. Right: Right-hand buffer zone. STRATA=0.23g Abaqus 50m PGA=0.23g, Abaqus 10m=0.25g,

2.2.5. Testing FLAC3D

FLAC3D is based on the finite-difference method using an explicit time integration scheme. An interesting comparison between implicit and explicit time integration schemes can be found in Andreotti and Lai (2017a, b). In contrast to Abaqus, FLAC3D has the free-field boundary condition implemented. To use them in this program, we need to append a buffer zone to any irregular geometry so as to provide a smooth transition to the regular geometry that is the basis of the free-field model. As rule of thumb, we consider that the width of a buffer zone should be equal to the width of the main model.

We also note that within an explicit integration scheme the dynamic time step changes according to the level of damping. The higher the damping, the smaller the time-step becomes, which means that analysis will take longer.

Above Abaqus is tested for simple geometries, i.e. a single layer soil column. To check its behaviour for more complex situations, we need to compare it to another software that is also capable of 2D SRA. 2D models can be developed in FLAC3D by developing a 3D model with a unit width in the breadth direction.

A test of the Rayleigh damping was made for FLAC3D because, as previously mentioned, this software uses a simplified formula using only a single control frequency, f_{\min} . We test the influence of the control frequency choice for a simple model (Table 2.2.4, Figure 2.2.11). The results show that by fixing the control frequency as the natural frequency, $f_{\min} = f_0$, the first amplitude is overestimated, while $f_{\min} = f_1$ as control frequency tends to underestimate the first peak, but has a good match for the second and third peaks. Choosing $f_{\min} = f_a = (f_0 + f_1)/2$ appears as the best compromise between the two, because overall it leads to the best fit.

K [MPa]	1340
G [MPa]	446
ρ [kg/m ³]	2200
V_s [m/s]	450
H [m]	50
f_0 [Hz]	2.25
f_1 [Hz]	6.75
f_a [Hz]	4.5
ξ [%]	1

Table 2.2.4. Characteristics of the model in FLAC3D

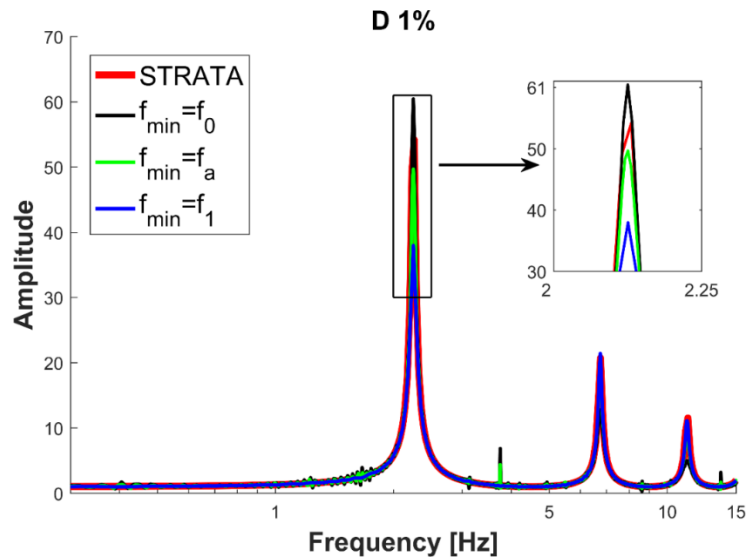


Figure 2.2.11. The influence of the control frequency in FLAC3D on the transfer function. STRATA, f_0 , f_a PGA=0.52g, f_1 PGA=0.51g

2.2.5.1 Comparing Abaqus and FLAC3D

In this section a comparison between the results from Abaqus and FLAC3D for an irregular 2D geometry is made. Viscously damped elastic analyses for a stratigraphy consisting of three layers (Table 2.2.5, Figure 2.2.1) are made.

Total width [m]	120
Buffer zone width [m]	40
Central region width [m]	40
H1 left [m]	10
H2 left [m]	20
H3 left [m]	30
H1 right [m]	13
H2 right [m]	20
H3 right [m]	27

Table 2.2.5. Geometries of the three dipping layers considered

The properties of the model are reported in Table 2.2.6.

	LAYER1	LAYER2	LAYER3
<i>H</i> [m] (centre)	11.5	20	28.5
<i>K</i> [MPa]	298	1500	1800
<i>G</i> [MPa]	170	500	700
ρ [kg/m ³]	1800	1900	2200
<i>V_s</i> [m/s]	307	513	564
<i>f_{control 1}</i> [Hz]	6.6	3.2	1.9
<i>f_{control 2}</i> [Hz]	20	9.8	5.9
α	0.31	0.15	0.093
$\beta \times 1000$	0.119	0.24	0.404
f_{\min} [Hz]	2.6		

Table 2.2.6. Properties of the model with three dipping layers

Results for three locations: one in the left part of the model, one in the centre and one in the right part of the model are shown in Figure 2.2.12. These comparisons show that both Abaqus and FLAC3D produce similar transfer functions. In particular, the same resonant frequencies are identified, although the maximum amplitudes differ because of their different Rayleigh damping formulations. Specifically, FLAC3D uses a single control frequency, which means there is less control on the frequency dependence of the damping.

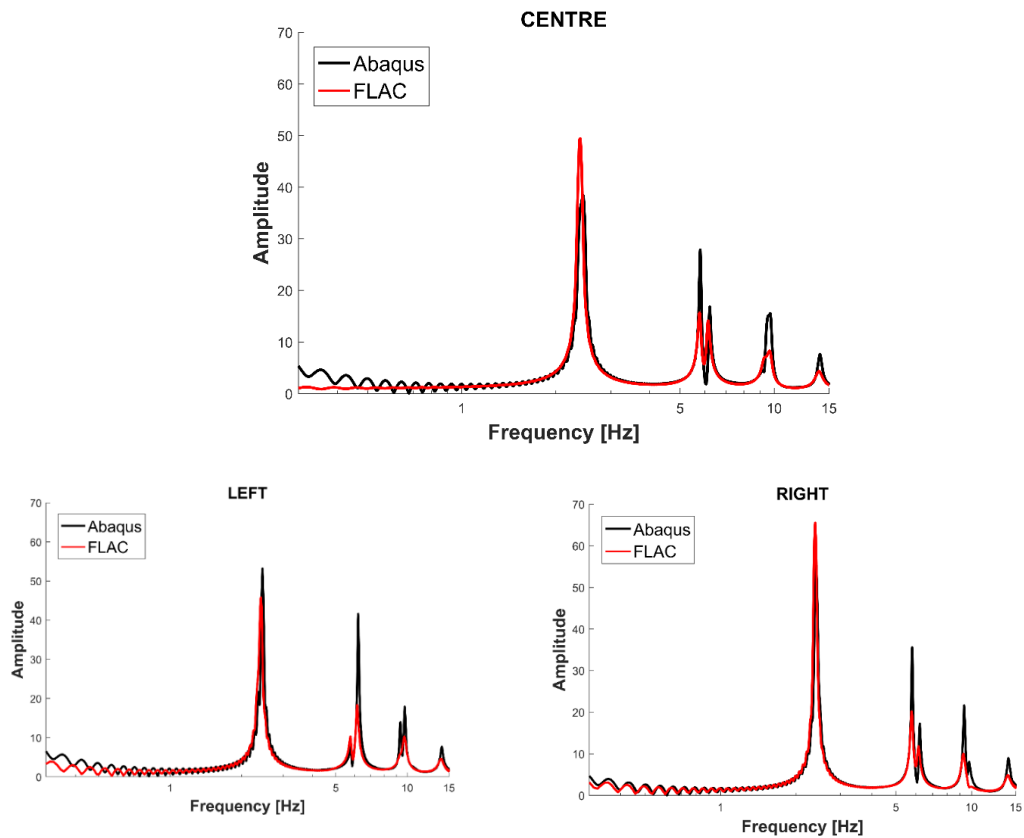


Figure 2.2.12. Abaqus and FLAC3D transfer functions for the three dipping layers model, Abaqus centre PGA=0.045g, FLAC PGA=0.05g

These results suggest Abaqus can simulate free-field boundary conditions in a satisfactory way. Moreover, we found that Abaqus is faster for linear-elastic analyses than FLAC3D.

2.2.6. Conclusions

In this work, a finite-element code (Abaqus) has been tested for 1D and 2D dynamic site response analyses. As a general-purpose FE application, Abaqus does not have the specialised boundary conditions required for this type of analysis. Abaqus does provide infinite elements for both static and dynamic analysis, but they are not optimal

for SRA. The free-field boundary conditions as developed by Nielsen (2006, 2014) are more appropriate for SRA of irregular sites. The free-field boundaries were tested in different configurations, and satisfactory results were found. Specifically, we found that:

- models with free-field boundaries provide the correct solutions for regular sites (by comparison with tied boundaries and STRATA solutions);
- choosing the appropriate element dimensions is crucial, especially for low values of damping ratio;
- the free-field boundaries can be used with symmetric matrices which permits faster solutions; and
- the Hashash and Park (2002) recommendations for the evaluation of control frequencies for Rayleigh damping are suitable.

Having clarified these aspects, we tested the importance of the buffer zone for models with irregularities. As a rule of thumb, the width of the buffer zone should be about the same as the width of the central region of the main model. However, we recommend that the adopted buffer zone width be validated for each case, for example by increasing the width until the output time history (or response spectrum) in the region of interest converges to a stable value.

Finally, we compared the Abaqus results with results from the finite-difference program, FLAC3D, where the free-field boundary condition is already implemented. Results have shown that the Abaqus implementation works properly when the guidance provided in this article is followed.

Acknowledgements

We would like to thank the anonymous reviewers for their useful comments on a previous version of this technical note.

Bibliography

- Abaqus, 6.13 © 2002-2018 Dassault Systèmes - All rights reserved
- Andreotti G, and C. G. Lai, (2017). A nonlinear constitutive model for beam elements with cyclic degradation and damage assessment for advanced dynamic analyses of geotechnical problems. Part I: theoretical formulation. *Bulletin of Earthquake Engineering*, 15(7): 2785–2801. [DOI: 10.1007/s10518-017-0090-1](https://doi.org/10.1007/s10518-017-0090-1)
- Andreotti G, and C.G. Lai, (2017). A nonlinear constitutive model for beam elements with cyclic degradation and damage assessment for advanced dynamic analyses of geotechnical problems. Part II: validation and application to a dynamic soil-structure interaction problem. *Bulletin of Earthquake Engineering*, 15 (7):2803–2825. [DOI: 10.1007/s10518-017-0091-0](https://doi.org/10.1007/s10518-017-0091-0).
- Bard, P.-Y., and M. Bouchon, (1980,a). The Seismic Response of Sediment-Filled Valleys. Part 1. The Case of Incident SH Waves.” *Bulletin of the Seismological Society of America*, 70 (4): 1263-1286.
- Bard, P.-Y., and M. Bouchon, (1980, b). The Seismic Response of Sediment-Filled Valleys. Part 2. The Case of Incident P and SV Waves. *Bulletin of the Seismological Society of America*, 70 (5): 1921-1941.
- Bard, P.-Y., and M. Bouchon, (1985). The Two-Dimensional Resonance of Sediment-Filled Valleys. *Bulletin of the Seismological Society of America* 75 (2):519–41.

- Bathe K.-J., and E. L. Wilson, (1976). Numerical methods in finite element analysis, Englewood Cliffs, NJ: Prentice-Hall.
- Bonilla, L.F., (2000). NOAH: Users Manual, Institute for Crustal Studies, University of California, Santa Barbara
- Chávez-García, F.J., and E. Faccioli, (2000). Complex Site Effects and Building Codes: Making the Leap. *Journal of Seismology*, 4 (1):23–40.
- Chopra, A.K., (1995). Dynamics of Structures: Theory and Applications to Earthquake Engineering. Prentice-Hall, New Jersey.
- Hashash Y.M.A., and D. Park, (2002). Viscous damping formulation and high frequency motion propagation in non-linear site response analysis, *Soil Dynamics and Earthquake Engineering*, 22:611–624
- [Itasca Consulting Group Inc. FLAC, \(2012\)](#). Itasca Consulting Group Inc. FLAC 3DFast Lagrangian Analysis of Continua: User's Manual, Minneapolis.
- Kaklamanos J., B. A. Bradley, E. M. Thompson, and L. G. Baise, (2013). Critical Parameters affecting Bias and variability in Site-Response analysis using Kik-net downhole array data, *Bulletin of the Seismological Society of America*, 103(3): 1733-1749, <https://doi.org/10.1785/0120120166>
- Kaklamanos J., L. G. Baise, E. M. Thompson, and L. Dorfmann, (2015). Comparison of 1D linear, equivalent-linear and nonlinear site response models at six KiK-net validation sites, *Soil Dynamics and Earthquake Engineering*, 69: 207-219, <https://doi.org/10.1016/j.soildyn.2014.10.016>
- Kimball A.L., and D. F. Lovell, (1927). Internal friction in solids, *Physics Review* 30 , 948

- Kottke, A. R., and E. M. Rathje, (2008). Technical Manual for Strata, PEER Report 2008/10, Pacific Earthquake Engineering Research Center College of Engineering, University of California, Berkeley.
- Kramer, S. L., (1996). Geotechnical earthquake engineering, Prentice Hall, Upper Saddle River, N.J
- Kuhlemeyer, R.L., and J. Lysmer, (1973). Finite Element Method Accuracy for Wave Propagation Problems. *Journal of the Soil Dynamics Division*, 99: 421-427.
- Lysmer, J., and R. L. Kuhlemeyer, (1969). Finite dynamic model for infinite media, Proceedings of the ASCE – *Journal of the Engineering Mechanics Division*, 95, no. EM4, 859-876
- Luzi L., F. Pacor, and R. Puglia, (2017). Italian Accelerometric Archive v2.3. Istituto Nazionale di Geofisica e Vulcanologia, Dipartimento della protezione Civile Nazionale, doi:10.13127/ITACA.2.3.
- Nielsen, A. H., (2006). Absorbing Boundary Conditions for Seismic Analysis in ABAQUS. *ABAQUS Users' Conference*, 359–76.
- Nielsen, A. H., (2014). Towards a Complete Framework for Seismic Analysis in Abaqus, *Proceedings of the ICE - Engineering and Computational Mechanics*, 167(1):3–12.
- Rayleigh J.W.S., and R. B. Lindsay, (1945). The theory of sound, 1st American edition. New York: Dover Publications.
- Schnabel, P.B., J. Lysmer, and H. B. Seed, (1972). Shake: a computer program for earthquake response analysis of horizontally layered sites, Report EERC 72-12, Earthquake Engineering Research Center, University of California, Berkeley

- Schnabel, P.B., J. Lysmer, and H. B. Seed, (1991). SHAKE-91: Equivalent Linear Seismic Response Analysis of Horizontally Layered Soil Deposits
- Seed, H. B., P. P. Martin, and J. Lysmer, (1975). The Generation and Dissipation of Pore Water Pressures During Soil Liquefaction, University of California, Berkeley, Earthquake Engineering Research Center, NSF Report PB-252 648
- Stewart, J. P., K. Afshari, and Y. M. A. Hashash, (2014). Guidelines for performing hazard-consistent one-dimensional ground response analysis for ground motion prediction, PEER Report No. 2014/16, Pacific Earthquake Engineering Research Center, UC Berkeley, CA.
- Stewart, J. P., K. Afshari, and C. A. Goulet, (2017). Non-Ergodic site response in seismic hazard analysis, *Earthquake Spectra*, 33: 1385-1414.
- Thompson, E. M., L. G. Baise, Y. Tanaka, and R. E. Kayen, (2012). A taxonomy of site response complexity, *Soil Dynamic and Earthquake Engineering*, 41: 32–43.
- Vidale, J., and D. V. Helmberger, (1988). Elastic finite difference of the 1971 San Fernando earthquake, *Bulletin of the Seismological Society of America*, 78(1):122-141
- Volpini, C., and J. Douglas, (2018). An accessible approach for the site response analysis of quasi-horizontal layered deposits, *Bulletin of Earthquake Engineering*, <https://doi.org/10.1007/s10518-018-0488-4>
- Wolf, J.P., (1994). Foundation Vibration Analysis Using Simple Physical Models, Prentice Hall.
- Wolf, J.P., (1988). Soil-Structure Interaction Analysis in Time Domain. Prentice Hall.

- Zienkiewicz, O.C., N. Bicanic, and F.Q. Shen, (1989). Earthquake input definition and the transmitting boundary conditions, *Proceedings Advances in Computational Nonlinear Mechanics I*, 109- 138, Springer-Verlag

Chapter 3

3.1 Introduction

This chapter describes in detail the uncertainties in site response analysis due to irregular stratigraphy. In particular, I study the effect of non-horizontal layers (with a gentle inclination) and whether it is recommended to undertake studies with 2D/3D software instead of the classic and more common 1D codes. 2D/3D behaviour, in certain situations, is also confirmed by Pilz & Cotton (2019), where they built a quantitative criteria and reproducible method to identify KiK-net sites in Japan with a significant deviation from 1D behaviour. From their analyses, they found that, at least half of the sites show 2D/3D effects, extending the resonance towards shorter periods and changing the classical 1D configuration.

As seen in the previous chapter, the study is performed with the Abaqus software (Dassault Systèmes, 2013), which has been verified thanks to another software package, FLAC3D (Itasca group, 2009). Before considering the use of a 2D software, the problem was first analysed with other techniques using just 1D calculations. On that occasion, the Toro (1995) model was introduced for the first time.

Specifically, the idea was to undertake a study on a geometry, like the one in Figure 3.1, where:

- All the layers are inclined at the same angle; and
- We consider vertical shear wave velocity (V_s) profiles at each 50m from the origin of the axis (top-left), where the thickness of the first layer is the one increasing.

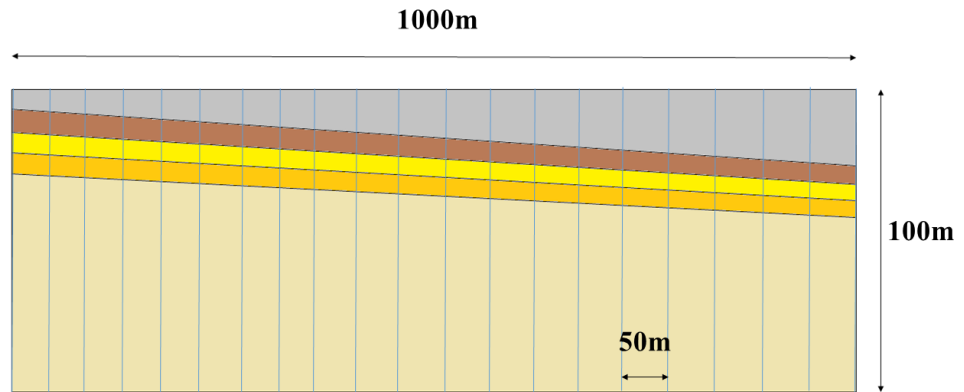


Figure 3.1. Geometry of the considered site (Modified from Appendix

1)

Layer Number	Vs [m/s]
1	300
2	350
3	400
4	500
Bedrock	1000

Table 3.1: V_s profile

We examine the influence of the increasing thickness and the intrinsic uncertainties in the V_s measurements, through the Toro (1995) randomization technique, in the following way. The blue curve (Figure 3.2) has been computed in this way: a matrix of n-rows (each row represents a single meter thickness) and m-columns (equal to

the number of profiles chosen) has been created. This matrix contains V_s profiles (Eq.21):

$$\begin{bmatrix} V_{1,1} & \cdots & V_{1,m} \\ \vdots & \ddots & \vdots \\ V_{n,1} & \cdots & V_{n,m} \end{bmatrix} \quad [21]$$

Then, logarithms of each element of this matrix are evaluated and finally, for each row of this matrix a standard deviation is computed. The result is represented by the blue curve in Figure 3.2.

The red curve in Figure 3.2 represents both the geometrical aspects of the model as well as the variability from the randomization. To compute this each of the 21 profiles has been randomized 100 times, using the Toro (1995) technique to randomize the V_s of each layer. This randomization has been evaluated using the coefficients from Toro (1995) (Table 3.2) for the appropriate $V_{s,30}$ for this site, i.e. for 180-360m/s as the models have V_{s30} between 200 and 400 m/s. Below are a brief description of the parameters of the Toro (1995) model. In this model, the shear wave velocity at the mid-point of each layer is described by a log-normal distribution, where:

- $\sigma_{\ln V_s}$ is the standard deviation of the natural logarithm of the shear-wave velocity;
- ρ defines the inter-layer correlation. Correlation is a measure of the strength and direction of a relationship between two random variables. In this case, the inter-layer correlation is a function of depth of the layer and its thickness. In particular: ρ_0 is the initial correlation, whereas ρ_{200} is the correlation coefficient at 200m;
- Δ is a model fitting parameter

- d_0 is the initial depth parameter.
- b is an exponent of the expression to define ρ_d .

$\sigma_{\ln V_s}$	ρ_0	ρ_{200}	Δ	d_0	b	Profile
						s
0.31	0.99	0.98	3.9	0	0.344	266

Table 3.2. Parameters of the Toro (1995) model for $V_s=180-360$ m/s, where ρ_0 , ρ_{200} , Δ , d_0 are respectively the initial correlation, correlation coefficient at 200m, model fitting parameter, initial depth parameter.

According to Table 3.2, coefficient $\sigma_{\ln V_s}$ leads to the starting point of the red curve. The biggest gap between the two curves, which is represented by the green one, is close to the surface and at maximum depth. The peak of the standard deviation (red and blue curves) is roughly at half of the maximum depth reached. This happens mainly for geometrical reasons and is understandable when looking at Figure 3.1.

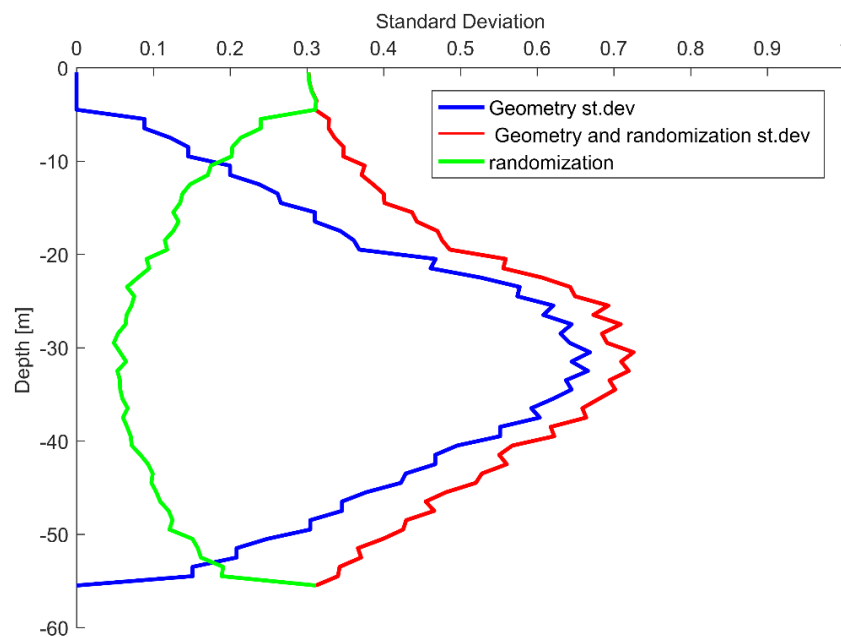


Figure 3.2. Comparison among the standard deviations of the logarithms of the velocity profiles with only geometric effects (blue), with geometric and randomization effects (red) and the difference between the two (green) [from Volpini & Douglas (2017) – see appendix 1]

This procedure was then abandoned in favour of a 2D approach, which is more realistic for such kinds of geometry. In fact, despite this 1D method having brought interesting results in terms of uncertainties, it was necessary to check the results, using a 2D model.

A finite element code, Abaqus, was chosen. The initial idea was to consider the output (in terms of time history) along the surface, compute the transfer function (the ratio between the output and input in terms of Fourier spectrum) and compare them with the analogous 1D transfer function computed as if we were considering the single soil column (Figure 3.3). As the aim of this chapter is to find a criterion to understand the acceptance limits of 1D analyses with irregular geometries, the first criterion I developed was the one described in Figure 3.3.

After comparing the two transfer functions (1D and 2D), I increased the 1D transfer function by different factors until it enveloped the entire 2D transfer function. This can be seen as a factor of safety procedure. In spite of the mathematical accuracy of the method, it is not acceptable from an engineering point of view. For instance, the example chosen below (Figure 3) displays a factor of safety of 200%, which is unrealistic from a practical point of view. The criterion finally adopted is explained in detail later on in this chapter.

To conclude, it is worth mentioning the original intention of testing my method on a real site. The ideal test site would have an irregular stratigraphy and in particular,

shallow dipping layers. The one considered for the test was Turkey Flat (Figure 3.4) (Real and Shakal, 2005), a sedimentary valley near Parkfield, California. The California Geological Survey (CGS) established a test area in this valley, where the California Strong Motion Instrumentation Program (CSMIP) installed a relatively dense strong-motion array. This array consists of surface and downhole accelerometers, with surface instruments at the two valley edges, at one quarter of the valley width, and at the centre of the small, shallow (25m) stiff soil sedimentary valley. After much effort, I eventually abandoned the hope of using this site to test the method due to the intrinsic difficulty in modelling this large site using the Abaqus software. In particular, I encountered problems with the mesh as the valley is very shallow but broad.

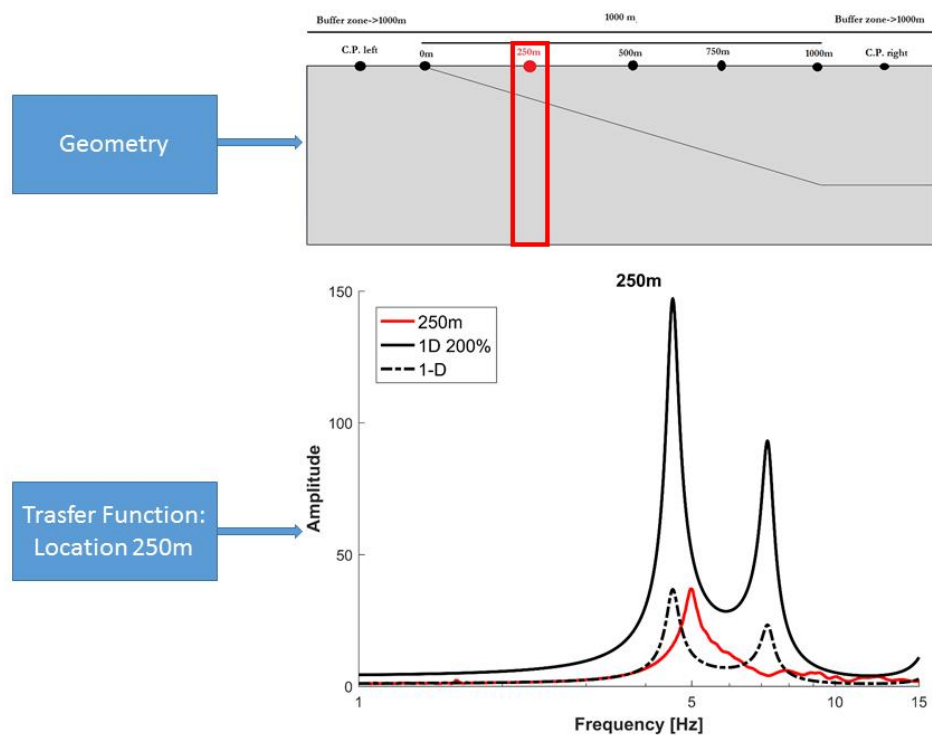


Figure 3.3. First criterion considered. Top: Geometry of the model, with the soil column and the control point chosen for the comparison; Bottom:

comparison of 1D and 2D transfer functions, plus the 1D transfer function
increased by 200%.

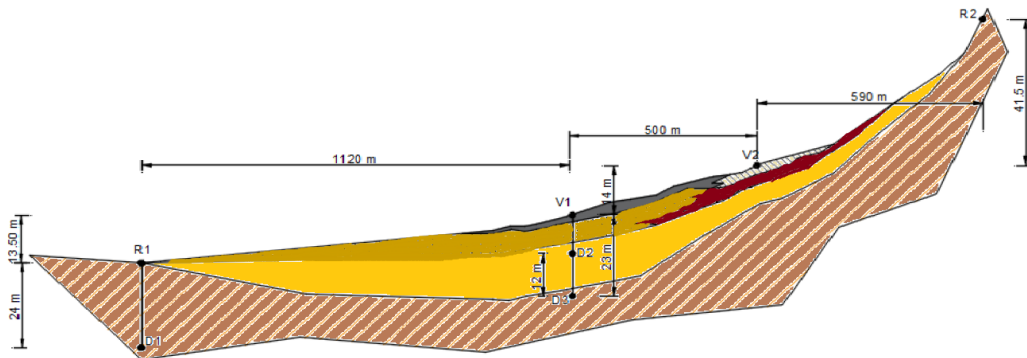


Figure 3.4. Turkey Flat valley scheme.

References

- Dassault Systèmes – SIMULIA (2013). Abaqus Analysis User's Guide, v6.13.
- Itasca Consulting Group, Inc., (2009). Fast Lagrangian Analysis of Continua in 3 Dimensions User's Manual, Minneapolis, Minnesota, U.S.A.
- Pilz, M. and F. Cotton (2019). Does the 1D assumption hold for site response analysis? A study of seismic site responses and implication for ground motion assessment using KiK-net strong-motion data. *Earthquake Spectra*, In-Press. <https://doi.org/10.1193/050718EQS113M>
- Real, C. R. and A. F. Shakal, Turkey Flat, USA, Site effects test area, report 7, Strong-Motion test: prediction criteria and data formats, CSMIP Report 0SMS 05-1, California Geological Survey Department of Conservation

- Toro, G. R., (1995). Probabilistic models of site velocity profiles for generic and site-specific ground-motion amplification studies. Technical Rep. No. 779574, Brookhaven National Laboratory, Upton, N.Y

3.2 An accessible approach for the site response analysis of quasi-horizontal layered deposits

Carolina Volpini & John Douglas

*Department of Civil and Environmental Engineering, University of Strathclyde
Glasgow (UK)*

carolina.volpini@strath.ac.uk,

john.douglas@strath.ac.uk <https://orcid.org/0000-0003-3822-0060>

Abstract

This study focusses on sites that are neither strictly one-dimensional (with flat parallel soil layers) nor clearly two-dimensional (steep valleys, canyons and basins). Both these types of geometries are well studied in the literature. There is a lack of studies, however, for all those geometries that are in between these two worlds, such as sites with gently dipping layers. Theoretically, such sites should be studied with a two-dimensional approach because of the formation of surface waves due to the non-horizontal layering. In certain situations, however, the one-dimensional assumption leads to minor errors and it may save a lot of effort in terms of defining a two-dimensional model, computing the response and interpreting the results.

As result of these practical advantages, an accessible approach is presented here to determine when one-dimensional analysis can be used for geometries consisting of quasi-horizontal layers. The methodology is based on the construction of a chart, delimiting the applicability of the one-dimensional approach, by using simple but valid variables, such as slope of the critical subsurface interface and the impedance contrast at this interface. Indeed, we propose our guidance on the limits of the one-dimensional

analysis in the form of a power law separating the one-dimensional and two-dimensional regimes: $I_z = 6.95 \gamma^{-0.69}$, where I_z is the impedance contrast and γ is the angle in degrees of the sloping critical subsurface interface. Site response for geometries with values of I_z below this critical value can be computed using a standard one-dimensional approach without large error whereas geometries with values of I_z above this threshold require two-dimensional calculations.

Keywords

Site response analysis; one-dimensional; two-dimensional; seismic hazard; dipping layers; site effects

3.2.1 Introduction

Site response analysis (SRA) is one of the most powerful tools within engineering seismology as it models the influence of the near-surface layers on earthquake ground motions. These near-surface layers act as a filter that amplify/de-amplify the seismic waves coming from the earthquake source. Based on the complexity of the near-surface geometry and the characteristics of the layers, several SRA approaches are possible.

From all we know in the literature, we can distinguish between two macro-worlds with regards subsurface geometry: flat layered sites and valleys or canyons. Each of them has its best approach for SRA. Indeed, the easiest method, one-dimensional (1D) SRA, should be used whenever the stratigraphy and/or the geometry of the soil deposit is flat. This method, in fact, simplifies the reality with a single multi-layered column (Kramer, 1996). Whenever, on the contrary, the stratigraphy/ topography requires a more complex model, two or three-dimensional (2D/3D) SRA should be used. This is the case for a steep valley or canyon, where the wave path cannot be described with a 1D model. Note that in this work 3D SRA will not be discussed. Some authors have also discussed that, among geometries such as valleys, there is a critical shape ratio, which delimits the two-dimensional resonance response from the one-dimensional and lateral propagation (Bard and Bouchon, 1980). Despite this, they are still focusing on valleys (edges with an angle larger than five degrees). This means that there is a gap in the literature of how to treat all those geometries with quasi-horizontal layers (from zero to five degrees). Most of the time, these sites are investigated by adopting the simplest and fastest method, which is the one-dimensional, but this does not mean that it is always the most correct one.

This study provides an accessible approach to identify the best option to study these particular geometries, which are neither strictly 1-D nor 2-D. To understand and identifying a threshold between these two worlds (1D and 2D), first we need to define a model that serves as a basis for comparison. This model must present a basic geometrical irregularity, like a gentle dipping layer (slope angles of 5 degrees or less). Indeed, we do not want to study either clearly flat layers or clearly steep valleys. For this model, we conduct a parametric analysis examining the effects of the sloping angle and the stiffness of the material on the difference between 1D and 2D results. After probing these variables and collecting the results, we define a criterion to quantify these differences and finally we test it with other simulations and observations taken from the literature. The following section discusses previous studies on the limits of 1D SRA before we present our results.

3.2.2 Previous studies on the limits of 1D SRA

Let us consider a simple stratigraphy: flat and without significant spatial variability. For these conditions it is possible to use 1D SRA, where the soil deposit and the bedrock are assumed to extend infinitely in the horizontal direction and just a single column is studied. The main hypothesis of this method is that the majority of the response is caused by SH-waves propagating vertically from the underlying bedrock. Ignoring the different ways of treating soil characteristics (linear, equivalent-linear, nonlinear), the result of a 1D SRA is displayed in Figure 3.2.1.

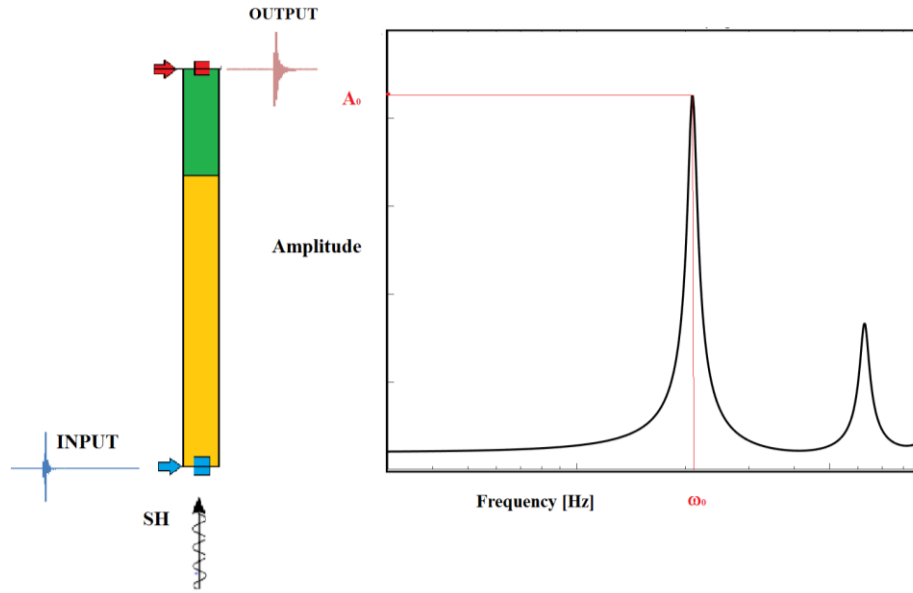


Figure 3.2.1. 1-D SRA transfer function.

The amplification caused by the difference in stiffness between the soil deposit and the bedrock (impedance contrast) peaks at certain angular frequency values (ω_n), which are functions of the thickness of soil deposit (H) and of its shear wave velocity (V_s):

$$\omega_n \approx \frac{V_s}{H} \left(\frac{\pi}{2} + n\pi \right) \quad n = 1, 2, \dots, \infty \quad [22]$$

The amplitudes associated with these resonance frequencies are given by equation [23] for the viscoelastic case (the one used throughout this study):

$$A_{r,max} \cong \frac{2}{(2n-1)\pi D} \quad n = 1, 2, \dots, \infty \quad [23]$$

where D is the damping value, which characterizes the reduction in wave energy.

This approach is not valid for geometries such as steep valleys, canyons and basins. These geological formations cause a series of phenomena, related to both its geometry and also the soft material infill. Indeed, the softer the material of the alluvial basin compared to the bedrock, the higher is the effect of the waves trapped within it. These trapped waves are incident body waves that propagate through the alluvium as surface waves (Vidale and Helmberger, 1988), which are responsible for stronger and longer shaking than would be predicted by 1D SRA, which only considers the vertical propagation of SH-waves.

The direct consequence of this complexity is the lack of analytical solutions for the transfer function. A single smooth peak at certain resonance frequencies is no longer valid and complex amplification at many frequencies can be seen (e.g. Figure 3.2.2).

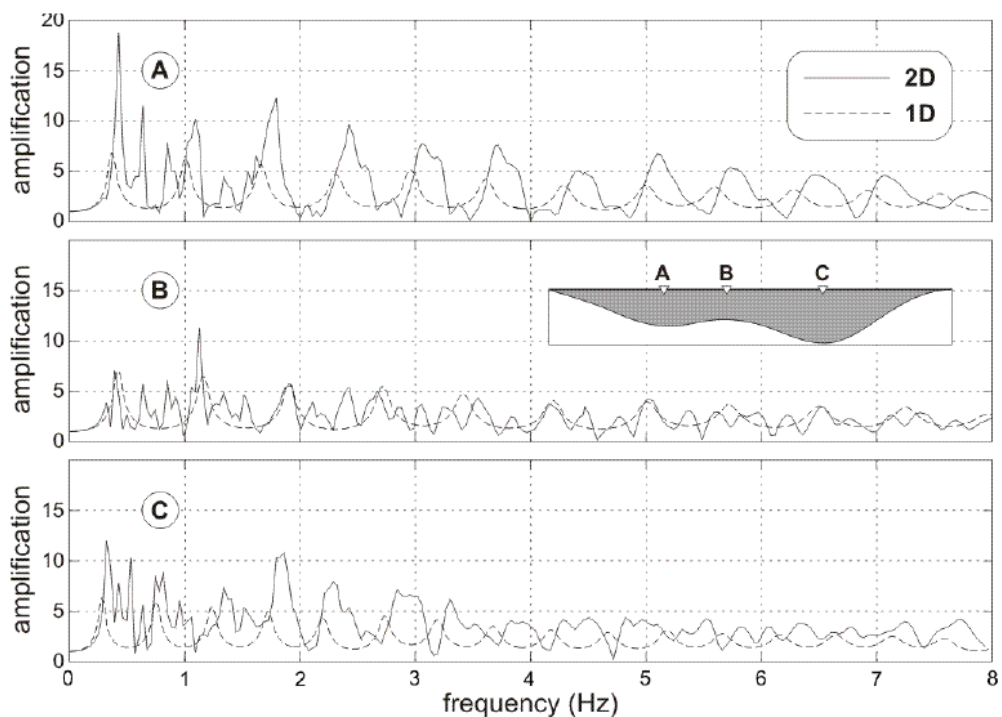


Figure 3.2.2. Example 1D and 2D transfer functions in a valley (Delépine and Semblat 2012).

Many studies have been conducted on the effects of this kind of geometry on earthquake ground motions. Bard and Bouchon (1980a,b) extended the work of Aki and Larner (1970) to demonstrate how effective inclined interfaces are at generating surface waves, in particular Love waves, which can cause larger amplitudes in comparison with the direct incident waves. Bard and Bouchon (1980a,b) also studied the influence of a high velocity contrast between the soil deposit and the bedrock and showed that it can trap the surface waves within the basin and cause multiple reflections of them at the edge of the valley. This results in ground shaking of a longer duration in comparison with a flat site.

Bard and Bouchon (1985) show that there is a critical shape ratio (Figure 3.2.3), depending on the velocity contrast, controlling whether the response of the valley is governed by lateral propagation or by 2-D resonance. This critical shape ratio has the following equation [24]:

$$(h/l)_c = \frac{0.65}{\sqrt{C_v - 1}} \quad [24]$$

where $(h/l)_c$ is the shape ratio; and C_v is the velocity contrast, which is the ratio between the shear-wave velocities of the bedrock and the soil deposit. For our analyses we use the impedance contrast (I_z) which takes into account the change in density as well as velocity.

Chávez-García and Faccioli (2000), focusing on incorporating 2D site effects in seismic building codes, extend the work of Bard and Bouchon (1985). They study a simple geometry of alluvial basins (symmetrical and homogeneous) to explore the impact of the impedance contrast and the shape ratio on site amplification. They report

their results in a similar graph to Bard and Bouchon (1985) showing the different alluvial valleys analyzed (Figure 3.2.3).

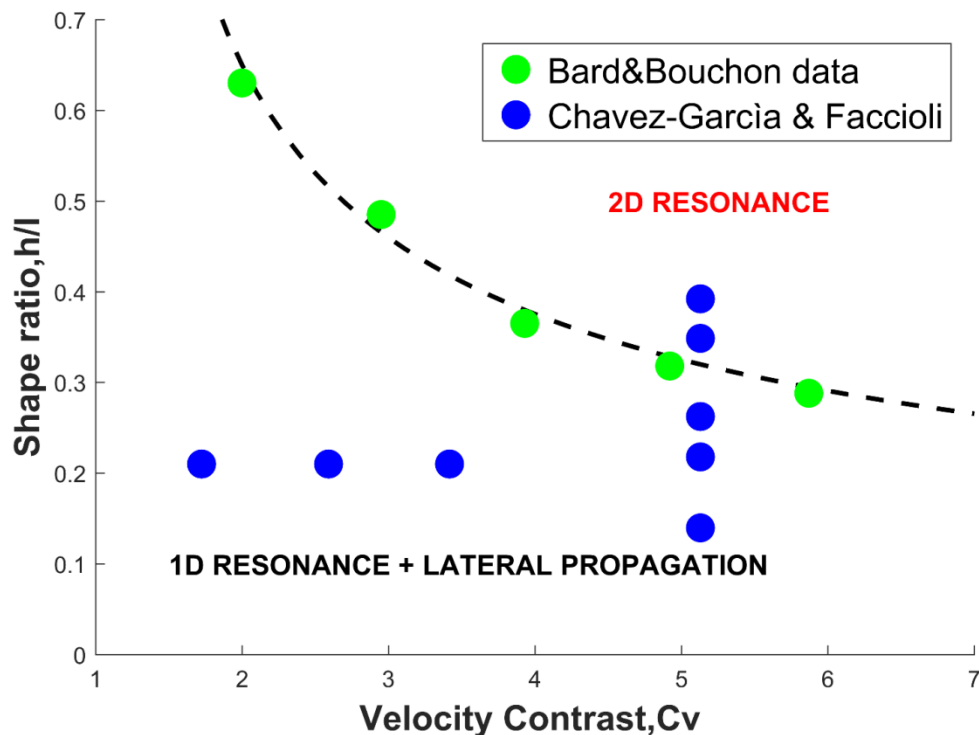


Figure 3.2.3. The critical shape ratio equation of Bard and Bouchon (1985) and the parametric analyses conducted by Chavez-García and Faccioli (2000) to validate this equation.

It is important to notice that we cannot use this graph for our study because it refers to shape ratios that go from 0.1 to 0.5, which means sloping angles greater than 5 degrees. The focus of Bard and Bouchon (1985) and Chavez-Garcia and Faccioli (2000) on high shape ratios is understandable because of their interest in valley/basin behaviour. However, our study focuses on geometries with gentle dipping layers. All of the cases we study here are within the region entitled “1D RESONANCE+ LATERAL PROPAGATION” on Figure 3.2.3 because we focus on slopes between 0 and 5 degrees. Our study shows that even within this section of their graph there is a

threshold separating geometries that clearly behave in a 2D manner and those where the 1D assumption roughly holds.

Another interesting study for our purposes was performed by Hasal et al. (2018), who conducted a parametric study for the Duzce basin (Turkey). They show the effect of the edge inclination (slopes of 6° , 11° , 27° and 45°) on the variation in surface motion under earthquake excitations with different frequency content. They investigate the variation of the aggravation factor (the 2D/1D spectral acceleration ratio) with distance from the basin edges. Figure 3.2.4 summarizes their findings on when 1D and 2D SRA apply. In the context of our study it is important to note that this graph does not apply to our geometries, because their range of H/D goes from 0 to 10, which means slope angles between 6° and 45° , steeper than our slopes.

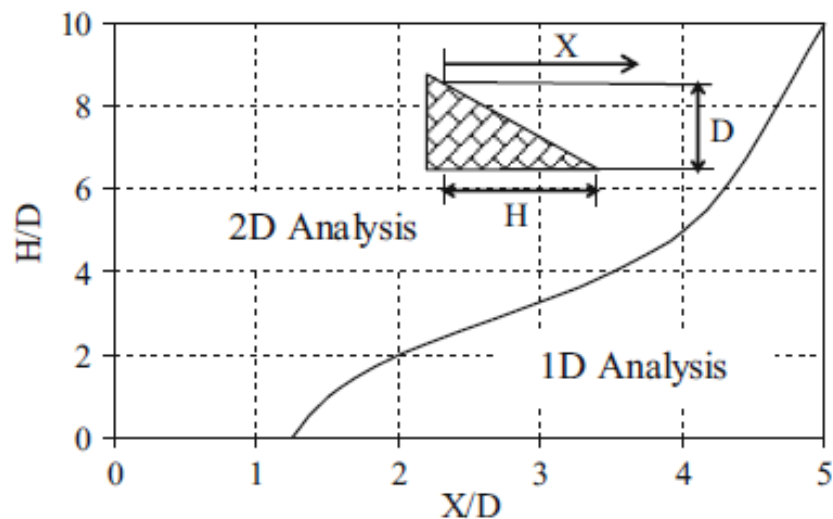


Figure 3.2.4 The threshold between 1D and 2D SRA at the edge of the Duzce basin proposed by Emre et al. (2017).

The use of an aggravation factor is also supported by Makra (2012) who compared the results of different software for 2D SRA of a basin. The use of an aggravation factor is shown to be a powerful tool to quantify the additional amplification in response

spectra in comparison with 1D SRA because of 2D effects. Makra et al.(2012) showed that the aggravation factors for the basins studied could be divided into three groups: a region on rock site outside the basin, a region at the edge of the basin and a third region far from the edge of the basin. They concluded that the aggravation factor could be used to provide guidance on site amplification depending on the position within the basin.

Vessia et al (2011) have reprised the problem of valley effects, stating the fact that these kind of phenomena can only be estimated on a case-by-case basis through specific numerical simulations. The aim of this work was to produce a sort of “geometric coefficient” to identify the so-called “valley effects”. To do that, they propose a simple approach to predict valley effects by using 2D simple sketches of 30m depth valleys, with a $V_{s,30}$ characterization (according to the Italian building code), where $V_{s,30}$ is the average shear-wave velocity in the top 30m.

Thompson et al. (2012) propose a method to classify sites that require a complex SRA from those where the standard assumptions are sufficient. Their taxonomy is based on two criteria, the second of which is a goodness-of-fit metric between the theoretical and the empirical transfer functions. For their comparison, Thompson et al. (2012) focus on the alignment of the resonances. As shown by equation [22], the resonance frequency depends on the geometry of the model (H), whereas the amplitude of the resonance peaks (at least for viscous-elastic analysis) depends on the material damping, which is uncertain and difficult to determine. These uncertainties come from both laboratory test data and modeling issues. In a viscous-elastic analysis, the amplitude depends completely on the damping value (equation [23]). For this reason, they have chosen to compare the theoretical and empirical transfer functions using the Pearson’s sample correlation coefficient, r , which captures how well the peaks are aligned. This correlation coefficient varies from -1 to 1, where -1 means completely

negative correlation, 0 means no correlation and 1 means perfect correlation. Thompson et al. (2012) choose $r=0.6$ as the threshold between poor ($r<0.6$) and good ($r\geq 0.6$) fits.

Sanchez-Sesma and Velazquez (1987) derive a closed-form solution for the seismic response of an elastic dipping layer using specific geometrical analysis. The exact solution is given for dipping angles of the form $\frac{1}{2}\pi/N$, where N is an odd integer. Using this formula they have shown the importance of modelling this kind of geometries, such as valley edges.

Furumoto et al (2006) proposed a method to compute the transfer function of dipping layers by superposing 1D transfer functions of the upper and lower side of the slope. Then they have compared their results to a 2D SRA showing that lateral site effects modify the dominant frequency.

In our previous study (Volpini and Douglas, 2017), we have already studied the effect of gently dipping layers and suggested that it could be captured by conducting 1D SRA with randomized profiles. We considered a five-layer model using both 1D and 2D SRA. The large number of layers considered did not allow us to generalize our findings. That is why in this article we have considered just two layers, in order to understand a simpler situation.

3.2.3 Comparing 1D and 2D SRA

The purpose of this study is to investigate those geometries, which are neither strictly 1D nor 2D/3D. In reality no site is perfectly 1D and hence it is important to know when the assumptions of 1D SRA breakdown. It is clear that when possible (good knowledge of the site in terms of characteristics of material, stratigraphy and records of input

motion; availability of appropriate software and skills in using these software; and time to conduct the analysis) it is worth undertaking a 2-D/3-D SRA for all sites significantly deviating from perfectly horizontal layering. Theoretically 2D/3D SRA should model the site amplification at such sites better than 1D SRA. From a practical viewpoint, however, 2D/3D SRA can produce erroneous and unpredictable results when there is a lack of detailed information about the site. Moreover, the more complex is the model, the higher the time taken to run the analyses, interpret the results and simplify them for engineering applications.

In the previous section, various studies on the importance of taking into account 2D effects related to the basin shape were summarized. In this study, we conduct a more general survey of stratigraphic irregularities and provide some general and simple guidance on a better method to adopt in engineering practice for sites with near-surface geometries that are at the boundaries between the 1D and 2D worlds. The guidance is in the form of site characteristics that can be known *a priori*, such as sloping layers and the geo-mechanical characteristics of the soil, so as to avoid the need to compare the results of 1D and 2D SRA for the site.

The following sections present:

- 1) a parametric study on the seismic response of a 2D model with different dipping layer geometries and impedance contrast ratios;
- 2) a comparison of the 2D results with a 1D analytical solution;
- 3) a numerical criterion based on the comparison between the 1D and 2D transfer functions;
- 4) definition of a boundary between the two approaches; and
- 5) verification of this guideline using other results from literature.

3.2.3.1 Defining the tools

To study this problem in a parametric way, a simple geometry has been chosen. The aim of this first part of the work is to analyze three main aspects, similarly to Bard and Bouchon (1985) and Chavez-Garcia and Faccioli (2000):

- the influence of the dipping layer and the angle of the slope;
- the influence of the impedance contrast;
- the influence of location within the model;

Figure 3.2.5 shows the situation analyzed. The model is composed of two layers. The first one is dipping layer, which corresponds to a soil deposit. Four dip angles are considered: 2° , 3° , 4° and 5° , leading to values of Δh of 35m, 52m, 70m and 87m, respectively.

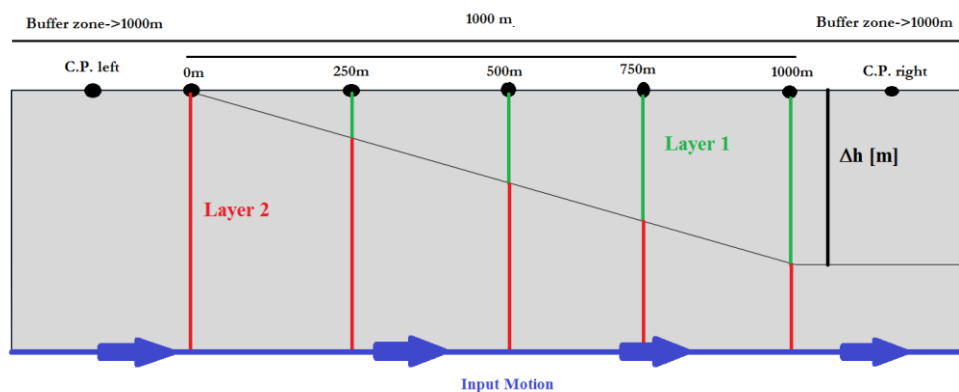


Figure 3.2.5 Geometry of the model considered.

Seven different shear-wave velocities are assumed for layer 1: 200, 300, 400, 500, 600 and 700 m/s. Therefore, there are six analyses for each geometry and, in total, 4 angles \times 6 velocities=24 analyses. The shear-wave velocity for layer 2 is kept constant at 1000 m/s for all calculations. This leads to a variation in the impedance contrast:

$$I_z = \frac{\rho_2 V_{s,2}}{\rho_1 V_{s,1}} \quad [25]$$

where: ρ_2 and $V_{s,2}$ are respectively the density and the shear wave velocity of the second layer; and ρ_1 and $V_{s,1}$ are respectively the density and the shear wave velocity of the first layer. The densities of layers 1 and 2 are 1750 and 2200 kg/m³ respectively and the Poisson's ratios are 0.35 and 0.25. It is worth mentioning that the main contribution to the impedance contrast ratios is the shear-wave velocity of layer 1. Density and Poisson's ratio do not have large effects on viscoelastic analyses.

The length of the model is 1000m plus two buffer zones of 1000 m each, which are fundamental to carry out the analysis in the 2D finite element software used here, Abaqus (Dassault Systèmes Simulia Corp, 2013). The dimensions have been chosen following the guidance provided by Nielsen (2006, 2014) as well as the boundary conditions (a rigid base and lateral free-field boundaries).

Time-domain viscoelastic analyses are conducted. Several (four rock outcropping motion and a within motion) input accelerograms have been tested, all of them taken from the Italian ITACA database (Luzi et al., 2017). The accelerogram is input at the horizontal base of the model (Volpini et al., 2018).

We tested inputting both the horizontal and vertical accelerograms simultaneously in the model but in the final calculations we decided to input just the horizontal component because of two reasons. Firstly, making a comparison with 1D SRA is clearer in this case. Indeed, in 1D SRA the basic hypothesis is to analyze the vertical propagation of the SH wave. Inputting a vertical motion into the 2D SRA would produce P and SV waves, changing the sense of the comparison. Secondly, there is still debate over the best way of conducting vertical SRA in the site response research community (Han et al., 2017).

Figure 3.2.6 displays one of the accelerograms used for the calculations shown here. From a theoretical point of view, the input motion should not make any difference to the transfer function, because we are dealing with linear analysis, whereas in a non-linear analysis the choice of the time history is important (Rathje et al., 2010)

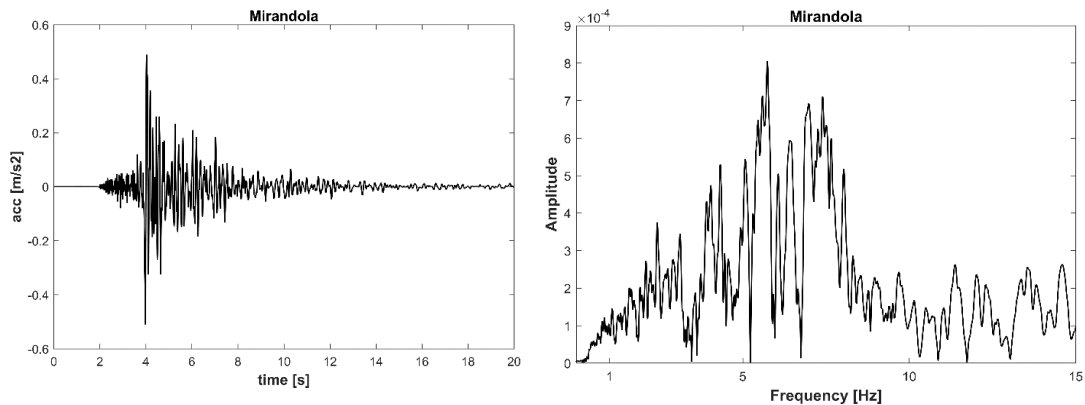


Figure 3.2.6 Examples of input motion chosen from the ITACA database.

The ground motions at several equally-spaced control points (Figure 3.2.5) are studied to investigate the spatial variability in the transfer functions, similarly to the approach of Makra et al.(2012). In addition, two other control points outside the main model, called C.P left and C.P right, are used to test the effect of the buffer zone. (Volpini et al., 2018). The resulting transfer functions are compared to those from 1D viscous-elastic SRA computed using STRATA (Kottke and Rathje, 2009) and the vertical soil column below each control point.

The damping ratio chosen for both sets of analyses is 3%, which results in a smooth transfer function where the effect of noise is minimized. The choice of this damping ratio is based on the results of the Prenolin project (Régnier et al. 2016), where a series of tests were conducted to determine the most appropriate damping value for viscous-elastic analysis. It is easy to fix the damping ratio in STRATA but more challenging in Abaqus because it treats damping in a different way. (Volpini et al., 2018)

3.2.3.2 Results

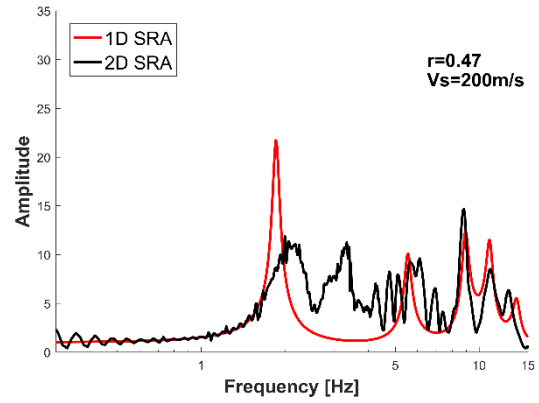
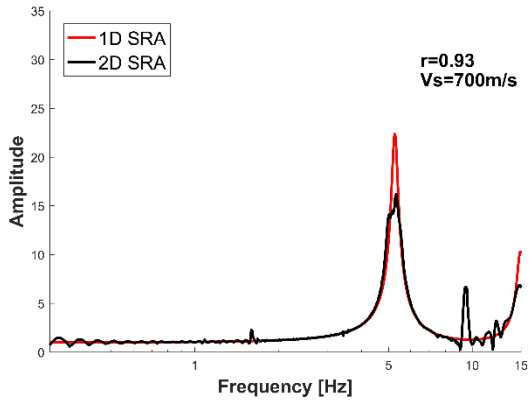
The purpose of this section is to compare the results of the 1D and 2D SRA for the 24 cases introduced above. Following the approach of Thompson et al. (2012) we make the comparison in terms of the transfer functions rather than the response spectral ordinates. Hence, time-domain results obtained with Abaqus were then converted to the frequency domain. It is well known that the frequency content of the input motion becomes very important in SRA, especially in non-linear analyses, whenever it is linked to a certain kind of soil deposit. Assimaki and Lee (2012) have defined a frequency index that is a cross-correlation between the transfer function and the input motion's amplitude spectrum. The higher this value is the more similar are these two functions, implying resonance.

For each geometry (2° , 3° , 4° 5°), a good match and a poor match are plotted (Figure 3.2.7). We have decided to plot the transfer functions for 250m and 750m, for good and poor match respectively, for consistency and for the results of the quantitative analysis discussed in the next section. For example, a good match (i.e. the 2D transfer function is similar to that from 1D SRA) is shown by the results for 700 m/s and control point 250 m whereas a poor match (i.e. the two transfer functions are dissimilar) is obtained for 200 m/s at control point 750 m. In general, a good match is obtained for a low impedance contrast and a shallow angle. Conversely, a poor match happens with high impedance contrast and a steeper angle.

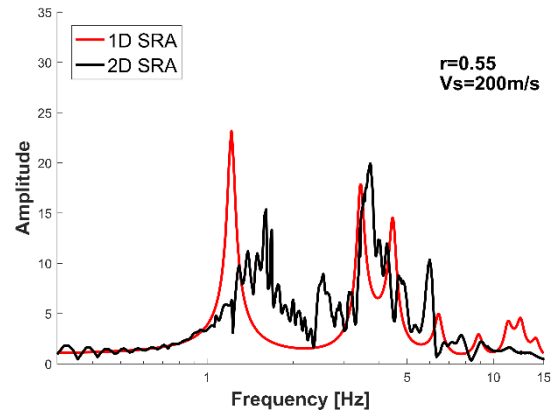
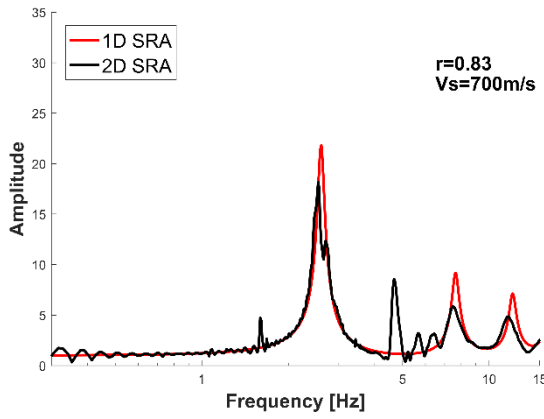
CONTROL POINT: 250m

CONTROL POINT: 750m

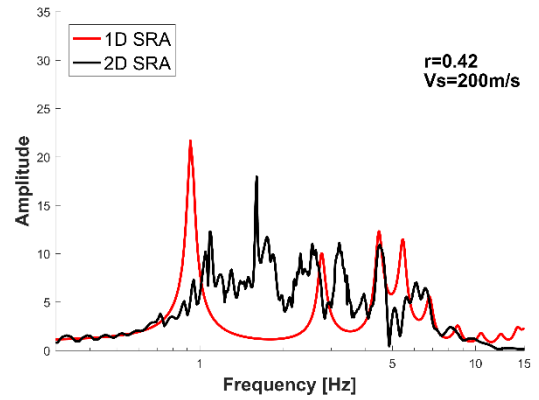
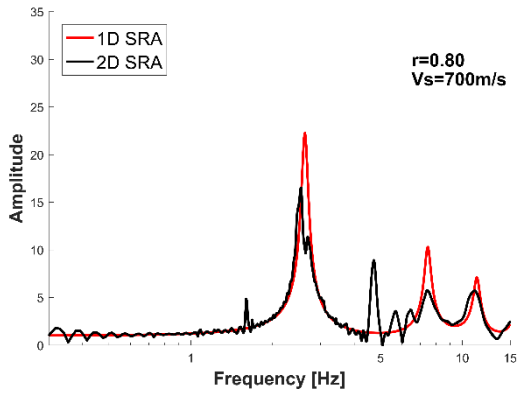
2°



3°



4°



5°

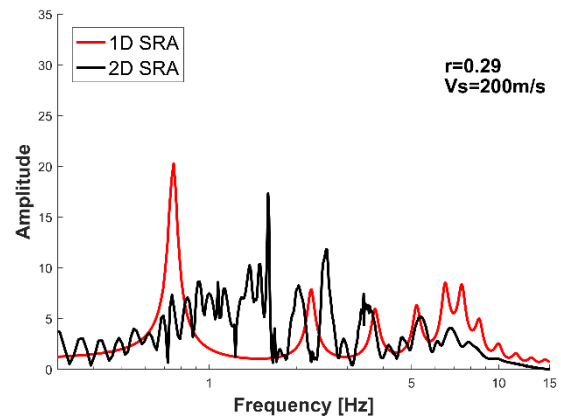
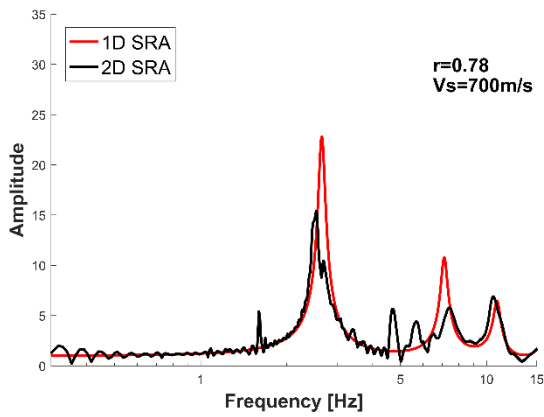


Figure 3.2.7 Comparison between 1D SRA and 2D SRA. 1a-b 2° good and poor match, 2a-b 3° good and poor match, 3a-b 4° good and poor match, 4a-b 5° good and poor match.

3.2.4 Investigating numerically the boundary between 1d/2d for quasi-horizontal layers

In the previous section, a qualitative comparison of the transfer functions was shown. For the chosen examples, it was clear which graph represented a good and poor match. Indeed, they have been selected with that aim. It is important to quantify the match, especially for those situations that are at the boundaries between visually good and poor matches. Indeed, although the transfer function plot immediately indicates the match between 1D and 2D SRA it does not measure it. Hence, following the approach of Thompson et al. (2012), the Pearson's sample correlation coefficient (r), is used to measure the goodness of fit between the two transfer functions. As discussed above r can vary from -1 to 1. In this context measures the alignment of the resonance frequencies.

To compute r the transfer functions for 1D and 2D for a set of consistent frequencies are plotted against each other. An example of such a plot is shown below in Figure 3.2.8. If the two curves were aligned perfectly r would equal one and if they showed no alignment r would equal zero. In this example, as is clear from a visual comparison of their transfer functions, the match is good; r in this case equals 0.8. Therefore, r is a useful parameter to measure the goodness of fit in a single number.

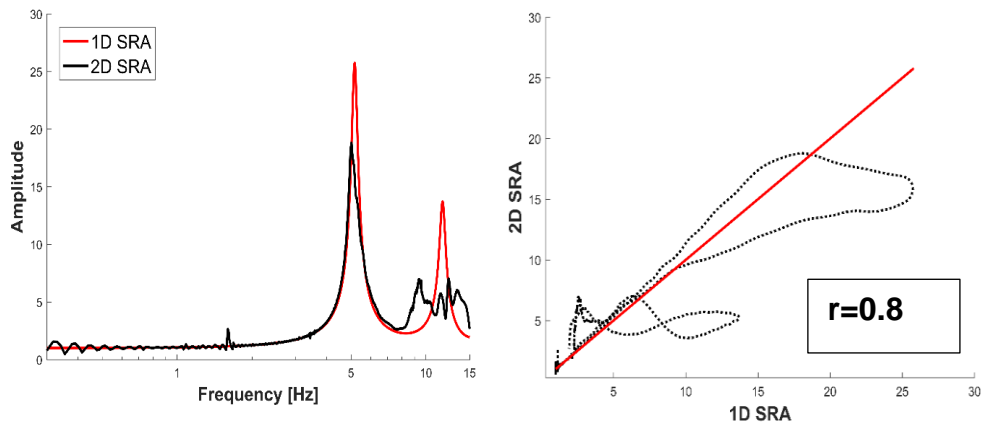


Figure 3.2.8 Comparison of the 1D and 2D transfer functions for the 2° model and $V_s=400\text{m/s}$ at control point 250m as well as the graph for computing the goodness of fit parameter r .

The value of r has been computed for every analysis and all considered control points. The values obtained are plotted together in a single graph (Figure 3.2.9). From this graph it can be seen, as expected, that: r increases as the angle of the slope decreases while it decreases with increasing impedance contrast. These trends are seen for all controls point except at 0m.

As the angle of the slope increases the fewer analyses pass the threshold of $r=0.6$, which Thompson et al. (2012) suggests indicates the boundary between poor and good matches. For example, for 2° only the results for 200 m/s are below the threshold, whereas for 5° most of the results for 200, 300, 400 m/s are below the threshold, thereby showing the strong impact of the slope on the match between 1D and 2D SRA. To make the influence of the three factors clearer on Figure 3.2.10 only the results for the highest and lowest impedance contrast are plotted. The values of r for 700m/s are always above the threshold whereas r for 200m/s is often below the threshold, which is in agreement to that presented by Bard and Bouchon (1980a, b, 1985) .

Figure 3.2.11 shows the results plotted in a different way to examine the influence of the location of the control point. The red dots indicate r values below the threshold whereas the black dots signify results above the threshold. In other words, red dots identify those situations where 2D SRA should be used because there is too large a difference between the 1D and 2D transfer functions.

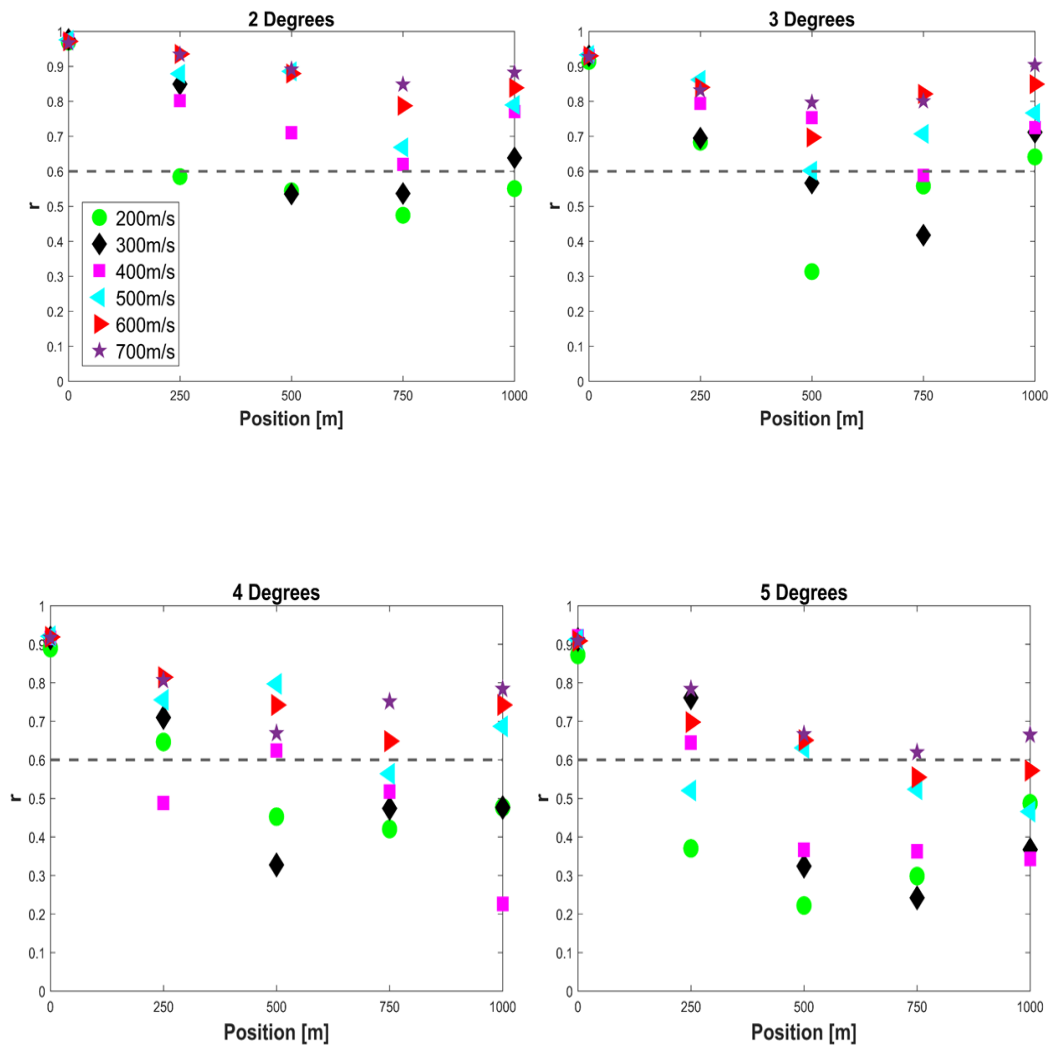


Figure 3.2.9 Summary of the Pearson's sample correlation coefficient, r , for all analyses. The colours and symbols identify different impedance contrasts. Each subplot is for a different slope angle and on each the results for every control point are plotted.

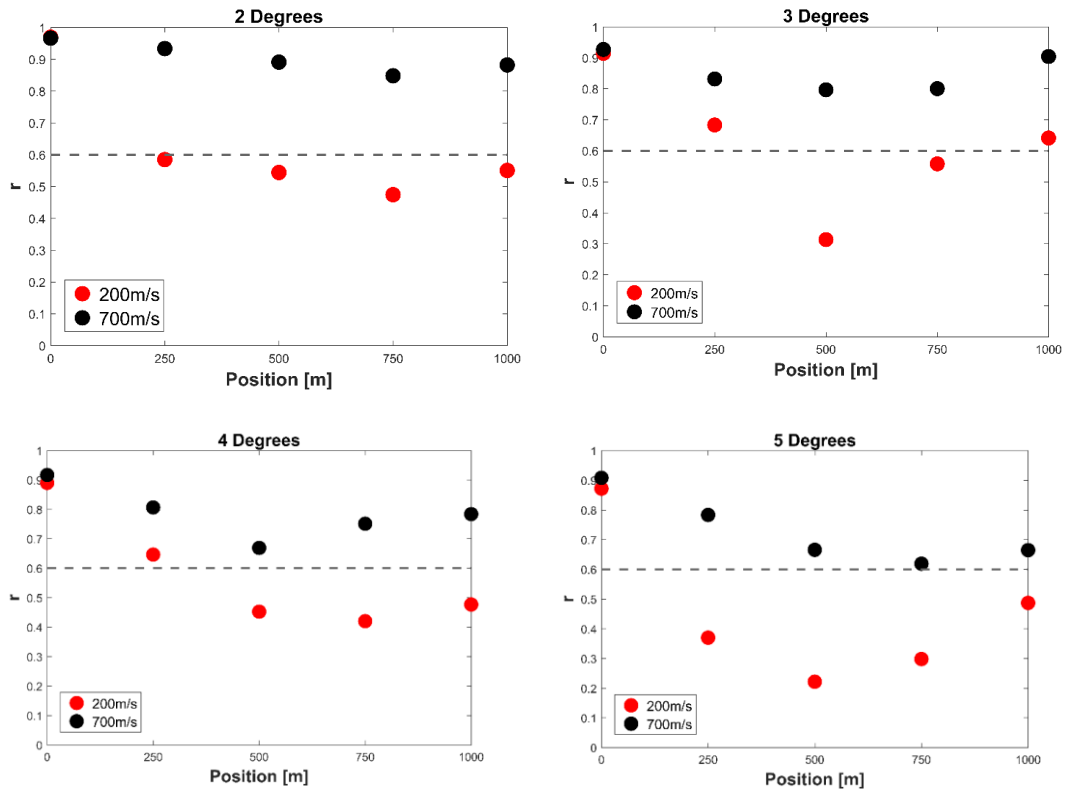


Figure 3.2.10 Summary of the Pearson's sample correlation coefficient, r , for the 200 m/s and 700 m/s analyses.

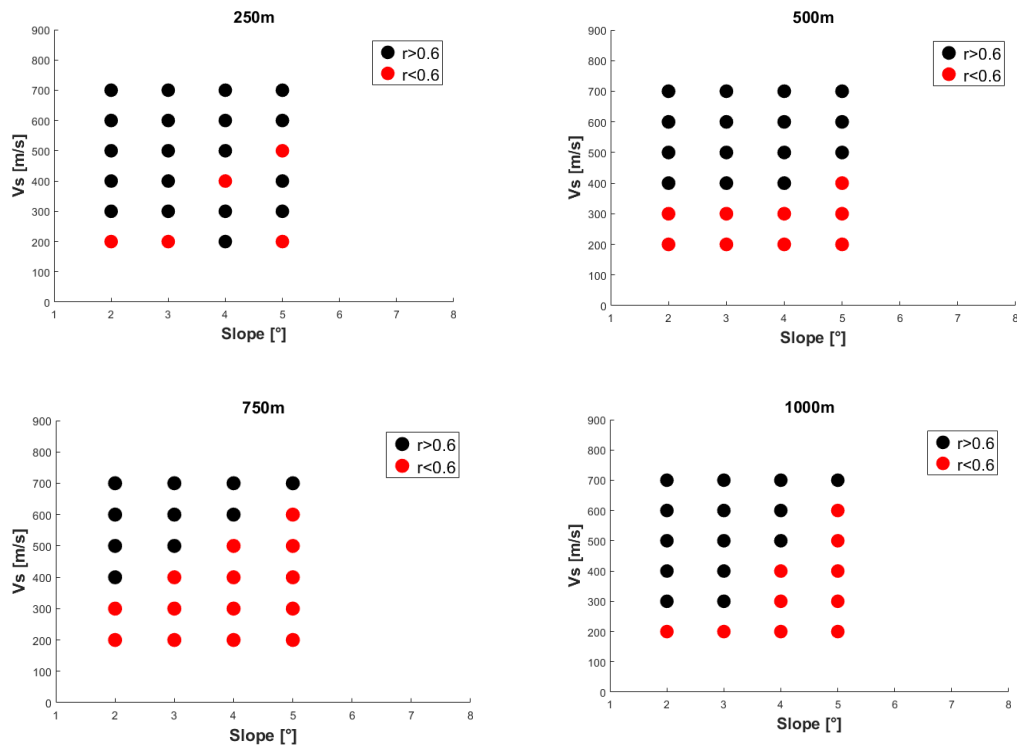


Figure 3.2.11 Summary of when the Pearson's sample correlation coefficient, r is above or below the 0.6 threshold. Each subplot is for a given control point: 250, 500, 750 and 1000m. The red dots indicates $r < 0.6$ and black dots $r > 0.6$.

From Figure 3.2.11 it can be seen that at the control point of 750m most r values are below the threshold of 0.6. To be conservative this location is chosen as the basis for the guidance derived below. Other analyses were conducted for control points 300m, 600m 700m, 800m and 900m to check whether 750m is indeed the most critical location. These analyses demonstrated that the worst match between 1D and 2D SRA occurs at the farthest distances from the origin. We have decided to base the guidance on the results for 750m because the results are more consistent here than at 800m and 900m. To check the robustness of this methodology, we have, firstly, reproduced the same geometry but for different widths. As well as the original one, which is 1000m

wide, we have selected two other widths: 500m and 2000m. In both cases, we have chosen the 2° and 4° models with $V_{s,1}=400\text{m/s}$. Results are reported in terms of Pearson's sample correlation coefficient in Table 3.2.1, demonstrating that this method gives stable results, except for certain location points of the 4° model. In particular, we should notice the 1000m Pearson's sample correlation coefficient, which is about 0.22 in the original model and 0.68 in the 2000m width model. This indicates that we are being conservative in the use of the results for 1000m.

	LOCATION	125	250	375	500	750	1000	1250	1500	1750	2000
	[m]										
2°	ORIGINAL	x	0.8	x	0.71	0.62	0.77	x	x	x	x
	(1000)										
	2000	x	0.88	x	0.88	0.86	0.73	0.68	0.73	0.74	0.77
	500	0.92	0.6	0.5	0.71	x	x	x	x	x	x
4°	ORIGINAL	x	0.49	x	0.68	0.52	0.22	x	x	x	x
	(1000)										
	2000	x	0.81	x	0.67	0.85	0.68	0.6	0.62	0.64	0.7
	500	0.68	0.7	0.47	0.6	x	x	x	x	x	x

Table 3.2.1 Pearson's sample correlation coefficient for geometries with different widths.

Secondly, to make the soil profile considered more realistic than a single soil layer overlying a stiff bedrock layer, the analysis was repeating using an idealized shear wave velocity profile from the Prenolin project (Régnier et al. 2016), described by this equation:

$$V_s = V_{s1} + (V_{s2} - V_{s1}) \left(\frac{z - Z_1}{Z_2 - Z_1} \right)^\alpha \quad [26]$$

Where: V_{s1} is the initial velocity; V_{s2} is the final velocity; $Z_1=0\text{m}$; Z_2 is the depth of the soil deposit, depending on the slope considered; and α is a parameter that denotes the shape of the curve (if $\alpha=1$, the equation describes a linearly increasing velocity). The soil deposit of Figure 3.2.5 is now divided into several sublayers using equation 26. Different values of α were tested. The results of this analysis are considered when checking the guidance derived from the simple profile (see below).

We also made calculations using the shear-wave velocity profile from an invasive test (cross-hole, from Fugro) performed in Mirandola (Italy) for the Interpacific project (Garofalo et al. 2016a; Garofalo et al. 2016b). Results from these calculations are also considered when checking the guidance (see below). In addition, results from our previous study (Volpini and Douglas, 2017) for extreme cases are also considered below. It should be noted that following publication of that study in the conference proceedings we found errors in our calculations, which have been corrected for consideration here.

Finally, we need to consider the possibility of irregularities on the dipping interface as the straight line geometry of Figure 3.2.5 is probably unrealistic for most locations. Therefore we also consider the interfaces shown in Figure 3.2.12a and b, which have the same overall slope as the interface of Figure 3.2.12c, which is used for the other calculations shown here.

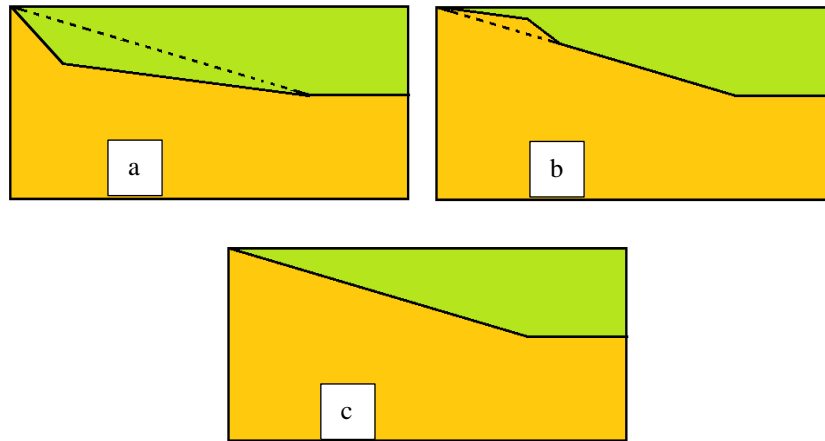


*Figure 3.2.12 Examples of irregularities that can be encountered on real sites
(a-b) and its simplification (c).*

A test is performed for 3° and velocity 300 m/s. Table 3.2.2 reports the results for the original interface (c) and the two irregular interfaces (a-b). The values obtained confirms the trend of the original calculations (c), except for control point 250m, where geometry b does not pass the threshold $r=0.6$.

Location [m]	0	250	500	750	1000
R_{,C}	0.93	0.70	0.56	0.41	0.71
R_{,A}	0.91	0.71	0.53	0.53	0.70
R_{,B}	0.94	0.57	0.45	0.43	0.70

Table 3.2.2 Pearson's sample correlation coefficient for geometries a, b and c.

To double-check this test, we have performed another analysis (3° , geometry b and $V_{s,1}=200\text{m/s}$). The results are shown in Table 3.2.3, which suggest that there is some minor uncertainty in the boundary between 1D and 2D response for irregular interfaces.

Table 3.2.3 Pearson's sample correlation coefficient for geometries b, c,
 $V_s, l=200\text{m/s}$ and 3°

LOCATION [m]	0	250	500	750	1000
$r_{,c}$	0.91	0.68	0.31	0.35	0.64
$r_{,b}$	0.92	0.58	0.26	0.54	0.64

3.2.5 Development of the chart

As discussed above, the 750m control point (Figure 3.2.11) is the worst location in terms of values of r and, therefore, to be conservative (i.e. to recommend 2D SRA when there is a doubt) results for this location are used in this section to develop the guideline. The purpose of this guideline is to choose on the best analysis method (1D or 2D SRA) *a priori* based on the slope angle and the impedance contrast.

To determine this guideline, in this section we: firstly determine a relation from the 750m location point graph separating the regions when 1D SRA gives acceptable results from those regions when it does not; and secondly to verify this relation with additional calculations taken from the literature as well as computed here for more realistic shear-wave velocity profiles.

Figure 13 again shows the results for the 750m control point trend, but this time using the impedance contrast. Bard and Bouchon (1985) and Chávez-García and Faccioli (2000) use the shape ratio parameter to characterize their basins. In this work, we do not want to concentrate on a specific type of 2D structure, e.g. basin or canyon, but to

develop a more general rule. Therefore, we use the average angle of the sloping interface, which can characterize basins and valleys as well as gently dipping layers.

This simple power law separates the two regions of Figure 3.2.13:

$$I_z = 6.95\gamma^{-0.69} \quad 0 < \gamma < 13^\circ \quad [27]$$

where γ is the sloping angle. To make this graph clearer, consider two situations. If we have a site with an irregularity such as a gentle dipping layer with a slope of two degrees (2°) and the soil deposit is stiff ($I_z = 3$), we could use a 1D SRA without large errors as the critical I_z for this case is $6.95 \times 2^{-0.69} = 4.3$. Conversely, let us consider the same geometry but with a very soft soil deposit ($I_z = 7.5$), in this case this graph suggests that a 2D SRA is required because the transfer function from a 1D SRA would not capture the strong 2D effects present.

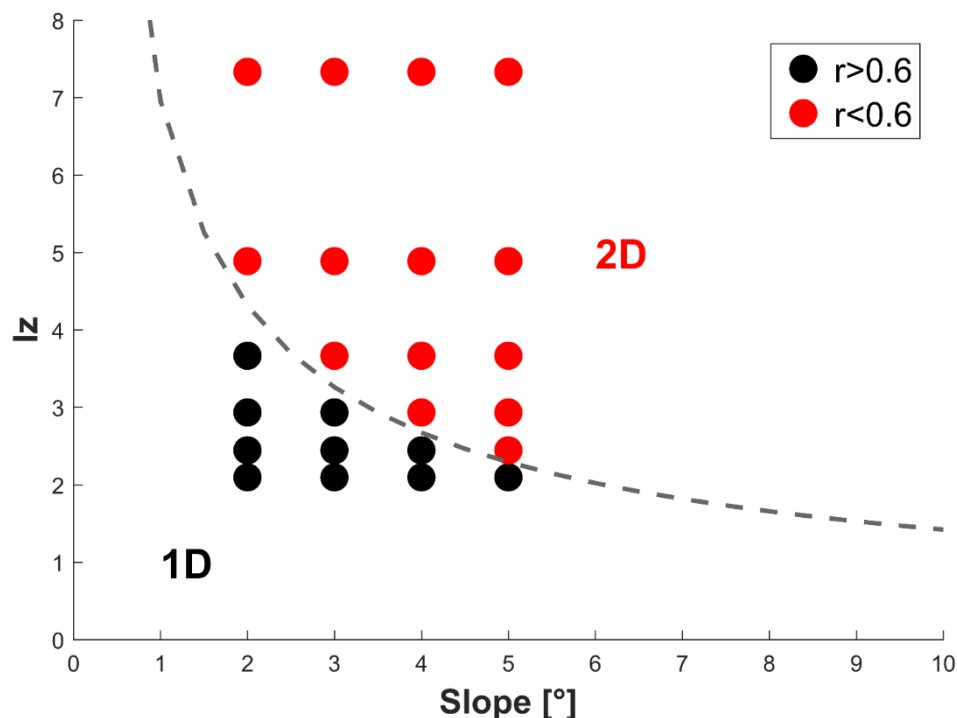


Figure 3.2.13 Summary of when the Pearson's sample correlation coefficient, r is above or below the 0.6 threshold for a control point of 750m, which is used

as the basis of the guidelines. The threshold indicates the boundary between 1D being acceptable and 2D being required.

3.2.6 Probing the guidelines

To check the guidance shown in Figure 13 it is useful to consider simulations or observations from the literature. We do not consider valleys with slopes larger than about 15° and “sine” shape because it is commonly agreed that beyond a certain level ($h/l=0.25$, narrow valley) (Silva, 1988) 1D SRA will always give incorrect results. It is important to include both sites that are clearly 1D and clearly 2D but also cases between these two worlds. Each site will be classified by two parameters: slope and impedance contrast.

The types of studies considered are the following, along with the methods to simplify them.

- 1- The paper must present the geology of the site as well as geo-mechanical characteristics.
- 2- A study is excluded from consideration if a 1D SRA is presented without giving a rough estimation of the subsurface stratigraphy/geology because we cannot estimate the slope for this situation.
- 3- In case of an irregular shape, a simplified shape will be taken into consideration (e.g. Figure 3.2.12).
- 4- As previously mentioned, the sloping angle must be $<15^\circ$. Our focus is on studies for slopes between 2 and 8° as this is the critical zone between 1D and 2D response.
- 5- The results of Bard and Bouchon (1980a, b, 1985) and Chávez-García and Faccioli (2000) are also considered.

While it is very easy to find clearly 2D/3D examples in literature, it is more difficult to find examples of 1D cases with sufficient information to confirm that they are 1D because such sites are often less appealing from a research point of view (if potential nonlinear behavior is ignored). Despite this lack of studies, we were able to find sufficient cases where the stratigraphy is not perfectly flat, but, because of a low impedance contrast or weak ground motions, 1D SRA has been used. Table 3.2.4 summarizes the examples considered here. To evaluate the impedance contrast ratio, we have computed an average value of both shear-wave velocity and density for each of the real geometries.

A comparison between the guidance derived in the previous section and the results from previous studies is shown in Figure 14. As is clear from the graph, there are cases (valley) in which 2D SRA is clearly needed. An interesting comparison is between the basins in Nice and Caracas (Semblat et al., 2002). They have chosen these two basins as examples of a 1D case (Nice) and 2D (Caracas). This decision is clearly highlighted in the graph as these basins are on opposite sides of the line. Considering the parametric analyses of Bard and Bouchon (1980a, b, 1985) and Chavez-García and Faccioli (2000), we can say that our guidance confirms their studies. For example, Bard and Bouchon (1985) did not consider the case of 4° and low impedance contrasts because their aim was to evaluate 2D effects. Considering our additional calculations using the Prenolin (equation 26) and Mirandola profiles, these also confirm the guidance in most cases. We should note that the Prenolin profile with $\alpha=1$ gives an inconsistent (but conservative) answer in comparison with the guidance. For this case all simulations had $r>0.6$, indicating a good match between 1D and 2D SRA. The results for Mirandola are also on the threshold; again all our simulations give $r>0.6$. The conclusion of the checking of the guidance with other more realistic profiles and geometries is that there is some uncertainty in the location of the threshold of when

1D SRA applies but our proposed threshold is generally conservative, i.e. it recommends 2D SRA when 1D SRA may in fact be acceptable.

Site	Reference	Description/Info	Slope [°]	Impedance contrast ratio, Cv	1D	2D
[-]	Bard and Bouchon., 1980a	type 1	4	2.2	x	
		type 1	4	8.2		x
		type 2	12	2.2		x
		type 2	12	8.2		x
[-]	Chavez-Garcia and Faccioli, 2000	HC	9	5.2		x
		same angle	13	1.8		x
				2.6		x
				3.5		x
				5.2		x
Thessaloniki, Greece	Raptakis et al., 2004	LEP	7	3.5		x
Val di Sole, Trento, Italy	Faccioli et al., 2001	[-]	13	3.0		x
Kirovakan Valley, Armenia	Bielak et al, 1999	zone 3	6	1.7	x	
		zone 2	>20	2.3		x
Grenoble, France	Bonilla et al,2006	[-]	12	5.2		x
[-]	Prenolin Project	alpha<1	3	2.4	x	
		alpha<1	4	2.4		x
		alpha=2.5	5	4.5		x
		alpha=1	5	3.3	from the analysis	x
Mirandola, Italy	Interpacific Project- Mirandola	Fugro -Crosshole	2	4.4	x	
			5	3.3		x
Nice basin, France	Semblat et al., 2004	[-]	3	4.6	x	
Caracas basin, Venezuela			10	5.5		x
Mississippi enbayment, U.S.	Park and Hashash, 2001	[-]	0	2.5	x	
[-]	Volpini and Douglas, 2017	[-]	1	2.4	x	
			5	3.4		x

Table 3.2.2 Summary of the real cases added to the guideline. For the definition of alpha please see Equation 26.

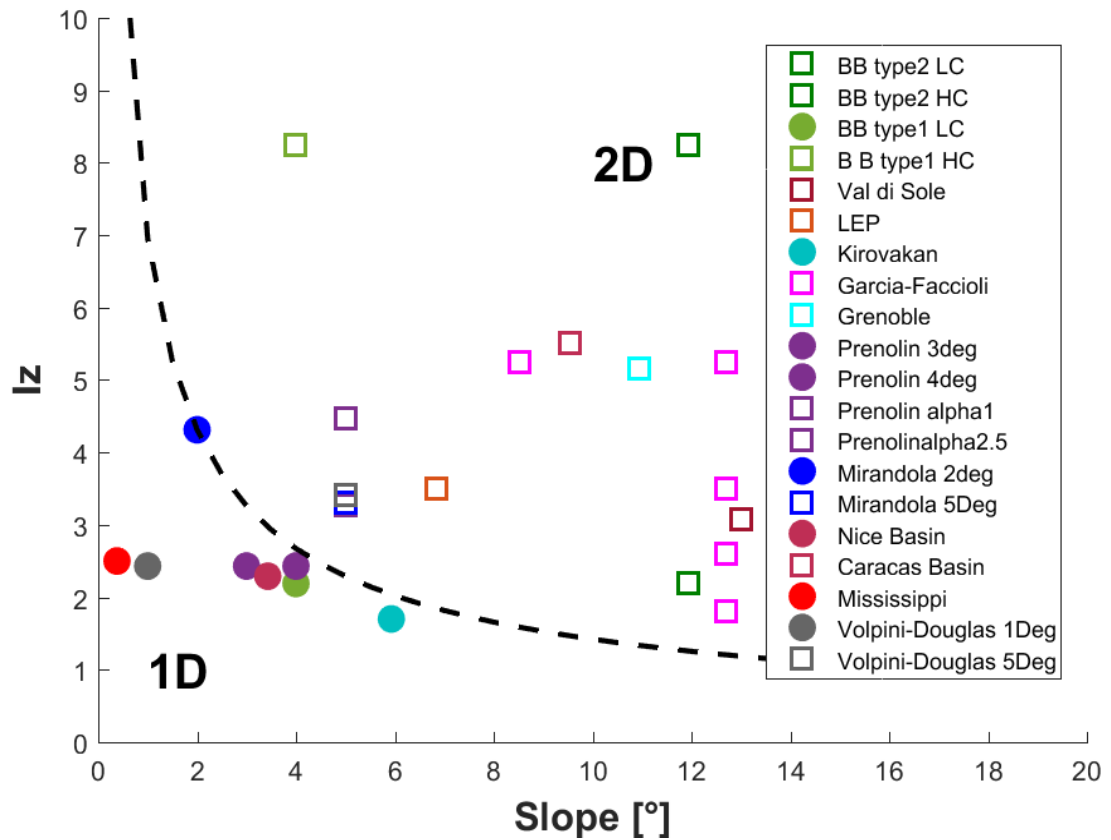


Figure 3.2.14 Comparison between the guidance proposed in this study and previous studies.

3.2.7 Conclusions

In this article, a comparison between transfer functions from 1D and 2D site response analysis was presented. 1D analyses are easy to understand, they are rapid and uncertainties in the geomechanical properties of the soil layers can be easily incorporated. When the subsurface geometry/stratigraphy does not present marked derivation from the assumption of flat layers 1D analysis can provide accurate results.

In contrast, 2D analyses are more complex and require much more detailed information about the site. In addition, they require more computational resources and time, especially if uncertainties in the site properties are considered. For these reasons, most of the time 2D analyses are not used in engineering practice unless strictly necessary, e.g. a steep valley. The result of this study was guidance in the form of a power law, based on the subsurface slope of the soil deposit and the impedance contrast, was proposed to decide on when 1D analysis provides acceptable results or in contrast when 2D analysis is required. Linear viscoelastic analyses were performed, where the main geomechanical characteristic is the material stiffness (expressed through the shear-wave velocity). The model proposed presents a simple geometry, defined by two layers, where the shallowest one is inclined. This configuration can be seen as the edge of a valley.

This guidance was the result of a parametric analysis, which was then checked using results from the literature. In future it will be interesting to add non-linearity to this parametric study, which could bring more realistic results.

Acknowledgements

The first author of this article is undertaking a PhD funded by a University of Strathclyde “Engineering The Future” studentship, for which we are grateful. We thank: Stella Pytharouli; CH2M Hill (now Jacobs), in particular, Iain Tromans, Guillermo Aldama Bustos, Manuela Davi and Angeliki Lessi Cheimariou; Andreas Nielsen; and Alessandro Tarantino for their help with various aspects of this study. Finally we thank an anonymous reviewer for their detailed comments on a previous version of this study.

Bibliography

- Abaqus, © 2002-2018 Dassault Systèmes - All rights reserved
- Aki, K., and K. L. Larner, (1970). Surface motion of a layered medium having an irregular interface due to incident plane SH waves, *Journal of Geophysics*, Res. 75, 933-954.
- Bard, P.-Y., and M. Bouchon, (1980,a). The Seismic Response of Sediment-Filled Valleys . Part 1. The Case of Incident SH Waves, *Bulletin of the Seismological Society of America*, 70 (4): 1263-1286.
- Bard, P.-Y., and M. Bouchon, (1985). The Two-Dimensional Resonance of Sediment-Filled Valleys.” *Bulletin of the Seismological Society of America*, 75(2):519–41.
- Bielak, J., J. Xu, and O. Ghattas, (1999). Earthquake Ground Motion and Structural Response in Alluvial Valleys, *Journal of Geotechnical and Geoenvironmental Engineering*, 125(5): 413-423
- Bonilla, L. F., P. Liu, and S. Nielsen, (2006). 1D and 2D linear and nonlinear site response in the Grenoble area, *Third International Symposium on the Effects of Surface Geology on Seismic Motion*, Grenoble ESG2006, Paper Number: 082/S02
- Chávez-García, F. J. and E. Faccioli, (2000). Complex Site Effects and Building Codes: Making the Leap, *Journal of Seismology*, 4(1):23–40.

- Delépine, N. and J. F. Semblat, (2012). Site Effects in an Alpine Valley with Strong Velocity Gradient : Interest and Limitations of the ‘classical’ BEM, *Soil Dynamics and Earthquake Engineering*, 38: 15–24.
- Emre, M., R. Hasal, and H. Iyisan, (2017). Basin Edge Effect on Seismic Ground Response : A Parametric Study for Duzce Basin Case, Turkey, *Arabian Journal for Science and Engineering*. <https://doi.org/10.1007/s13369-017-2971-7>
- Faccioli, E., M. Vanini, and L. Frassiné, (2002). Complex site effects in Earthquake ground motion, including topography, *12th European Conference of Earthquake Engineering*, Paper Reference: 844
- Furumoto, Y., Y. Saiki, and M. Sugito, (2006). On a simple modeling for seismic transfer function of ground on inclined based layer, *Third International Symposium on the effects of surface geology on seismic motion*, Grenoble, Paper number:098
- Garofalo, F., S. Foti, F. Hollender, P. Y. Bard, C. Cornou, B. R. Cox, M. Ohrnberger, et al., (2016). InterPACIFIC Project : Comparison of Invasive and Non-Invasive Methods for Seismic Site Characterization . Part I : Intra-Comparison of Surface Wave Methods, *Soil Dynamics and Earthquake Engineering* 82:222–40. (<http://dx.doi.org/10.1016/j.soildyn.2015.12.010>).
- Garofalo, F., S. Foti, F. Hollender, P. Y. Bard, C. Cornou, B. R. Cox, A. Dechamp, et al., (2016). InterPACIFIC Project : Comparison of Invasive and Non-Invasive Methods for Seismic Site Characterization . Part II : Inter-Comparison between Surface-Wave and Borehole Methods, *Soil Dynamics and Earthquake Engineering*, 82:241–54. (<http://dx.doi.org/10.1016/j.soildyn.2015.12.009>).

- Kottke, A. R., and E. M. Rathje, (2009). PACIFIC EARTHQUAKE ENGINEERING Technical Manual for Strata.”, PEER Report 2008/10
- Kramer, S. L., (1996). Geotechnical earthquake engineering, Prentice Hall, Upper Saddle River, N.J
- Luzi, L., F. Pacor, and R. Puglia,(2017). *Italian Accelerometric Archive v 2.3*” Istituto Nazionale di Geofisica e Vulcanologia, Dipartimento della Protezione Civile Nazionale. doi: 10.13127/ITACA.2.3"
- Makra, K., F. Gelagoti, O.-J. Ktenidou, and K. Pitilakis, (2012). Basin Effects in Seismic Design : Efficiency of Numerical Tools in Reproducing Complex Seismic Wavefields, 15th WCEE, Lisboa 2012
- Nielsen, A. H. (2006). Absorbing Boundary Conditions for Seismic Analysis in ABAQUS, *2006 ABAQUS Users' Conference*, 359–76.
- Nielsen, A. H. (2014). Towards a Complete Framework for Seismic Analysis in Abaqus, *Proceedings of the ICE - Engineering and Computational Mechanics*,167(1):3–12.
<http://www.icevirtuallibrary.com/content/article/10.1680/eacm.12.00004>).
- Park, D., and Y. M. A. Hashash, (2004). Estimation of Non-linear Seismic Site Effects for Deep Deposits of the Mississippi Embayment, Report, National Science Foundation Mid America Earthquake Center.
- Raptakis, D., K. Makra, A. Anastasios, and K. Pitilakis, (2004). Complex Site Effects in Thessaloniki (Greece): I. Soil Structure and Comparison of Observations with 1D Analysis, *Bulletin of Earthquake Engineering*, 2: 271-300.

- Rathje, E. M., A. R. Kottke, and W. L. Trent, (2010). Influence of Input Motion and Site Property Variabilities on Seismic Site Response Analysis, *Journal of Geotechnical and Geoenvironmental Engineering*, 136(4):607–19.
- Régnier J. et al. (2016). International Benchmark on Numerical Simulations for 1D , Nonlinear Site Response (PRENOLIN): Verification Phase Based on Canonical Cases, 106(5):2112–35.
- Sanchez-Sesma, F. J. and S. A. Velazquez, (1987). On the Seismic Response of a Dipping Layer, *Wave Motion* 9(5):387–91.
- Semblat, J. F., P. Dangla, M. Kham, and A. M. Duval, (2002). Seismic site effects for shallow and deep alluvial basins: in depth motion and focusing effect, *Soil Dynamics and Earthquake Engineering*, 22 (9-12):849-854
- Silva W.J., (1988). Soil response to earthquake ground motion, EPRI Report NP-5747, Electric Power Research Institute, Palo Alto, California.
- Thompson, E. M., L. G. Baise, Y. Tanaka, and R. E. Kayen, (2012). A Taxonomy of Site Response Complexity, *Soil Dynamics and Earthquake Engineering*, 41:32–43. Retrieved (<http://dx.doi.org/10.1016/j.soildyn.2012.04.005>).
- Vessia, G., S. Russo, and D. Lo Presti, (2011). A new proposal for the evaluation of the amplification coefficient due to valley effects in the simplified local seismic response analyses, *Rivista italiana geotecnica* 4/2011
- Vidale, J. and D. V. Helmberger, (1988). Elastic finite difference of the 1971 San Fernando earthquake, *Bulletin of the Seismological Society of America*, 78(1): 122-141

- Volpini, C., and J. Douglas, (2017). Examining the assumption of homogenous horizontal layers within seismic site response analysis , *PBD III Earthquake Geotechnical Engineering*, Vancouver, 144
- Volpini, C. and J. Douglas, A.H. Nielsen (2019). Guidance on Conducting 2D Linear Viscoelastic Site Response Analysis Using a Finite Element Code, *Journal of Earthquake Engineering*, DOI: 10.1080/13632469.2019.1568931

Chapter 4

4.1 Introduction

The fourth chapter of this thesis does not concern lateral uncertainties due to non-horizontal layers. Instead, I focus on another aspect of imperfect knowledge of site conditions and its influence on site effects. In particular, I study the uncertainties related to deep soil deposits.

A deep soil deposit in this context is one that does not reach high shear-wave velocity until a considerable depth. This situation is relatively common and the main issue associated with it is the lack of reliable *in situ* tests beyond a certain depth. In fact, most invasive/non-invasive tests give an accurate answer only in the shallow portion

of a soil deposit. Then, either for economic/technical reasons (for invasive tests) or due to intrinsic difficulties in interpreting the test results (non-uniqueness of the solution/loss of resolution along the vertical) (for non-invasive tests), the deep portion of a soil deposit cannot be defined with accuracy. In Figure 4.1 the generic scheme of different investigated volumes of invasive and non-invasive tests is displayed (Comina et al., 2011). Despite the volume of non-invasive tests appears to be much larger than the volume of invasive ones, it is well-known that this kind of tests has a lower resolution at greater depths.

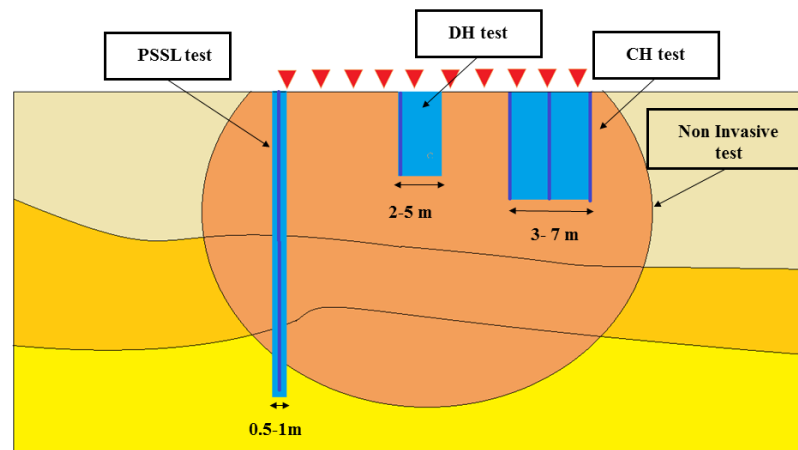


Figure 4.1. Investigated volumes of invasive and non-invasive test. In particular a suspension logging test (PSSL), down-hole test (DH), cross-hole test (CH) and a general volume referred to as non-invasive test

Connected to the influence on site response analysis of the generic uncertainties in a deep profile, there is also the uncertainty linked to the bedrock. Typically, an engineering bedrock should reach at least 800m/s from an engineering point of view. Most of the time, once found a value similar to this is reach the site investigation could be considered concluded. Several studies, however, focused their attention on the

portion of soil immediately after the seismic bedrock and they questioned whether this deep portion is important or not. Consider, as an example, the soil profile in figure 4.2. This profile is both a deep profile and it presents several uncertainties in the determination of its deep portion. Similar soil deposits will be investigated in the main body of the chapter. Boore and Joyner (1997) proposed a method to estimate the seismic shear-wave velocity as a function of depth for generic rock sites, from borehole data and studies of crustal velocities. This is one of the main approaches that tries to analyse this kind of profile that will be illustrated in the following section.

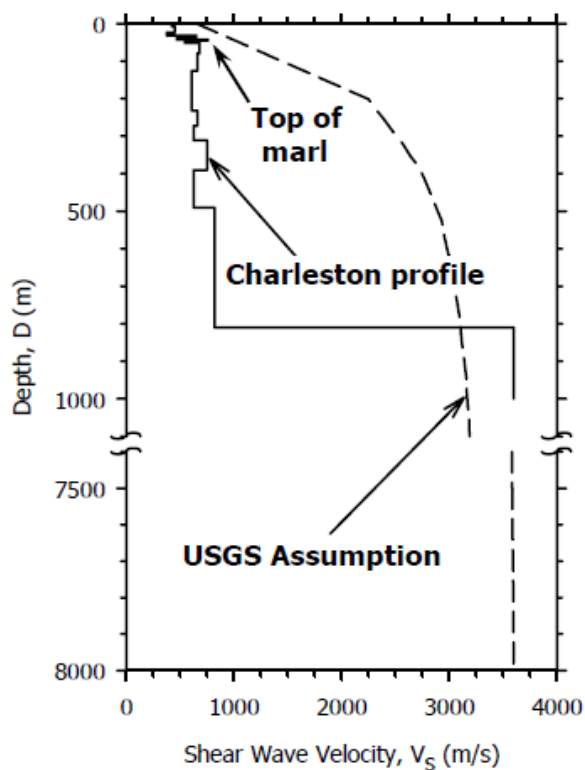


Figure 4.2. Example of a deep shear wave velocity profile (Charleston) from Chapman et al. (2006) showing a comparison between it and the general USGS assumption.

References

- Boore, D. M., and W. B. Joyner, "Site amplification for generic rock sites". *Bulletin of Seismological Society of America* 1997; 87:327-41
- Comina, C., Foti, S., Boiero, D., and L. Socco, (2011). Reliability of VS, 30 evaluation from surface-wave tests. *Journal of geotechnical and geoenvironmental engineering*, 137: 579-586.

4.2. The influence of limited knowledge of deep (>100m) shear-wave velocities on estimated site amplifications

Carolina Volpini & John Douglas

Department of Civil and Environmental Engineering,

University of Strathclyde, Glasgow (UK)

Abstract

Here we consider sites with a suspected deep (>100m) impedance contrast and high but unknown bedrock velocity (shear-wave velocities >1000m/s). Current standard methods using ground motion prediction equations to assess the input motion for such bedrock are problematic due to a lack of observed strong-motion data to constrain these equations. It would be helpful to have knowledge of velocities at greater depths for all records in current strong-motion databases. Because most often this information are lacking, should the deep impedance contrast be omitted when conducting site-response analyses (SRA) for these sites? And what are the implications of this choice? By not considering the deep impedance contrast we are potentially ignoring an important aspect of the site but one for which we have little constraint.

An approach to simulate the deep portion of the full profile, based on a large database of profiles, is proposed here. Firstly, sites are classified into three categories based on the depth to the bedrock (D). The portion of the profile below this interface is then removed and substituted with simulated profiles to account for uncertainty in the deep properties. The effect of these uncertainties on the results of SRA are then assessed. We find that the simulations are robust for profiles with $D \leq 100\text{m}$, whereas it is more difficult to constrain profiles with higher D , due to the lack of real measurements. Particular attention is given to the influence of softer layers within the soil deposit

(inversions of velocity). It is found that such layers often have little impact on the SRA. Finally, the results of the full SRA are compared to those obtained by the quarter wavelength method and we find that this approach should only be considered as a first step of a complete analysis.

4.2.1 Introduction

In Douglas et al. (2009) a framework for the inclusion of site effects in empirical ground-motion prediction equations (GMPEs) was proposed. They characterized stations through the quarter wavelength method (QWM) (Joyner et al., 1981) and assessed confidence limits on their shear-wave velocity (V_s) profiles and also the predicted amplification using the QWM. Their aim was to take advantage of all the possible information about a given site (e.g. surface geology, soil profile, in situ tests, near-surface velocity estimated from the topographic slope, depth to bedrock and crustal structure) to constrain the V_s profile down to a few kilometers, where it is appended to a model of the crustal velocity. One aspect they did not consider fully was the characterization of the deep portion of the profile. Does this deep portion of the profile have a strong impact on site amplification assessed through site response analysis (SRA)?

To study this question, it is useful to define various terms. We call the “deep portion of a profile” the part of profile that goes from engineering bedrock ($V_s=800\text{m/s}$) to a second bedrock (crustal velocity $\approx 3000\text{-}3500\text{m/s}$). These limits are chosen based on conventions in the engineering seismology community. Eurocode 8 (ENV 1998, hereinafter referred to as EC8) defines $V_{s,\text{bedrock}}$ as $V_s > 800\text{m/s}$. “Hard rock” is generally considered to have a V_s of 2000m/s to 3500m/s , which are similar to the velocities in the crust (e.g. Boore and Joyner, 1997; Laske et al., 2005; Tsang and Lam,

2007). It is common to have knowledge of the shallow V_s profiles thanks to invasive and non-invasive tests but not deeper and/or those materials with high V_s because of the difficulty in assessing their characteristics. V_s of the crustal structure at depths of 1km or more are determined using tomography of seismic wave travel times (e.g. Iyer and Hirahara, 1993; Kennett, 2002).

Techniques to measure near-surface V_s can be split into two categories. Firstly, invasive tests, which are generally considered more reliable because they are based on the interpretation of local measurements of shear wave travel times, giving a good resolution as a function of depth. The main drawback is that they require, at least, one borehole, making them quite expensive for obtaining deep information, in contrast to non-invasive technique. Examples of these measurements are cross-hole, down-hole and PS suspension logging. Secondly, non-invasive tests, also called surface-wave methods, are commonly employed because they are often cheaper as they do not need a borehole. Indeed, they are based on the analysis of surface-wave propagation and the dispersive characteristic of the site. In a layered medium (such as a soil deposit), surface waves propagation is governed by geometric dispersion. It is a multimodal phenomenon: at each frequency modes of vibration can exist and each one is characterized by its own propagation velocity (Aki and Richards, 1980). Non-invasive tests require usually little effort for field acquisition but the processing and inversion of the experimental data are much more computationally intensive than those required for invasive methods. The resolution is also not generally as good as for the invasive methods. Thanks to this kind of tests, it is possible to measure V_s at greater depths than is generally achieved through invasive tests. Non-invasive techniques fall into two groups: active (using an actual source generating the seismic waves) and passive (seismic waves are generated by ambient noise) methods. Examples of these

techniques are spectral analysis of surface waves, frequency wave-number spectrum method and multichannel analysis of surface waves (all active methods) and noise analysis of surface waves (a passive method). Another commonly-used passive method, which estimates the fundamental frequency, is the horizontal to vertical spectral ratio (HVSR) (Nakamura, 1989) technique. The main applications of this technique are the determination of the fundamental frequency of subsurface resonance as well as to provide a preliminary idea of the stratigraphy of the subsoil.

Despite all these techniques it is difficult to estimate the V_s of the central portion (roughly $>50\text{m}$ and $<1\text{km}$) of a deep profile (Passeri et al., 2018). That is why, most of the time, this portion is neglected and a site response analysis is performed using just a shallow profile (Bielak et al., 1999; Lanzo et al., 2011). The aim of this work is to understand what we miss when conducting a SRA if we do not have detailed information about the deep velocities. After a review of some relevant literature we develop a procedure to simulate V_s at depth ($>50\text{m}$). Then, we perform SRA for these simulated profiles to understand the importance of this portion of the profile.

4.2.2 Literature review

When estimating seismic site amplification several uncertainties must be taken into account. Some of them come from the lack knowledge about the mechanical characteristics of the soil, some from the topographic and stratigraphic uncertainties related to the site and some from numerical simplifications made to reproduce reality in a tractable way.

In this work, we pay particular attention to imperfect knowledge of V_s profiles and its effects on SRA. In this context, the epistemic uncertainty of the characteristics of each geophysical method on the resulting V_s profile was recently highlighted by Passeri et al. (2018) by providing examples for each seismic in-situ test. Another interesting study focused on the uncertainties associated with the measurement of V_s , earthquake magnitude and source-to-site distance is by Moss (2009) who noted that these uncertainties are often neglected when deriving GMPE. He presented a method to quantify the uncertainties and to consider them when developing GMPEs. Seyhan et al. (2014) improve the site database of NGA-West2 by providing and improving the documentation and consistency of site descriptors used to estimate $V_{s,30}$ (the average V_s to a depth of 30m) when actual measurements are not available. These estimators are surface geology, topographic slope, and geotechnical and geomorphic categories. Thanks to this approach, they found a way to minimize the bias and dispersion assign the best $V_{s,30}$ for each site.

Considering more closely our study, the first aspect that should be considered is the concept of deep deposit profiles. By this we mean a deposit with a V_s profile that does not reach a bedrock value until a considerable depth (>50m). The importance of the knowledge of deep V_s was discussed in Ohta et al. (1980), where they conducted measurements in deep soil deposits using a sophisticated down-hole method. They underlined the engineering importance of these measurements when calculating the amplification of seismic waves from the bedrock. Their work highlighted the large effect of deep soils on long-period ground motions. Similarly, Hashash et al. (2001) studied the uncertainties that a deep deposit can bring to SRA. They focused on the New Madrid Seismic Zone (NMSZ), which is the most seismically active zone in the eastern USA. They conducted a non-linear analysis to take into account the effect of

large confining pressures on the strain-dependent modulus degradation and damping of the soil. In their analysis, they considered a 1000m soil column, which is typical for Memphis within the NMSZ. They observed that significant high frequency components are propagated through such deposits. Moreover, the propagation of seismic waves through very deep deposits results in the development of large long-period ground motion. Boore and Joyner (1991) focus on the estimation of ground motion at typical deep-soil sites in North America. They modified their stochastic model for hard-rock ground motions to account for the effects of deep soils. They created a generic model of Vs and attenuation for these deep soil sites and then they proposed a filter modifying the stochastic model of Boore and Atkinson (1987) to obtain GMPEs for various ground-motion parameters.

A typical profile for Memphis (Gomberg et al., 2003; Cramer et al., 2004) is a perfect example of a deep soil deposit (Figure 4.2.1) considering that its seismic bedrock is located at more than 400m. As discussed above it is difficult and expensive to have detailed measurements to this depth. A “dark zone” can be identified below a depth of about 400m where little information is available. At great depths (>2km) the crustal velocity from seismic tomography is generally quite well known. In the case of Memphis the Vs profile features a velocity inversion. One of the goal of our study is to investigate the impact an inversion at these depths can have.

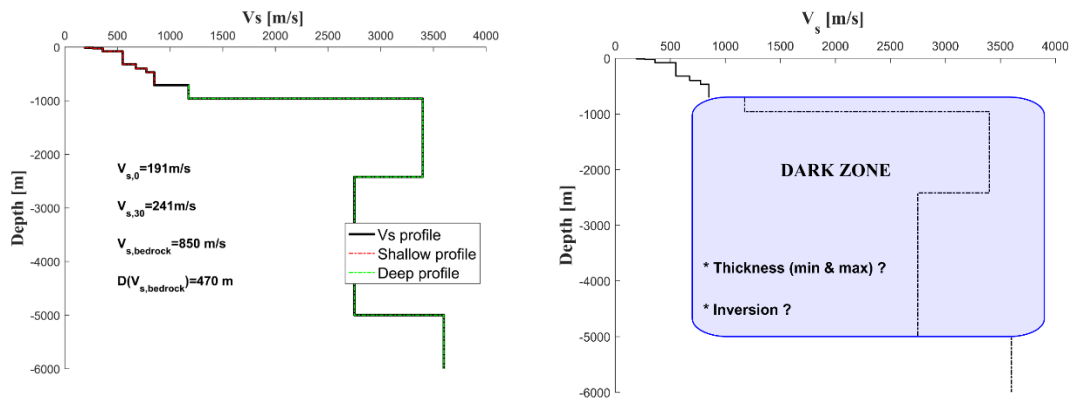


Figure 4.2.1: Memphis profile from Gomberg et al. (2003) and Cramer et al. (2004). Figure modified from Volpini and Douglas (2019) (see Appendix 2)

Using the techniques discussed above it is impossible to have a perfect knowledge of the whole Vs profile down to the crustal velocity. Based on the current literature it is not clear whether only the well-known shallow part of the profile should be considered or if the poorly-constrained deeper portion should also be included within the SRA. The QWM (Joyner et al., 1981), which is the main technique used in Douglas et al. (2009), could be useful in such situations because it only uses average Vs down to a depth equal to the quarter wavelength of seismic waves of the considered frequency. Therefore, it is less sensitive to the unknown details of the profile. Another option would be a full SRA considering a combination of randomized profiles around the central one. These methods are described in the following sections.

4.2.2.1 Quarter-wavelength method

In the QWM (Joyner et al., 1981) the amplification, A , is given by the square root of the ratio between the seismic impedance (velocity times density) averaged over a depth

corresponding to a quarter wavelength and the seismic impedance at the depth of the source, i.e.:

$$A[F(z)] = \sqrt{\frac{\rho_s V_s}{\bar{\rho}_s V_{s,average}(z)}} \quad [28]$$

where: $\rho_s V_s$ are the crustal density and the crustal shear-wave velocity respectively and $V_{s,average}(z)$ is the average velocity to depth z and it given by $z/S_{tt}(z)$ and the frequency corresponding to the depth, $f(z)$, equals $1/[4S_{tt}(z)]$.

To account for near-surface attenuation we need to multiply the $A[F(z)]$ by $\exp(-\kappa\pi f)$, where κ is the high-frequency attenuation parameter introduced by Anderson and Hough (1984) and f is the frequency. According to Anderson and Hough (1984), above a certain frequency the acceleration spectrum generally decays exponentially with frequency. This parameter is a subject of much recent research (e.g. Ktenidou et al., 2014) but it is not considered further here because our focus is on site amplification not attenuation.

The QWM can provide a first-order estimate of the site amplification (e.g. Figure 4.2.2). Cotton et al. (2006) present equations to provide a generic V_s profile given a value of $V_{s,30}$. In their formulation they used the V_s profiles of Boore and Joyner (1997) as end members and then interpolate between them.

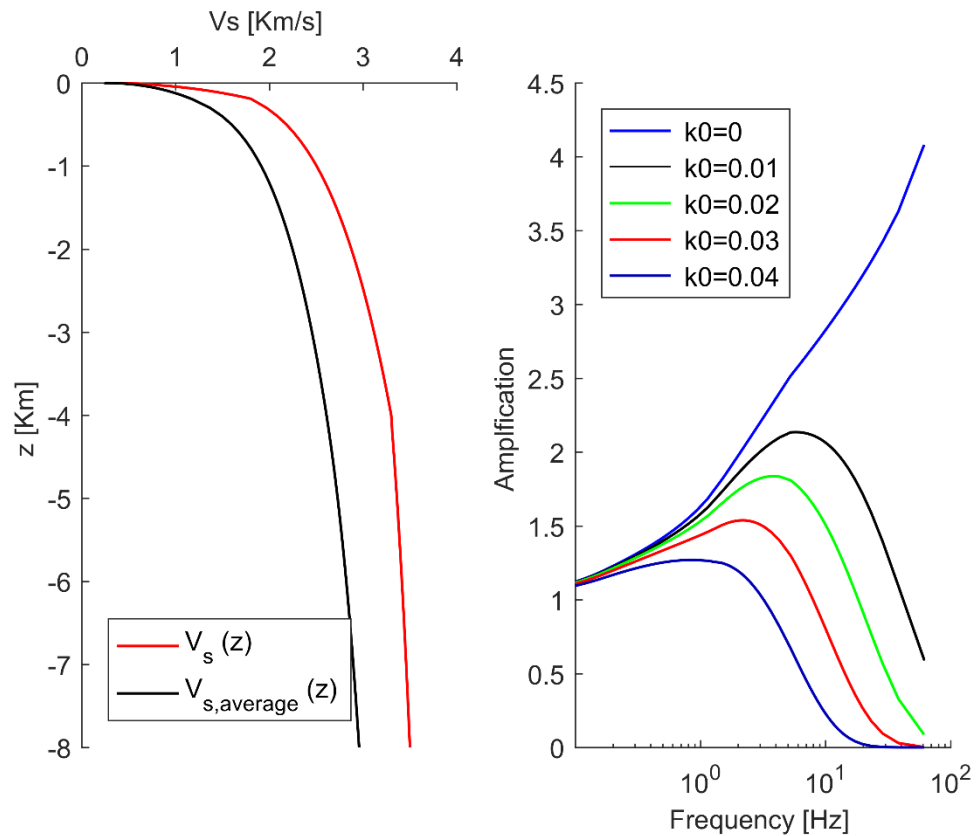


Figure 4.2.2: Example of QWM output. Left: the generic rock V_s profile for California (Boore and Joyner, 1997); Right: amplification with various levels of attenuation modelled using κ .

The main problem of this method is that it gives just a general idea of the amplification we expect, which is, at the same time, its strength. In the absence of information on the deep portion of V_s profiles, this method appears to estimate a reliable amplification as it is insensitive to uncertainties. For example, let us suppose there is an inversion of velocity in the deep portion of profile. Considering that the QWM considers an average V_s profile the influence of the inversion is partially lost.

4.2.2.2 Site response analysis

We define SRA as the sum of the modification/alteration of the seismic waves by variations in the near-surface V_s . SRA works as a filter that amplifies the motion at certain frequency and deamplifies it at others. A full SRA requires knowledge of the V_s profile, mechanical characteristics of the soil and stratigraphy/topography of the

deposit. It is usually common to start with a linear elastic analysis and then to consider more complex soil behavior (e.g. non-linear response). In this work, since we are dealing with deposits where we know little, it is not useful to perform complex (nonlinear) analyses. Viscous linear-elastic analyses will be performed here. These require the Vs profile, the density of each layer and the ratio of viscous damping.

Assuming a single layer of soil of thickness H with an input as an outcropping (bedrock) motion. The amplitudes associated with the resonance frequencies at the ground surface are given by this equation:

$$A_{r,n} = \frac{1}{I_z + (2n - 1) \frac{\pi}{2} q} \quad n = 1, 2, \dots, \infty \quad [29]$$

where q is the damping value, which characterizes the reduction in wave energy and I_z is the impedance contrast ratio. According to this equation, the maximum amplitude depends on the value of damping and on the impedance contrast ratio, whereas resonance frequencies depend on the Vs and H:

$$\omega_n \approx \frac{V_s}{H} \left(\frac{\pi}{2} + n\pi \right) \quad n = 1, 2, \dots, \infty \quad [30]$$

From this equation it is clear that knowing the Vs profile and the related thickness of each layer is fundamental to perform a consistent analysis. That is why it is not clear whether it is worthwhile to use this method when Vs and H are uncertain.

To account for uncertainty in the deep portion of a Vs profile, randomization of the profile has been proposed. The theory was firstly developed by Toro (1995) based on a database of 557 real Vs profiles. From these profiles, he derived a number of parameters for Geomatrix and USGS classifications using a maximum-likelihood procedure to constrain the randomized profiles. This procedure is implemented in two of the one-dimensional most known software for site response analysis (STRATA, Kottke and Rathje, 2013; Deepsoil, Hashash et al., 2016). The main problem with this approach is that the database used to derive the parameters was composed mainly of shallow profiles. Hence, it is not clear it can be used to constrain a deep profile. Passeri et al. (2018) developed an alternative method but also in this case they consider shallow profiles as the examples they have taken into account are: Mirandola (Italy) (InterPacific Project, Garofalo et al., 2016a-b) and the Seohae Grand Bridge site (South Korea) (Kim et al., 2013a). Montalva et al. (2010) develop a random field model for Vs profiles when lacking information, particularly when the only available information is a generic site classification. They compare their approach with an existing one in terms of the statistics of the Vs random field and in terms of the predicted site response.

Douglas et al. (2009) considered various data capable of constraining the Vs and density profiles down to a few kilometers (soil profile, crustal structure, generic Vs profiles, near-surface geology, microtremor measurements, site class and in situ invasive and non-invasive tests). They define a number of parameters to constrain the shallow part of the soil profile as they have lots of information from the database. Then, they were forced to reduce the number of parameters to create the central portion of the profiles (from D, depth of the bedrock, down to few kilometers) because of a lack of real profiles with measurements for this depth range (Figure 4.2.3). From their study, it is clear that the portion with the least information is the one identified by the

dashed line, $50\text{m} < H < 500\text{m}$ (the “dark zone” referred to above). For our study we have expanded their database to include more profiles with measurements in this “dark zone”.

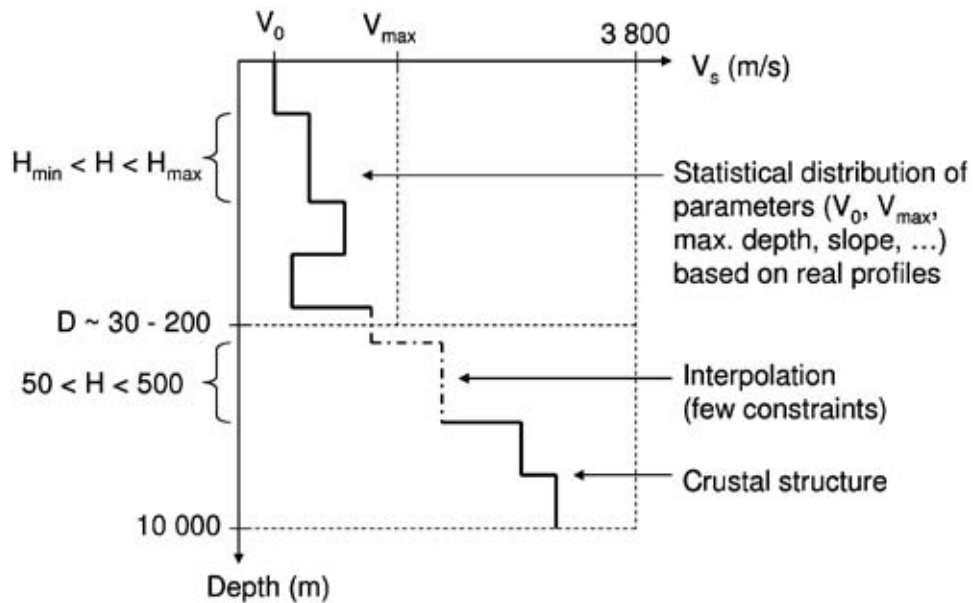


Figure 4.2.3: Procedure of Douglas et al. (2009) to generate V_s profiles. They identify the most uncertain zone by a dashed line [from Douglas et al. (2009)]

4.2.3 Database

A database of 1102 real shear-wave velocity profiles has been compiled for this study. It is composed of the 857 profiles from Douglas et al. (2009) (see that reference for details of these profiles) plus 245 profiles kindly provided by INGV from the Engineering Strong Motion database (Luzi et al., 2016). Figure 4.2.6 displays our classification scheme. The first separation is whether the profile features a softer layer between two surrounding layers (a velocity inversion) or not. The second separation concerns the the maximum V_s attained in the profile: the first category includes those profiles reaching a V_s of 800m/s and the second those, which have not (these are not

considered further in our analysis). This limit comes from an engineering classification of bedrock (e.g. Pitilakis et al., 2018), below which the V_s should not decrease.

1102 V_s Profiles

- Does the profile reach a $V_s \geq 800$ m/s?
- Does the profile present a softer layer? If No it will be considered
- If yes, where is the softer layer located?

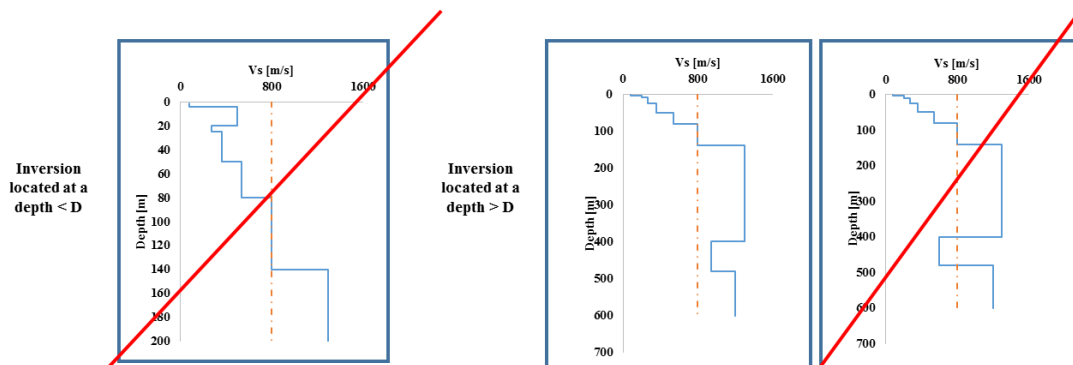


Figure 4.2.6: Description of the steps to come up with the final database.

4.2.4 Method

The method developed comprises the following steps.

- 1- Compile the database of 1,102 real shear-wave velocity profiles (see Section 3);
- 2- Determine the type of information needed to constraint the shape of a deep profile, as figure 4.2.7 displays:

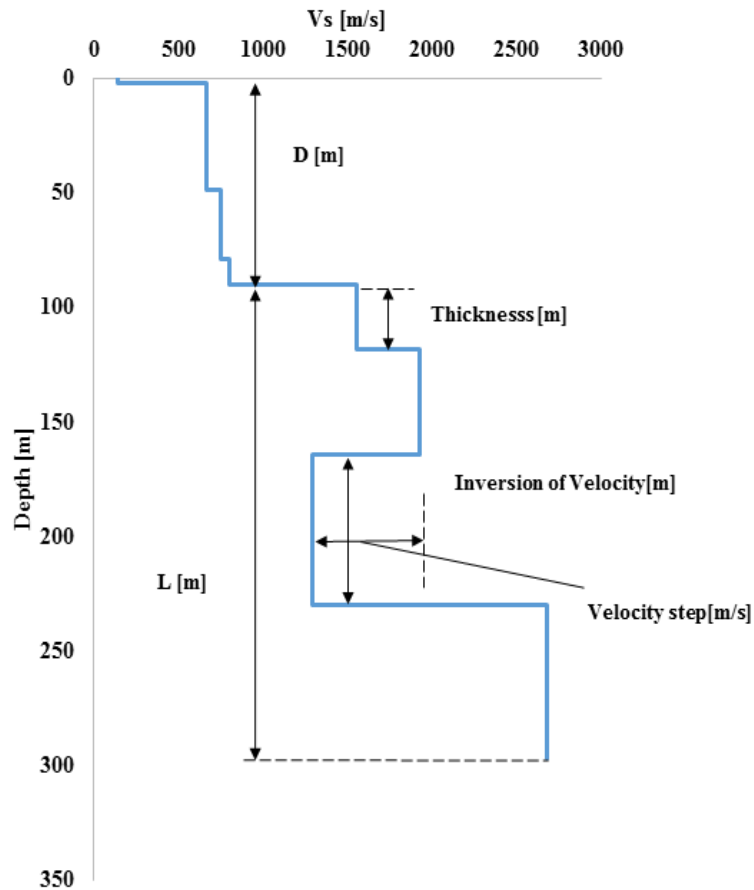


Figure 4.2.7: Scheme of the information taken from database needed to build randomized profiles

- i) Depth of bedrock (D), i.e. the depth where V_s reaches 800m/s. We consider three categories:
 - ◆ $D \leq 50$ m;
 - ◆ $50\text{m} < D \leq 100\text{m}$; and
 - ◆ $D > 100\text{m}$.
- ii) Length (L) of the profile after D ;
- iii) Thickness of the layers along L ;

iv) Presence of velocity inversion or softer layers. Inside this parameter, we search for thickness of the inverted layer, thickness above the inverted layer and the velocity step:

$$Velocity_{step} = V_{S_{layer_sup}} - V_{S_{inverted_layer}} \quad [31]$$

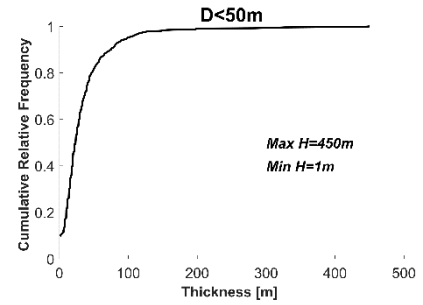
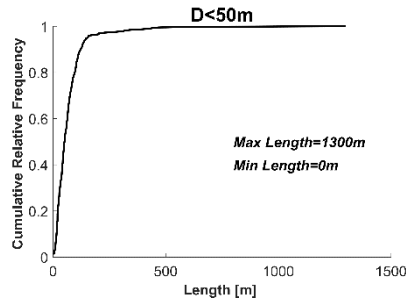
- 3- Find a number of profiles that are representative for our study;
- 4- Select a real reference profile where all this information is available as a basis for comparison;
- 5- Simulate random deep profiles on the basis of the database information;
- 6- Perform a SRA, using Seismo-soil software (Asimaki and Shi, 2017; see Appendix 4) to highlight the importance of the deep portion of the Vs profile;
- 7- Compare the SRA for the real reference profile and those simulated; and, finally,
- 8- Compare the SRA and QWM, which is the main method used in Douglas et al (2009).

Figures 4.2.8 displays the information determined in step 2 in terms of cumulative relative frequency plots.

Profiles:

$D \leq 50m$

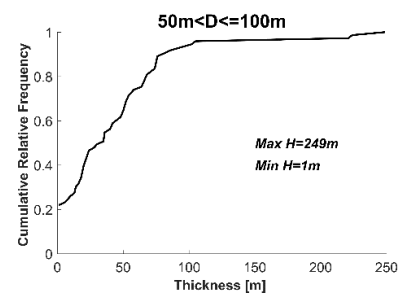
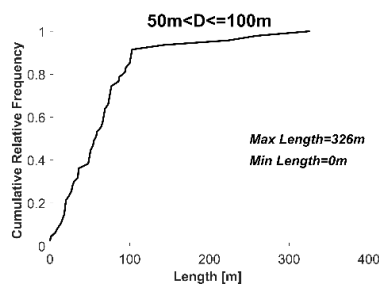
**Total Number
of samples: 373**



Profiles:

$50m < D \leq 100m$

**Total Number
of samples: 47**



Profiles:

$D > 100m$

**Total Number
of samples: 49**

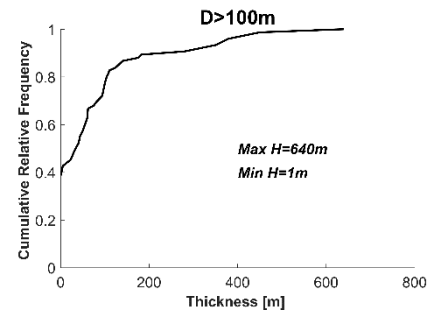
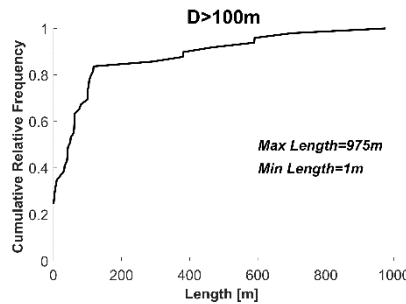


Figure 4.2.8a: Cumulative relative frequency plots of length after D and thickness of the layers. Top: $D \leq 50m$ profiles, center: $50m < D \leq 100m$, bottom: $D > 100m$.

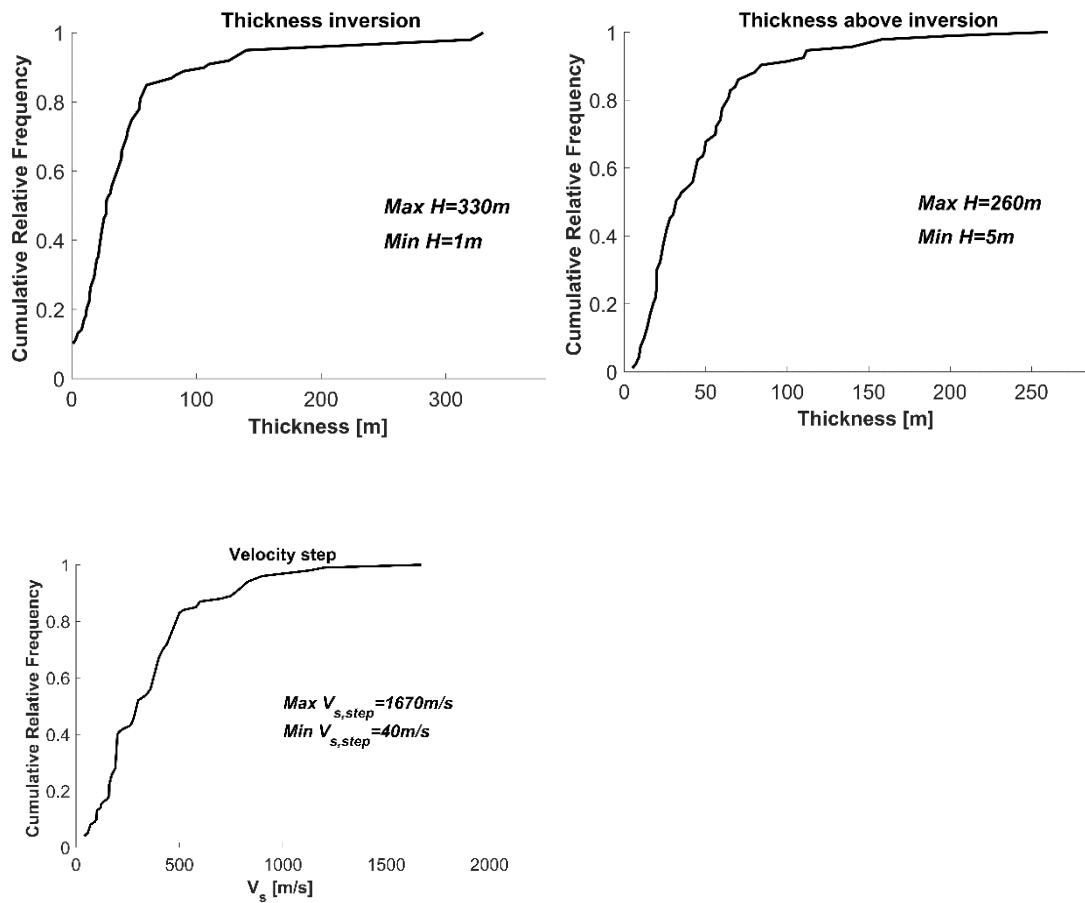


Figure 4.2.8b. Example for $D > 100m$. Top left: Thickness of velocity inversion; top right: Thickness of the top layer; bottom: velocity step in the inversion.

To test the influence of the deep portion of the V_s profile on the results of a SRA, we consider a selection of real profiles. Table 4.2.1 represents the relevant values for all the profiles (Figures 4.2.1 and 4.2.9) we consider. We should also mention that for all the profiles we chose a damping of 1%.

Shallow Profile (from surface to D)					
	D ≤ 50m (254)	D ≤ 50m (352)	50m < D ≤ 100m (1)	50m < D ≤ 100m (2)	D>100m (Memphis)
V ₀ [m/s]	540	80	140	340	191
V _{s,30} [m/s]	1053	161	486	488	241
Depth to the bedrock [m]	2.5	48	80	30	400
H min before D [m]	2.5	3	3	12	12
H max before D [m]	2.5	16	30	18	240
V _{bedrock} [m/s]	836	800	750	870	775
Deep profile (from D to Hard Bedrock)					
H min [m]	5	30	40	30	70
H max [m]	10	100	100	150	2580
Inversion Characteristics					
Velocity, step [m/s]	321	630	500	500	650
Thickness of the inversion [m]	5	100	40	150	2580
Thickness above the inversion [m]	10	32	100	30	1460

Table 4.2.1. Parameters defining the characteristics of the Vs profiles for the considered sites.

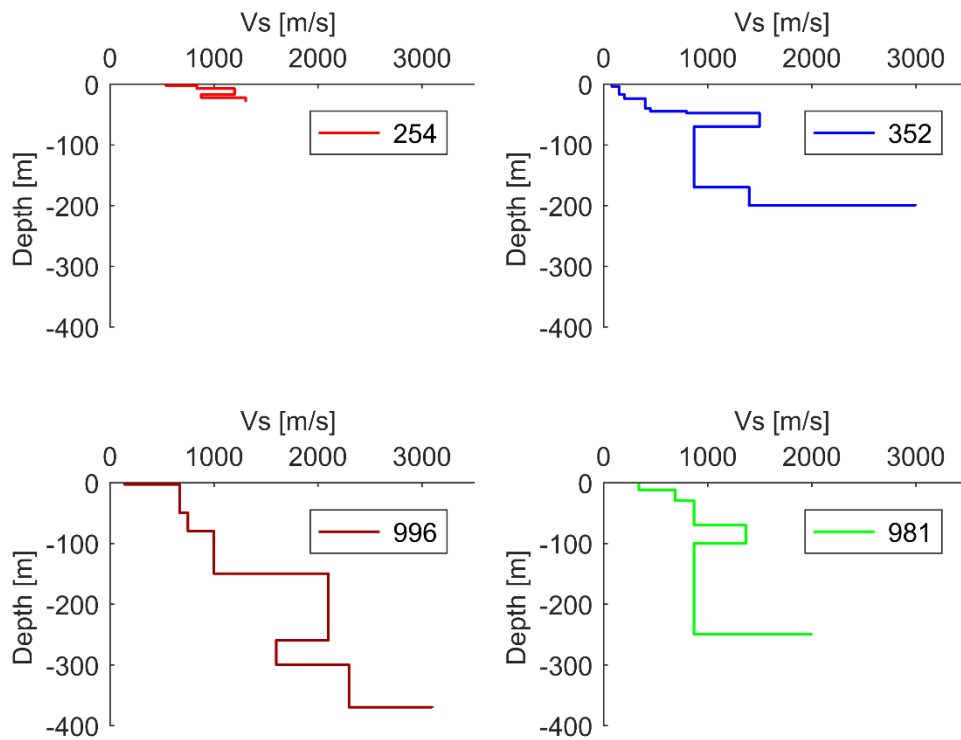


Figure 4.2.9. Vs profiles for considered sites.

Top: $D \leq 50m$, profiles 254 and 352 from the database.

Bottom: $50m < D \leq 100m$, profiles 996 and 981 from the database.

To compare the simulated and real Vs profiles and the results of SRA using these profiles the following steps are followed.

- 1- Remove the deep portion (depths $> D$) of the Vs profile because for most sites this is unknown;
- 2- Define the number of layers to create (we use five for the following calculations);
- 3- Define the starting value of velocity, which corresponds to $V_{s,bedrock}$, and the crustal velocity;
- 4- Consider various types of velocity inversion:

4a- Type 1: Velocity does not decrease below $V_{s,bedrock}$. This imposes the least restriction.

4b- Type 2: Like type 1 but also respecting the cumulative relative frequency plot for velocity step;

4c- Type 3: Like type 2 but also respecting cumulative relative frequency plots for the thicknesses of the inverted layer and the layer above. This is the most restrictive.

4.2.5. Results

4.2.5.1 First profile with $50m < D \leq 100m$

Many profiles belong to the category $50m < D \leq 100m$. Figure 8 displays the randomly chosen profile (number 996) and Table 4.2.1 reports its key characteristics. Figure 4.2.10 shows the simulated V_s profiles using the randomization procedure described above assuming the three types of inversion as well as the results of the SRA. It is interesting to notice that in this case, the original profile is well represented by the mean and its confidence limits. This is because the length of the original profile matches the database available. As shown below this is not the case for Memphis profile (see section 4.2.5.3).

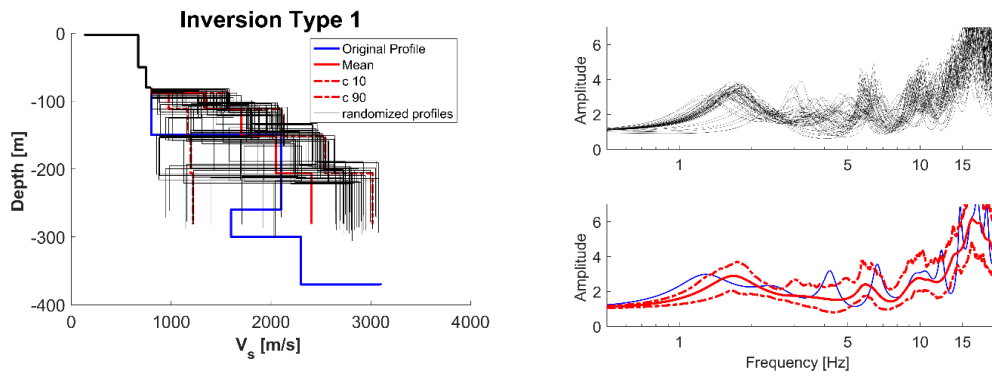


Figure 4.2.10a. Randomized profiles assuming an inversion of type 1 and the resulting amplifications.

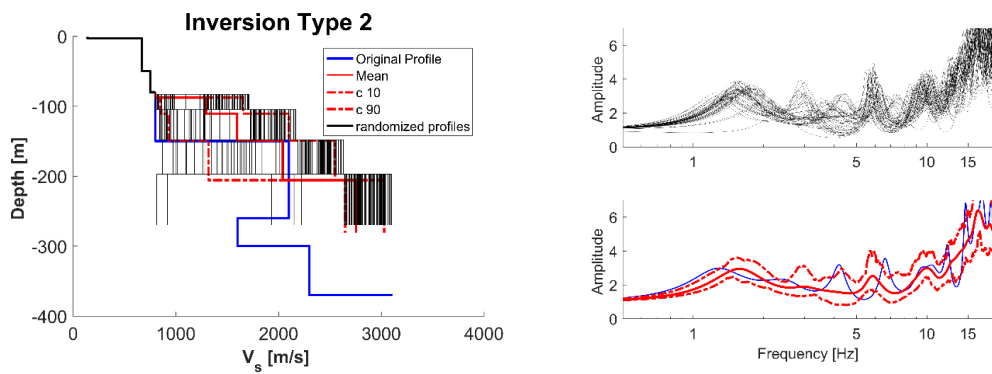


Figure 4.2.10b. Randomized profiles assuming an inversion of type 2 and the resulting amplifications.

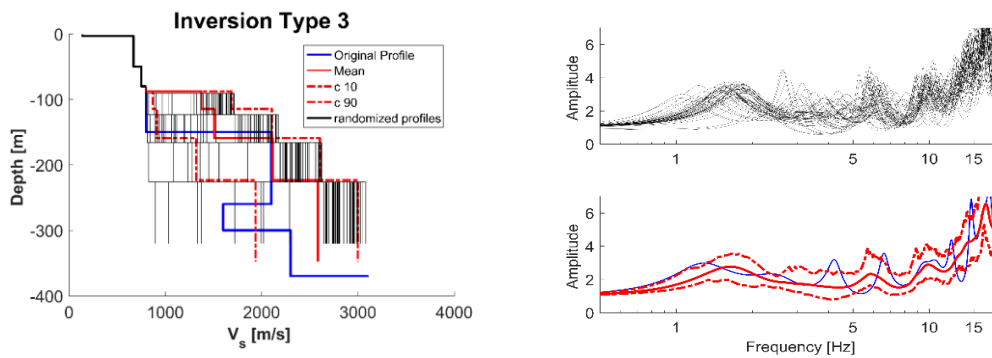


Figure 4.2.10c. Randomized profiles assuming an inversion of type 3 and the resulting amplifications.

From Figure 4.2.10 it can be seen that the sensitivity of the results to the type of inversion is small. Therefore, it appears that when we lack knowledge we could simply assume the minimal constraints (i.e. inversion type 1). This hypothesis is checked in the next section for another profile. It is also important to underline the shape of these simulated profiles. Most of these profiles lie in the upper portion of the confidence limits because one of the constraints removes the profiles that feature velocities below $V_{s,bedrock}$ due to the definition of bedrock assumed here (Pitilakis et al., 2018).

4.2.5.2 Second profile with $50\text{m} < D \leq 100\text{m}$

The second profile considered is number 991 (Figure 4.2.9, Table 4.2.1). Figure 4.2.11 displays the randomized profiles and the calculated site amplifications.

Inversions of type 2 are not considered as the main differences in the results were between assuming types 1 or 3.

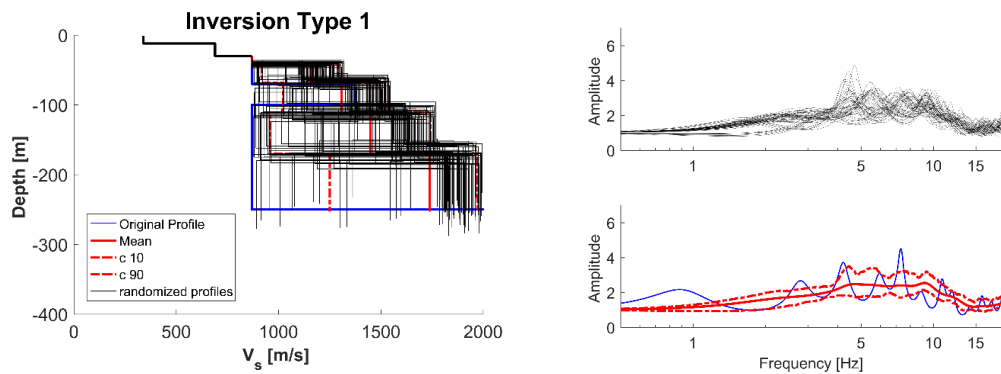


Figure 4.2.11a. Randomized profiles assuming an inversion of type 1 and the resulting amplifications.

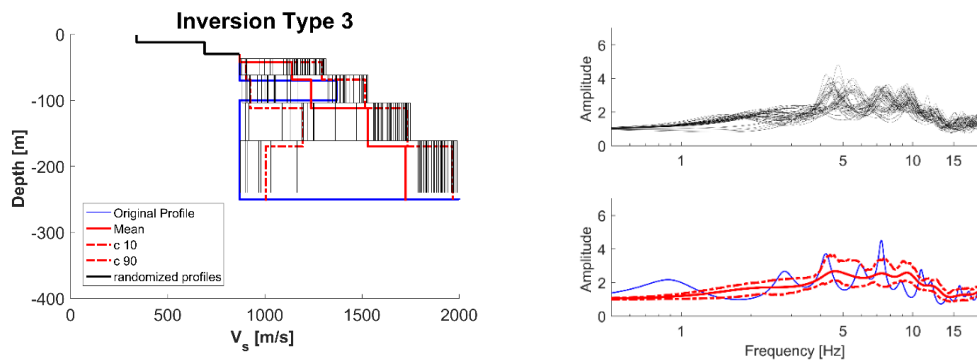


Figure 4.2.11b. Randomized profiles assuming an inversion of type 3 and the resulting amplifications.

Figure 4.2.11 shows that there is very little difference between the site amplifications computed assuming inversions of types 1 or 3, confirming the observation above. Velocity inversions occurring in the deep portion of a V_s profile have little impact on the computed site amplification.

4.2.5.3 Memphis profile with $D > 100\text{m}$

We next consider the very deep Memphis profile (Figure 4.2.9, Table 4.2.1). Figure 4.2.12 displays the randomized profiles and the calculated site amplifications. We can clearly see the influence of the constraints in inversion type 3 where the dispersion around the main curve is smaller. This is clearly visible in the low frequency range ($< 1\text{Hz}$). Despite this, neither inversions of type 1 nor type 3 can catch the fundamental frequency very well. We can clearly see this in the lower part of Figure 4.2.12a. This mismatch is due to the database itself: among the profiles with $D > 100\text{m}$ there are not many profiles with length comparable to the Memphis profile. Consequently, there is not much information about the deep layers, their thickness and their velocities with which to constrain the simulated profiles. In the absence of a large database, it is best to assume an inversion of type 1 because this does not generally lead to large errors. It

is clear that the more we know about the characteristics of deep profiles the better we can constrain the simulations.

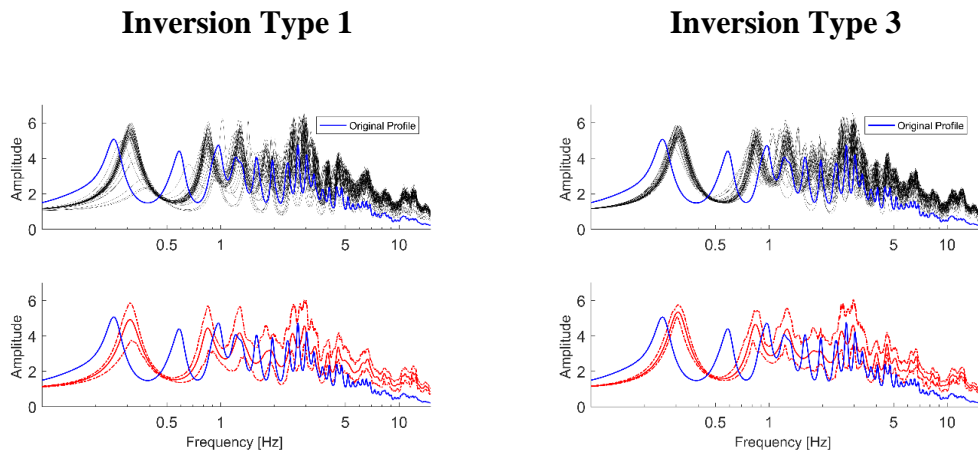


Figure 4.2.12a. Amplification function assuming inversions of type 1 (left) and type 3 (right).

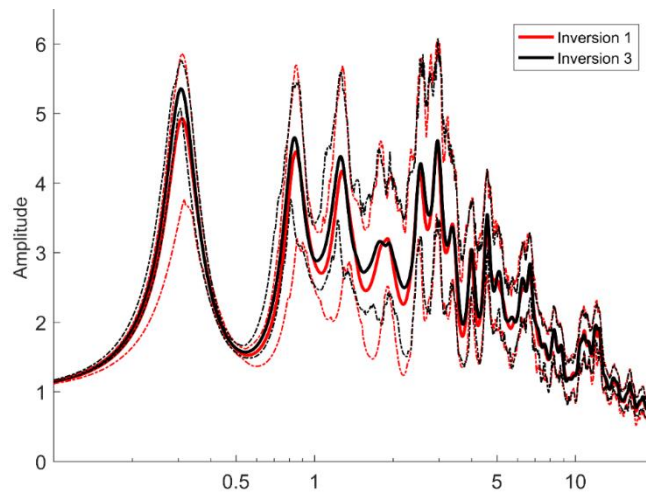


Figure 4.2.12b. Comparison of the results of the two methods, where the dashed lines indicate the 95% confidence limits.

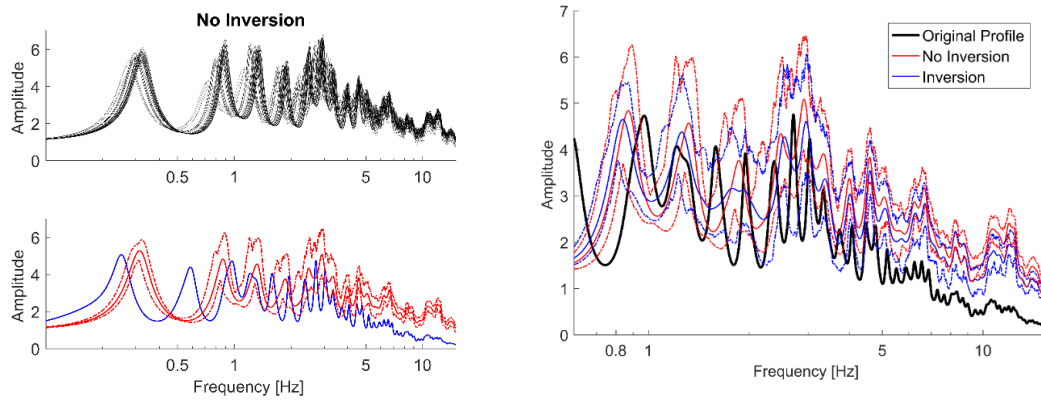


Figure 4.2.12c. Left: Profiles with no inversion of velocity; Right: Amplification functions of the original profile and the mean +/- confidence limits of the randomized profiles.

A comparison between the amplification from randomized profiles when an inversion is assumed for the Memphis profile and when it is not are displayed in Figure 4.2.12c. In reality the Memphis profiles contains a velocity inversion in its deep portion but Figure 4.2.12c shows that neglecting this inversion does not change the computed amplification by much. The main difference between the two analyses is mainly in the frequency range 1-5 Hz and that often the confidence limits of the computed amplification functions contain the amplification function for the original profile.

4.2.5.4 $D \leq 50\text{m}$ profile

In this section the effect of an inversion in the first 50m is examined. We have already seen that the influence of softer layers at great depths is not very important and can often be neglected if we do not have sufficient information. What if this softer layer is located at shallower depths? To answer this question two profiles with $D \leq 50\text{m}$ are considered: profile 254 (a very shallow profile) and profile 352 (a deeper profile)

(Figure 4.2.9, Table 4.2.1). The results of randomizing the lower parts of these profiles assuming an inversion type 3 are shown in Figure 4.2.13.

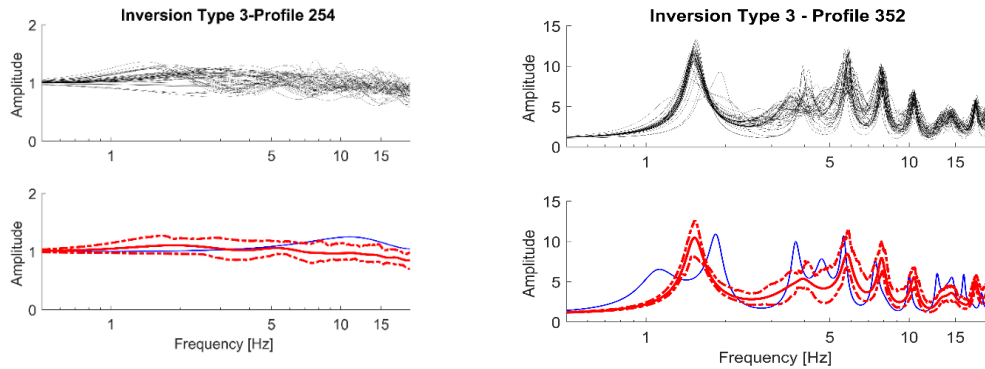


Figure 4.2.13. Amplification function assuming an inversion of type 3 for both profiles

We can observe a significant difference between the two. Profile 254 is particularly stiff while profile 352, despite its shallow D, is softer, which leads to a larger uncertainty on the amplification. Both of the profiles present an inversion but characteristics of the second profile mean that this inversion has a larger impact.

4.2.5.5 Influence of thickness and velocity step on the inversion

It appears to be interesting to check the influence of the velocity step and the thickness of the inversion on the computed amplification. Figure 4.2.14 displays various profiles that have been considered to investigate whether the thickness of the inversion or the size of the velocity step has a greater influence.

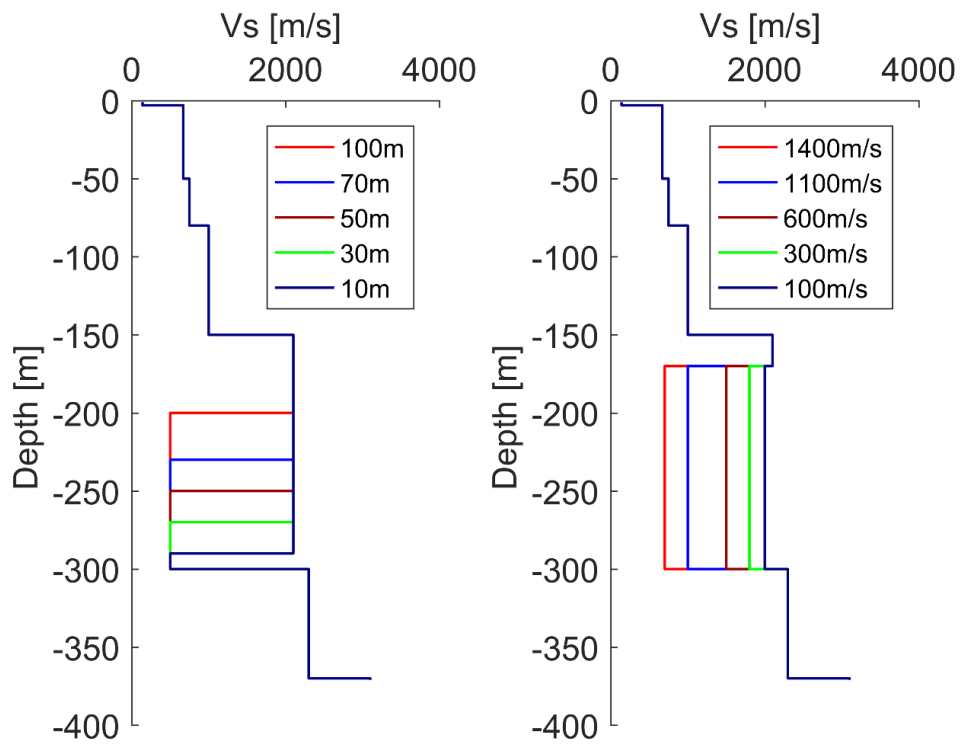


Figure 4.2.14. Left: Original Vs profile and inversions of different thicknesses;
 Right: Original Vs profile and inversions with different velocity steps.

Results for these profiles are displayed in Figure 4.2.15a. We notice that a large velocity step has a greater impact on the result than having a very thick inversion. However, considering smaller velocity steps of 600m/s to 100m/s (all with a thickness of 130m) does not change greatly the amplification function whereas changing the thickness of the inversion slightly does gradually shift and decrease the amplitude of the fundamental mode.

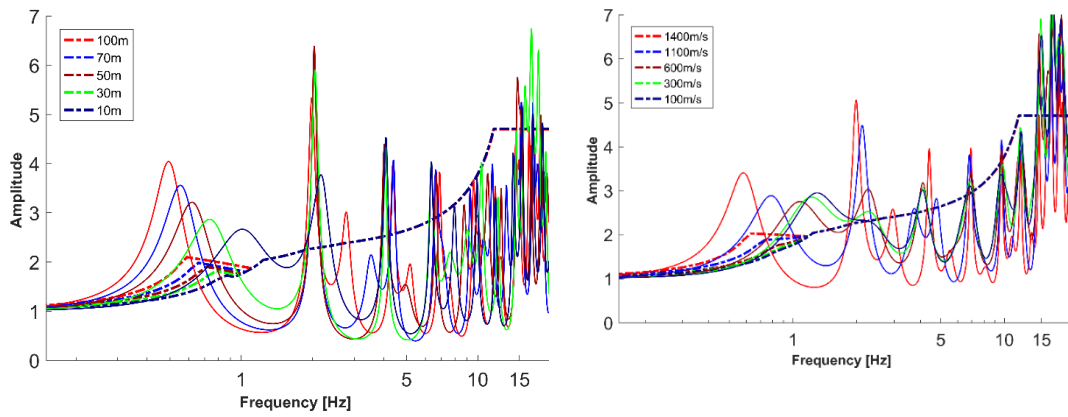


Figure 4.2.15a. Left: Comparison between results of QWM and SRA for different thicknesses. Right: Comparison between the results of QWM and SRA for different velocity steps. In both cases, the profiles refer to figure 4.2.14

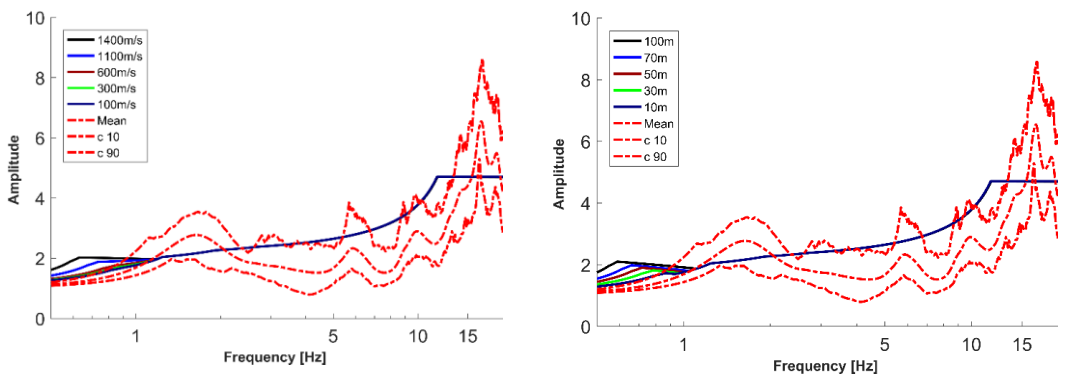


Figure 4.2.15b. Left: Results of QWM for different velocity steps; Right: Results of QWM for different inversion thicknesses. In both cases, QWM is performed using the V_s profiles from figure 4.2.14, whereas the red curves are the results of the randomized procedure proposed here.

Figure 4.2.15b shows using the QWM gives similar results for all inversions studied, i.e. it is not capable of catching the influence of the softer layers within the profile unlike SRA. QWM can give a first order approximation of the amplification but it is often best to proceed with a full SRA.

4.2.6 NALS station

The final example is the NALS station on shallow relatively soft sedimentary layers in Nice. The V_s profile for this site also presents an inversion starting from 24m. Douglas et al., (2009) compared the site amplification curves for this station considering: a) all available data (near-surface profile, depth to bedrock, and crustal structure); b) instead of using the full near-surface profile V_{s30} and V_0 have been used; c) not imposing the depth to bedrock as a constraint and d) only using V_{s30} and crustal structure as constraints.

We have generated random profiles assuming inversions of type 1 and type 3. Both the original shallow profile transfer function and the deep profile (developed in Douglas et al., 2009) transfer function together with our results are plotted in Figure 4.2.16. We should keep in mind that the Douglas et al. (2009) profile is not a measured profile but more an ideal one obtained from the shallow profile and by imposing a series of constraints. This is why we have chosen to plot both the original shallow transfer function, which may be the only one we have at disposal, and the Douglas et al. (2009) one. In Figure 4.2.15 the results of using SRA and QWM for the deep profile are compared. From these results, it is clear that the QWM tends to underestimate the amplification of the soil deposit.

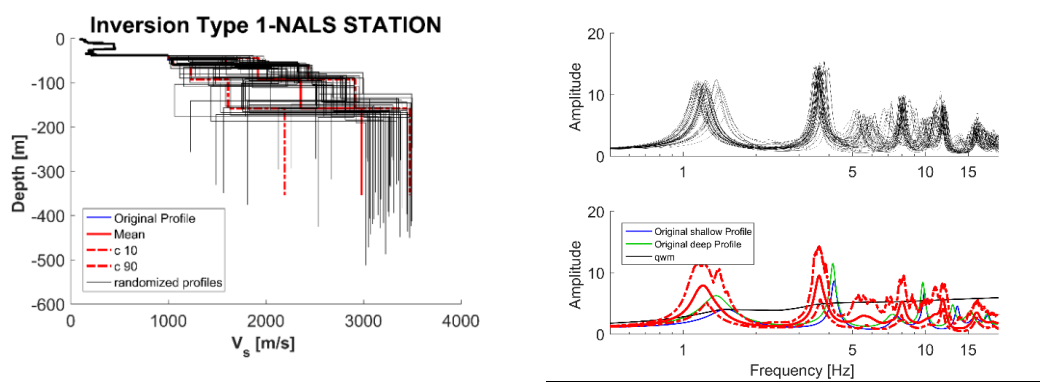


Figure 4.2.16a. Randomized shear-wave profiles and the related transfer functions (Inversion Type 1)

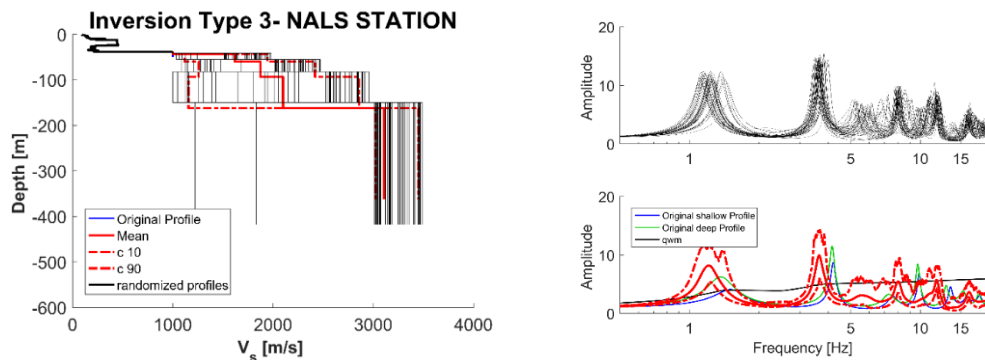


Figure 4.2.16b. Randomized shear-wave profiles and the related transfer functions (Inversion Type 3)

4.2.7. Conclusions

In this work, we have undertaken a study on deep soil profiles and especially on the influence of their central portions (i.e. roughly between depths of 50 and 1km). As is generally known, it is difficult measure the characteristics of this portion of the profile because of the high costs of investigations and the intrinsic uncertainties in the results. Generally, we have an idea of the shape of them and most of the time, we consider the shallow portion of the deposit (up to a depth equal to $V_{s,bedrock}$) to perform a site-response analysis. Here we considered nearly 500 real V_s profiles to define a series of

constraints to develop a method of randomization. This randomization approach can be used to generate a set of possible deep profiles for sites with only shallow V_s profiles to account for the uncertainties in their deep properties.

To test the potential of the method, we have chosen profiles with different depths to seismic bedrock (D). Only sites with $D \leq 50\text{m}$ and $50\text{m} < D \leq 100\text{m}$ can be used with our method because our database is rich in such profiles. For such sites the method gives robust results for amplifications computing using site response analysis. Conversely, due to a lack of profiles with $D > 100\text{m}$, our method does not give robust results, i.e. the comparison between the calculated amplifications for the simulated and real profiles is poor.

We also considered the presence of softer layers within harder layers (so called velocity inversions). These are a relatively commonly characteristic of V_s profile but they are sometimes difficult to identify. To analyse the influence of these inversions, we performed various analyses. For instance, for the very deep Memphis profile, which presents an inversion in its deep portion, we compared the amplification when this inversion is ignored with various methods of simulating an inversion. The conclusion is that in all the cases considered the inversion does not strongly influence the calculated amplifications.

To check the validity of the quarter-wavelength method in the presence of inversions, we compared the amplification predicted using this method and full site response analysis and found that the results of the quarter-wavelength method are insensitive to inversions, even if they are very large. Full site response analysis shows that the inversions do actually have an influence, especially on the location and amplitude of the fundamental mode. From the analyses performed, we suggest that the quarter

wavelength method is a valid starting point. However, it should always be used with caution.

Bibliography

- Aki, K. and P. G. Richards, (1980). Quantitative Seismology, Theory and Methods, San Francisco EEUU, Freeman and Company.
- Anderson, J. G. and S. E. Hough, (1984). A model for the shape of the Fourier amplitude spectrum of acceleration at high frequencies, *Bulletin of the Seismological Society of America*, 74: 1969-1993
- Asimaki, D. and J. Shi, (2014–2017). SeismoSoil User Manual, v1.3, GeoQuake Research Group, California Institute of Technology
- Bielak, J., J. Xu and O. Ghattas, (1999). Earthquake Ground Motion and structural response in alluvial valleys, *Journal of Geotechnical and Geoenvironmental engineering*, 125(5): 413-324
- Boore, D. M., and G. M. Atkinson (1987). Stochastic prediction of ground motion and spectral response parameters at hard-rock sites in eastern North America, *Bulletin of the Seismological Society of America*, 77, 440-467.
- Boore, D. M., and W. B. Joyner (1991). Estimation of ground motion at deep-soil sites in Eastern North America, *Bulletin of the Seismological Society of America*, 81(6), 2167-2185.
- Boore, D. M. and W. B. Joyner (1997). Site amplifications for generic rock sites, *Bulletin of the Seismological Society of America*, 87(2), 327-341.
- Campbell K. W. (2009), Estimates of shear-wave Q and k_0 for Unconsolidated and Semiconsolidated Sediments in Eastern North

America, *Bulletin of the Seismological Society of America*, 99(4):2365-2392, doi: 10.1785/0120080116

- Cotton, F., F. Scherbaum, J. J. Bommer and H. Bungum (2006). Criteria for selecting and adjusting ground-motion models for specific target regions: Application to central Europe and rock sites, *Journal of Seismology* 10:137-156 doi:10.1007/s10950-005-9006-7
- Cramer, C. H., J. S. Gombert, E. S. Schweig, B. A. Waldron and K. Tucker, (2004). The Memphis, Shelby County, Tennessee, seismic hazard maps, U.S. Geol. Surv. Open-File Rept. 04-1294.
- Douglas, J., P. Gehl, L. F. Bonilla, O. Scotti, J. Regnier, A. M. Duval and E. Bertrand (2009). Making the most of available site information for empirical ground-motion prediction, *Bulletin of the Seismological Society of America*, 99(3)1502-1520, doi: 10.1785/0120080075
- ENV (1998) EUROCODE 8, Design Provisions for Earthquake Resistance of Structures. Seismic Actions and General Requirements of Structures, CEN/TC 250, Draft, May 2002
- Garofalo, F., S. Foti, F. Hollender, P. Y. Bard, C. Cornou, B. Cox, M. Ohrnberger, D. Sicilia, M. Asten, G. Di Giulio, T. Forbriger, B. Guillier, K. Hayashi, A. Martin, S. Matsushima, D. Mercerat, V. Poggi and H. Yamanaka (2016). InterPACIFIC project: comparison of invasive and noninvasive methods for seismic site characterization. Part I: intra-comparison of surface wave methods. *Soil Dynamic and Earthquake Engineering*, 82:222-240. DOI 10.1016/j.soildyn.2015.12.010
- Garofalo F., S. Foti, F. Hollender, P. Y. Bard, C. Cornou, B. Cox, A. Dechamp, M. Ohrnberger, V. Perron, D. Sicilia, D. Teague and C. Vergnault (2016). InterPACIFIC project: comparison of invasive and non-

invasive methods for seismic site characterization. Part II: inter-comparison between surface-wave and borehole methods, *Soil Dynamic and Earthquake Engineering*, 82:241-254. DOI 10.1016/j.soildyn.2015.12.009

- Gomberg, J., B. Waldron, E. Schweig, H. Hwang, A. Webbers, R. Van Arsdale, K. Tucker, R. Williams, R. Street, P. Mayne, W. Stephenson, J. Odum, C. Cramer, R. Updike, S. Hutson and M. Bradley, (2003). Lithology and shear-wave velocity in Memphis, Tennessee, *Bulletin of the Seismological Society of America*, 93: 986–997.
- Hashash, Y. M. A., M. I. Musgrove, J. A. Harmon, D. R. Groholski, C. A. Phillips and D. Park, (2016). DEEPSOIL 6.1, User Manual.
- Hashash, Y. M. A., D. Park and J. Lee, (2001). Non-Linear Site response analysis for deep deposits in the new Madrid Seismic Zone, 4th *International conference of recent advances in geotechnical Earthquake engineering and soil dynamics*
- Joyner, W. B. and D. M. Boore, (1981). Peak horizontal acceleration and velocity from strong-motion records including records from the 1979 imperial valley, California, earthquake, *Bulletin of the Seismological Society of America*, 71 (6):2011-2038.
- Iyer, H. and K. Hirahara, (1993). *Seismic Tomography: Theory and Practice*, Chapman & Hall, London.
- Kennett, B. L. N., (2002). *The Seismic Wavefield, Volume 2: Interpretation of Seismograms on Regional and Global Scales*, Cambridge University Press, Cambridge.

- Kim, D., H. Park, and E. Bang, (2013a). Round Robin test for comparative study of in-situ seismic tests, 766 *Geotechnical and geophysical site characterization* **4**, 1427-1434.
- Kottke, A. and E. M. Rathje, (2013). Technical Manual for Strata. PEER Report, University of California, Berkeley.
- Ktenidou, O.-J., F. Cotton, N. A. Abrahamson and J. G. Anderson, (2014). Taxonomy of k : A review of definitions and estimation approaches targeted to applications, *Seismological Research Letters*, 85(1) doi:10.1785/0220130027
- Lanzo, G., F. Silvestri, A. Costanzo, A. D’Onofrio, L. Martelli, A. Pagliaroli, S. Sica and A. Simoncelli (2011). Site response studies and seismic microzoning in the Middle Aterno valley (L’Aquila, Central Italy), *Bulletin of Earthquake Engineering*, 9:1417-1442, doi: 10.1007/s10518-011-9278-y
- Laske, G., A. Dziewonski, and G. Masters (2005). The Reference Earth Model Web Site, <http://mafi.ucsd.edu/Gabi/rem.html> (last accessed December 2008)
- Luzi, L., R. Puglia, E. Russo and ORFEUS WG5 (2016). Engineering Strong Motion Database, version 1.0. Istituto Nazionale di Geofisica e Vulcanologia, Observatories & Research Facilities for European Seismology. doi: 10.13127/ESM
- Montalva, G. and A. Rodriguez-Marek (2010). Random Fields for Site Response Analysis. *Geotechnical Special Publication*. 2062-2072. 10.1061/41095(365)209.

- Nakamura, Y., A method for dynamic characteristics estimation of subsurface using microtremor on the ground surface, Railway Technical Research Institute/Tetsudo Gijutsu Kenkyujo, ISSN:0033-9008, Vol.30, Issue N.1
- Ohta, N., N. Goto, F. Yamamizu and H. Takahashi (1980). S-wave velocity measurements in deep soil deposit and bedrock by means of an elaborated down-hole method, *Bulletin of the Seismological Society of America*, 70(1): 363-377;
- Passeri, F., A. Rodriguez-Marek and S. Foti, (2018). Influence of epistemic uncertainty in shear wave velocity on seismic ground response analyses, *Earthquake Spectra*, doi: 10.1193/011018EQS005M
- Pitilakis, K., E. Riga, A. Anastasiadis, S. Fotopoulou and S. Karafagka, (2018). Towards the revision of EC8: proposal for an alternative site classification scheme and associated intensity dependent spectral amplification factors, *Soil Dynamics and Earthquake Engineering*, <http://doi.org/10.1016/j.soildyn.2018.03.030>
- Seyhan, E., J. P. Stewart, T. D. Ancheta, R. B. Darragh and R. W. Graves, (2014). NGA-West2 Site Database, *Earthquake Spectra*, 30(3): 1007-1024;
- Souriau, A., A. Roullé and C. Ponsolles (2007). Site effects in the city of Lourdes, France, from H/V measurements: implications for seismic-risk evaluation, *Bulletin of the Seismological Society of America*, 97(6): 2118–2136, doi 10.1785/0120060224.
- Toro, G. R., (1995). Probabilistic models of site velocity profiles for generic and site-specific ground-motion amplification studies, Technical Report 779574, Brookhaven National Laboratory, Upton, New York;

- Tsang, H.-H. and N. T. K. Lam (1997). The importance of crustal shear wave velocity profile for ground motion modelling, Proceedings of the 1st IASME/WSEAS International Conference on Geology and Seismology (GES'07), Portoroz, Slovenia,
- Volpini, C. and J. Douglas (2019). Assessing earthquake site amplification for deep soil sites with uncertain bedrock conditions, *VII International Conference on Earthquake Geotechnical Engineering*, Roma

Conclusions and future work

This study focused on improvements to seismic site response analysis for non-standard sites. In particular, I carried out detailed studies on the uncertainties in site amplification for:

- sites with peculiar stratigraphy (in particular non-horizontal layers); and
- sites where the deep portion of the shear-wave velocity profile is poorly known.

In Chapter 2, I tested the finite-element software “Abaqus”, which then was used to develop guidelines on how best to model sites with non-horizontal layers (Chapter 3). To check the performance of this finite element code under dynamic analysis, we performed a viscoelastic analysis of a simple layered column, comparing it with the results from a one-dimensional software. After checking the effectiveness of the software with this simple solution, we performed other analyses with a more complex geometry. This was essential to verify the free-field boundary conditions, which are not implemented in Abaqus. FLAC3D was used to check them.

Connected to the technical article included in Chapter 2, Chapter 3 focused on the influences of stratigraphic heterogeneities. Lateral uncertainties, due to non-horizontal layers were studied. The aim was to develop an accessible approach to define whether these soil deposits should be studied with one-dimensional or two-dimensional codes. The guideline proposed was built using two main parameters that characterize a soil deposit, which are the angle of the dipping layers and the impedance contrast ratio. The guideline was then testing using real case studies.

The main limitations connected with this analysis are the following.

- I did not perform any analyses for a real case, for example Turkey Flat (see section 3.1). In fact, despite the model used presenting a simple, ideal but quite realistic geometry, it would have been informative to check what happens for some real sites with more complex geometries and/or shear-wave velocity profiles;
- The choice of evaluating results in terms of only Fourier Amplitude Spectrum could be extended to also consider response spectral ordinates. In fact, the predicted one-dimensional site response presumes that strong resonances can develop. What happens in reality is that small heterogeneities, deviations from the assumed vertical and horizontal spatial variability would smooth the resonance peaks. Response spectra, since they measure the response of a single degree of freedom oscillator, act as a smoothing filter and hence reduce the resonances.

In chapter 4, I investigate another type of uncertainties when conducting site response analyses. This is the uncertainty connected, substantially, with the lack of information about shear-wave velocity profiles (V_s), particularly at depth. Neglecting the shallow portion, where we usually have the majority of the measurements, I consider the deep portion of a soil profile. For instance, for depths below the seismic bedrock ($V_s \geq 800$ m/s), the engineering community tends to stop site investigations unless they are explicitly requested. I focused my attention on the portion of soil that goes from the seismic to hard bedrock and whether this portion can significantly modify the site amplification function. A database of real profiles was used to simulate randomized deep profiles with realistic characteristics, which were then used in site response analyses. The main limitation connected with this method was the lack of

measurements for profiles with deep ($D \geq 100\text{m}$) depth to the seismic bedrock. This precluded the building of a reliable randomization technique for such sites.

Some additional work that would extend the analyses presented in this thesis are the following.

- Connected to Chapters 2 and 3, the basic model could be modified to introduce an absorbing boundary condition at the base of the model. In this way the bedrock would no longer be rigid, which would be more realistic.
- An interesting extension to the parametric simulations in Chapter 3 would be to introduce some degree of spatial variability to the 1D and 2D simulations to see to which degree the dividing boundary (Figure 3.2.13) is sensitive to the assumption of homogeneous velocities in the layers.
- Moreover, a more realistic soil constitutive model, including a fully non-linear one, could be used for the simulations to better represent true soil behaviour.
- Connected to Chapter 4, a useful development would be to improve the database of shear-wave velocity profiles. Having more information would lead to a more robust simulation procedure, especially for those sites with particularly deep profiles, e.g. the Memphis profile (see Figure 4.2.1).

Appendices

Appendix 1: Conference Paper “Examining the assumption of homogeneous horizontal layers within seismic site response analysis

Carolina Volpini and John Douglas

Department of Civil and Environmental Engineering – University of Strathclyde, Glasgow, UK

ABSTRACT

One-dimensional analyses can be conducted to estimate the impact of superficial soil layers on earthquake ground motions. Such analyses are based on the assumption that all boundaries are horizontal and that the response of a soil deposit is predominantly caused by horizontal shear waves propagating vertically from the underlying bedrock. This assumption is made even for sites with a relative large surface area, e.g. the footprint of large infrastructure such as power plants.

An important step then is to create a model of the near subsurface that is representative of the overall area under analysis. This means it is essential to evaluate geomechanical characteristics of the soil at certain locations and extend these measurements over the whole site. As a consequence of this, it is assumed that the soil characteristics, which include stratigraphy, geometry and geotechnical properties, are homogeneous. Recent observations, however, have clearly demonstrated that even over a small area ($\sim 1\text{km}^2$) ground conditions can vary greatly.

The purpose of this study is to examine the impact of relaxing the assumption of

infinite horizontal layers by undertaking a parametric study of the variability in amplification across areas with gently dipping subsurface layers. Starting from a 1D approach the influence of dipping layers is evaluated through simplified but geometrically representative models. Randomization of shear-wave velocity profiles using the Toro (1995) method, as implemented in STRATA, is used to compute the variability in site amplification that would be captured by a standard 1D technique. This provides a baseline for comparison with the variability introduced by the dipping layers. Subsequently, two-dimensional simulations are conducted for the same sites with dipping layers to estimate the error made through the assumption of 1D response. The goal of this study is to understand when the 1D assumption can be used in the presence of dipping layers.

INTRODUCTION

Seismic site response analyses are one of the most important aspects of seismic hazard assessment. This step is generally required for critical structures (such as power plants) and for buildings not located on hard rock.

A critical aspect of this kind of study is the capability to assess all the possible site uncertainties, which can arise both from geo-mechanical and geometrical points of view. Geological conditions can vary rapidly within a small area (e.g. within the roughly 1 km² footprint of some critical infrastructures). Generally *ad hoc* procedures are used to account for this variability (if it is known to exist), which can be difficult to justify, time-consuming and associated with an unknown level of conservatism.

Engineering judgement plays a key role in the final selection of the parameters for the analyses. A selection of the most relevant geological conditions are analyzed and then extended to the whole model. Furthermore, simplifying assumptions can be made, such

as 1D response can reproduce the real situation quite well, but again this needs to be judged on a site-by-site basis.

This approach has been the predominant approach for many years, because it leads to easy-to-understand and generally reliable results but the assessment of its associated uncertainties is still challenging.

Several authors have compared the response of 1D and 2D models, in particular for sedimentary valleys (e.g. Bard and Bouchon 1985). Some of the studies have focused on real cases, taking into account complex geometries and non-linear effects (e.g. Kapuskar et al. 1989), whereas others (e.g. Sanchez-Sesma and Velazquez 1987; Paolucci and Morstabilini 2006) have studied canonical forms, such as the response of a single dipping layer, and find closed-form solutions for them. This study starts from these previous studies and aims to assess the error we commit by making the 1D assumption instead of more complex solutions, which consider variability in terms of soil mechanical properties and variability in terms of geometrical characteristics of the site (e.g. gently-dipping layers). In contrast to previous studies, which were related to real locations, this one is more generic, since it is seeking to provide general guidance.

Review of the available methods

According to basic theory (e.g. Kramer, 1996), whenever the site presents a not very complex geometry (e.g. valleys) and the analysis that we want to conduct is a preliminary one (e.g. soil nonlinearity is not taken into consideration), a 1D linear viscous-elastic analysis can be used (Figure A1-A). The basis of this approach is to model the site as a series of parallel flat layers that extend infinitely in the horizontal direction excited by a horizontal input motion (SH waves), which can be a significant simplification.

Rathje and Kottke (2011) have added the possibility to make this simple model more realistic from the point of view of its geo-mechanical uncertainties. In their software STRATA, they have introduced the possibility of randomizing the shear-wave velocities profiles, using Toro (1995) technique (Figure A-2).

This should overcome, at least partially, the problem of lack of reliable site information (e.g. thickness of layers, stiffness of layers, depth of bedrock) over an entire building footprint, which is often the case for real projects.

What happens if the site is not anymore representable as a series of parallel flat layers? We are excluding from our discussion obviously 2D or 3D sites like alluvial basins or narrow valleys and focusing on geometries with gentle dipping layers, e.g. at edges of wide shallow valleys.

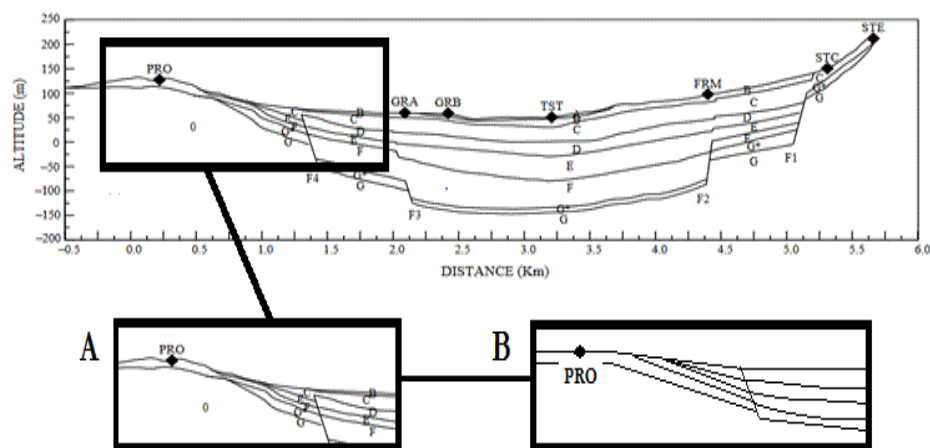


Figure A-1. Example of the edge of a valley. A) lateral edge zoom; B) lateral edge possible simplification. Example taken from (Makra and Raptakis 2007)

Could a situation like that be accurately studied with 1D model, with its advantages of speed and simplicity, or is it necessary to move to 2D analyses, which are generally much slower and more complex to set up (e.g. the need for many input parameters) and analyze?

In this work, the 1D approach both in the standard way and by using randomization are studied. The first version will result in a series of transfer functions computed by changing the thickness of the layers, per the geometrical situation (Figure A2-A). The second set, in addition to this variability, will account for the randomization of the shear-wave velocity profiles, trying to account for both geometrical and geomechanical issues (Figure A2-B). These second results will be compared to the 2D results, which are the most correct way to model response of such a site. A possible future step would also involve comparison of 1D and 2D simulations with actual observations.

The goal of the work is to try to estimate the standard deviation that when included in the randomized model leads to 1D results that are comparable to those from the 2D analyses. This would mean that 2D analyses could be avoided for these cases, thereby saving time and effort in modeling and interpretation of results.

Future steps will include randomization within the 2D model and understanding the implications of this on possible site response for this type of site.

Scheme of possible solutions

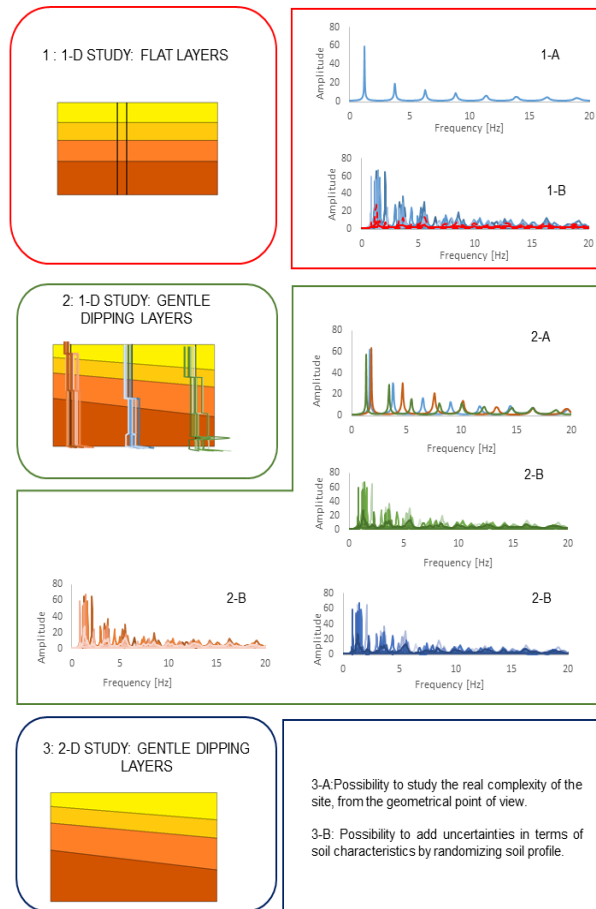


Figure A- 2. Above left: 1-D analysis with flat layers. Above right: comparison of transfer functions from classical analysis (1-A) and randomized one (1-B)

Centre: 1-D analysis for dipping layers. Comparison between classical analysis (2-A) and randomized one (2-B).

Bottom left: 2-D analysis of dipping layers. Bottom right: evaluation of the possible 2-D analyses (3-A), (3-B)

COMPARISON BETWEEN 1D AND 2D RESULTS

As indicated in Figure A-2, a series of steps will be taken to evaluate the difference between 1D and 2D results. Considered that the first model (1-A, 1-B) is well known, the second and the third ones will be studied here. First, a simple general geometry must be chosen that can be applied to many situations.

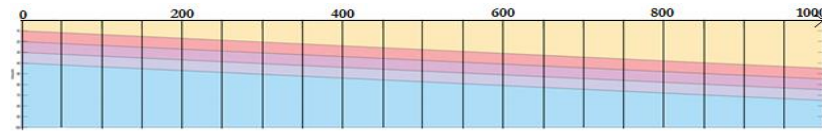


Figure A- 3. Scheme of the model used for the analysis

Figure A-3 represents the model selected for this purpose. Each different color represents a different layer, in terms of geotechnical properties. Furthermore, each of these layers is inclined at the same angle, which is a reasonable assumption when the same geological processes are acting on all layers. This geometry has been used because of its simplicity and potential for leading to general guidelines. Table 1 reports the shear-wave velocity of the model.

Table A-1. Shear-wave velocity of each layer of the model

Layer Number	Vs [m/s]
1	300
2	350
3	400
4	500
Bedrock	1000

RANDOMIZED PROFILES

The idea behind the second approach (Figure A-2) is that of linking both geo-mechanical issues and geometrical ones in a single 1D model. Indeed, several linear viscoelastic analyses will be computed along the x-axis (Figure A-3, black lines) and in each of them the shear-wave velocity profiles will be randomized.

Before anything else, it is useful to examine the consequences of both the geometrical aspects and the shear-wave velocity randomization on the model. To do this, a comparison in terms of standard deviation of the shear-wave velocities at each depth is carried out. Focusing on Figure A-3, 21 profiles have been selected (one every 50 m). The blue curve (Figure A-4) has been computed in this way: a matrix of n-rows (each row represents a single meter thickness) and m-columns (equal to the number of profiles chosen) has been created. This matrix contains shear-wave velocity profiles (Eq.31):

$$\begin{bmatrix} V_{1,1} & \cdots & V_{1,m} \\ \vdots & \ddots & \vdots \\ V_{n,1} & \cdots & V_{n,m} \end{bmatrix} \quad [31]$$

Then, logarithms of each element of this matrix are evaluated and finally, for each row of this matrix a standard deviation is computed. The result is represented by the blue curve in Figure A-4.

The red curve in Figure A-4 represents both the geometrical aspects of the model as well as the variability from the randomization. To compute this each of the 21 profiles has been randomized 100 times, using the Toro (1995) technique to randomize the V_s of each layer. This randomization has been evaluated using the coefficients from Toro (1995) for the appropriate $V_{s,30}$ for this site, i.e. for 180-360m/s as the models have $V_{s,30}$ between 200 and 400 m/s.

Coefficient $\sigma_{\ln V_s}$ leads to the starting point of the red curve. The biggest gap between the two curves, which is represented by the green curve, is close to the surface and at maximum depth. The peak of the standard deviation (red and blue curves) is roughly at half of the maximum depth reached. This happens mainly for geometrical reasons and is understandable when looking at Figure A-3.

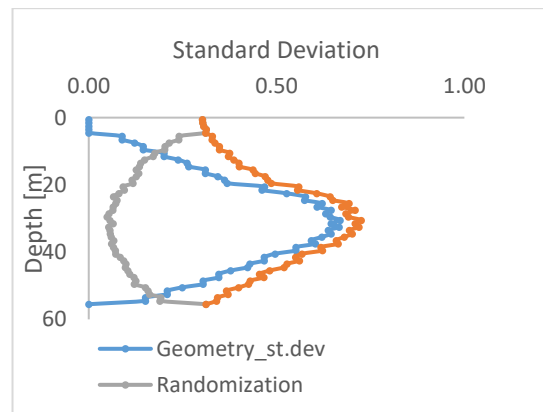


Figure A-4. Comparison among standard deviation of the logarithms of the velocity profiles with only geometric effects (blue), with geometric and randomization effects (red) and the difference between the two (grey).

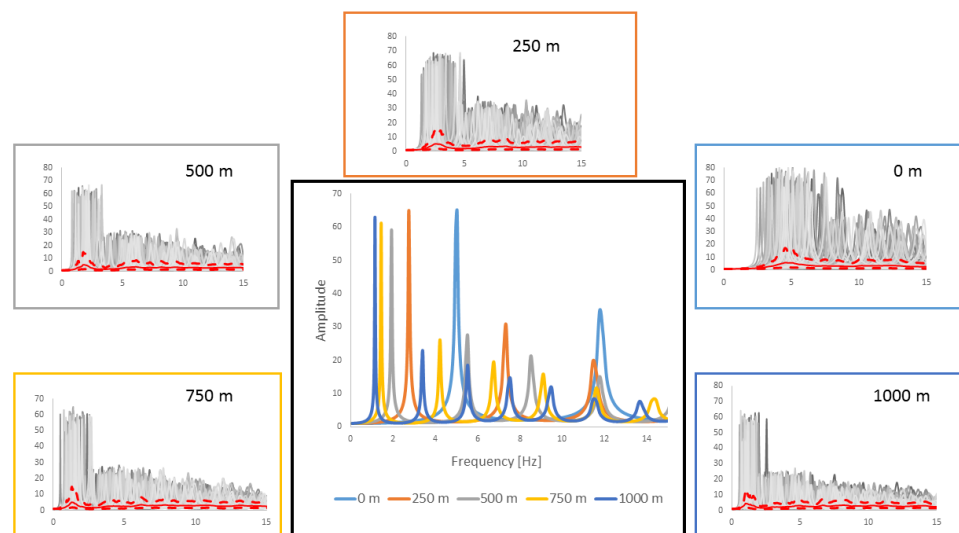


Figure A-5. Comparison between standard analyses (center) and randomized ones (0m, 250m, 500m, 750m, 1000m). The red curve is the median amplification and dashed lines are the 16th and 84th percentiles.

A comparison of transfer functions between 1D standard analyses and 1-D analyses with randomized profiles (both linear viscoelastic) is shown in Figure A-5.

2-D Analyses

The aim of this work is to assess the possibility of using 1D analyses instead of 2D analyses in some cases. To verify this possibility, a set of 2D analyses must be performed.

The general idea is to recreate the same model as shown in Figure 3 within a finite element software package. Currently we are using Abaqus (Simulia) for these simulations. When implementing the model several parameters, such as the dimension of the main model, the dimension of the single element, the correct boundary conditions, have to be carefully chosen.

Description of the model

The Abaqus model must be as similar as possible to the 1D analysis. This means that several rules have to be followed. First, a viscous linear elastic analysis is performed. Abaqus gives the possibility of defining the damping in terms of the Rayleigh formula, which is an artifice to reproduce the real damping. In this formula, the damping matrix, C is assumed to be a linear function of the mass matrix, M and the stiffness matrix, K , through two coefficients, α_R and β_R , in this way:

$$C = \alpha_R M + \beta_R K \quad [32]$$

Therefore, by imposing the damping value that should be reached, these two terms can be computed. The critical aspect of this method is that it is a frequency-dependent method. Consequently, it should be used with prudence, especially if the analysis is not linear.

The second aspect of this analysis is the way in which the bedrock is specified (this is also true in the 1D case). There are two principal ways to include bedrock within site response analysis: the first, which is used here, is the infinite rigid bedrock, whereas the second, which is more realistic from a geo-mechanical point of view, is considering the bedrock as “another” layer, with stiffer characteristics than the others. We could say that the first one is the preliminary choice, when there is a lack of information about the site. The second possibility allows a more realistic model to be produced, but it requires an in-depth knowledge of the site. As stated above, in this set of analyses an infinite rigid bedrock will be assumed and no dashpots introduced.

The third important concept that must be controlled is the dimension of the single element of the model (Lysmer and Kuhlemeyer, 1973), which should follow this rule:

$$\Delta l_{max} \leq \frac{\lambda_{min}}{10} \leq \frac{V_{s,min}}{10 \cdot f_{max}} \quad [33]$$

where:

- Δl_{max} is the maximum dimension of the element;
- λ_{min} is the minimum wavelength of the model;
- $V_{s,min}$ is the minimum shear wave velocity presented in the model;
- f_{max} is the maximum frequency for which we would like to obtain an accurate result;

Following this rule, the shallowest layer will be the one with the smallest elements. The final important issue is the boundary conditions, which are fundamental in finite element analyses. There are several approaches in the literature to model the boundary conditions for this kind of problem. The main issue is the reproduction

within a finite model of a semi-infinite phenomenon. It is understandable that the wave path is conditioned by this finite geometry and could alter the output.

To prevent this, a free-field (Wolf, 1988) boundary condition is created. Theoretically, it is a semi-infinite domain with horizontal layers of linear-elastic materials. In Abaqus, this has been implemented in a subroutine (Nielsen 2006, 2014), which allows the generation of free-field elements. This subroutine can be used either in 2D or 3D models, with complex morphologies, as long as a buffer zone, which has to link the main model (complex morphology) to the free field element, is provided.

Following this series of rules, the model has these characteristics:

- the main model length is 800m;
- the lateral buffer zones length is 600m;

Figure A- 6 shows an outline of the model.

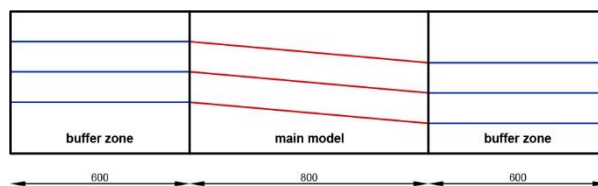


Figure A- 6. Outline of the model in Abaqus

Four different models have been generated, each of them presenting a different slope angle of the layers, from 1 degree to 4 degrees, which implies different thicknesses of the first layer (Table A-2).

Table A- 2. Evaluation of Δh , the additional thickness of the first layer coming from the geometry.

Sloping angle [°]	Δh [m]	Thickness first layer [m]
1	13.6	23.6
2	28	38
3	41.6	51.6
4	56	66

The maximum value of the dipping angle has been set to 4 degrees because, as Table A-3 shows, Δh starts to become too big, which means the geometry effect will dominate the site response analysis.

Finally, table A-3 displays geo-mechanical characteristics of each layer, apart from the damping ratio, which is of the order of 1%. Table A-4 does not show it, because it is represented through the Rayleigh method, which means different values of alpha and beta for each layer and for each model.

Table A- 3. Geo-mechanical characteristics of each layer

	Layer 1	Layer2	Layer 3	Layer 4
γ [KN/m ³]	1800	1800	2000	2000
V_p [m/s]	755.9	1530.5	982.0	1224.7
V_s [m/s]	308.6	362.5	400.9	500.0

ANALYSIS PROCEDURE AND RESULTS

From a theoretical point of view this analysis could be processed with any time-history because it is a linear viscoelastic model and here only the transfer functions are considered. A series of different input have been chosen to test the model, all of them taken from the Itaca database (Italian Accelerometric Archive). For each set of triaxial time-histories (N-S, E-W, U-D) belonging to a single earthquake, the maximum of the two horizontal and the vertical one have been chosen. Each of the geometries has been tested with the same set of time-histories. Previously it was checked that Strata and Abaqus give comparable results for the 1D case.

Figure A-7 displays an example of the time-histories selected for the bedrock.

Figure A-8 displays a comparison between an input motion and an output taken from 1 degree Abaqus analysis, at the central node of the surface.

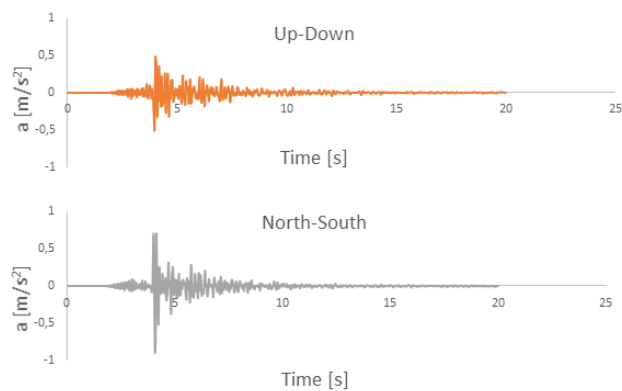


Figure A-7. Example of the input time history, taken from ITACA

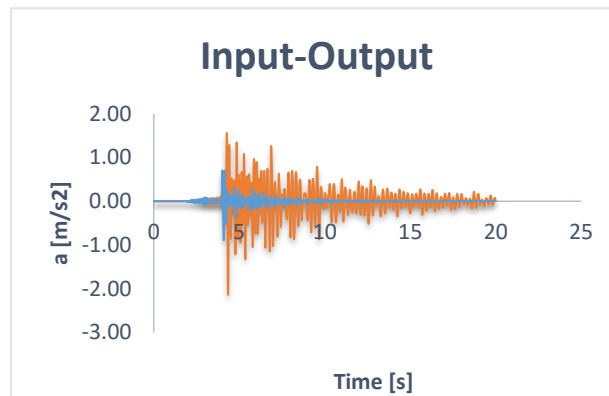


Figure A- 8. Input (blue) and Abaqus output (red) accelerograms, taken from the center of the model (400m).

To evaluate the effect of the sloping layers, transfer functions have been computed every 100m and they have been compared to those from STRATA. This procedure has been repeated for each of the geometries. For this purpose, the 1D profile at the center of the main model has been selected. Indeed, the goal of this work is to assess the reliability of 1D analysis for this kind of geometry. Therefore, it is interesting to make this comparison and to evaluate how far is the 1-D response from the 2D calculation that takes into account non-vertically incident waves. Figure A-9 and Figure A-10 display these results: Figure A-9 corresponds to 1 and 2 degrees slopes, whereas Figure A-10 shows the results for 3 and 4 degrees slopes. As expected the greater the slope the greater the mismatch, because geometrical complexity dominates.

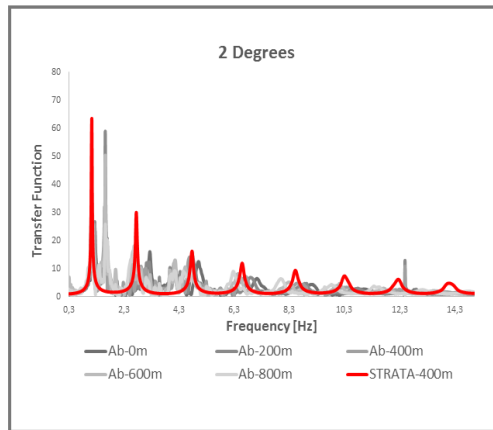
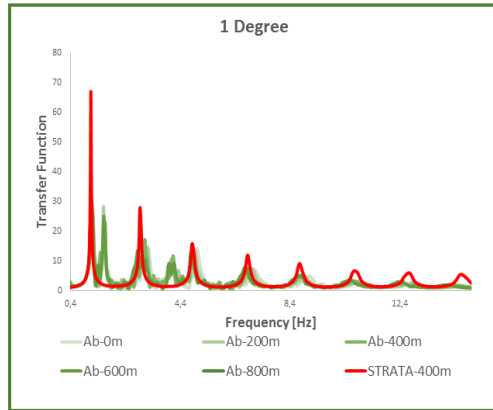


Figure A-9. Above: 1-degree comparison between Abaqus transfer functions (0m, 200m, 400m, 600m, 800m) and STRATA transfer function (400m); Below: 2-degree comparison between Abaqus transfer functions (0m, 200m, 400m, 600m, 800m) and STRATA transfer function (400m).

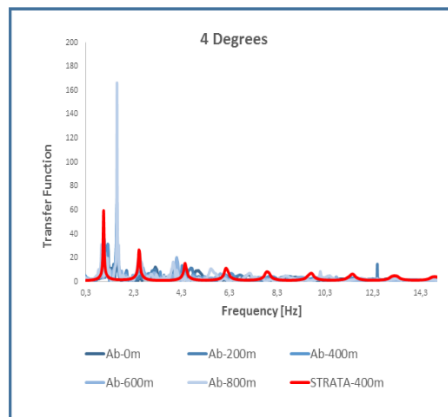
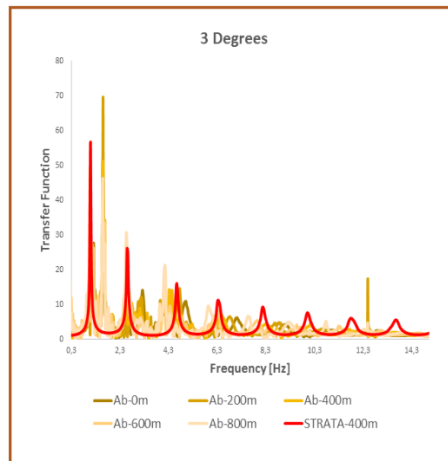


Figure A-10. Above: 3-degree comparison between Abaqus transfer functions (0m, 200m, 400m, 600m, 800m) and STRATA transfer function (400m); Below: 4-degree comparison between Abaqus transfer functions (0m, 200m, 400m, 600m, 800m) and STRATA transfer function (400m).

CONCLUSION

This work presents some preliminary evaluations of the capabilities of 1D analysis to compute the seismic response of gentle dipping layers. This is a kind of morphology that is quite common at the edge of large shallow valleys. The literature has clearly demonstrated that complex geometries, like narrow deep valleys, cannot be studied with 1D analyses. This work focuses on those geometries in a transition zone from flat

layers to valleys. To do that, a logical scheme has been followed. Starting from 1D analyses with flat layers, which is the classical configuration and the most used one, this work studied configurations with a more complex geometry, i.e. gently-dipping layers (Figure A-3) and they have been studied both with the classical method (1D) and in a more realistic way, using 2D models. Results from the two approaches have been compared in terms of transfer functions, to understand the error, we commit using simple 1D models.

This is a preliminary study, which is currently being expanded. New comparisons will be made in terms of elastic response spectra. Bigger models and higher complexities will be considered as well as more variations in the geo-mechanical properties, e.g. non-linear effects and different bedrock stiffness.

ACKNOWLEDGMENTS

We would like to thank CH2M Hill, in particular Iain Tromans, Guillermo Aldama Bustos, Manuela Davi and Angeliki Lessi Cheimariou, and Andreas Nielsen for their help with various aspects of this study.

BIBLIOGRAPHY

- Bard, P. Y., and M. Bouchon, (1985). Two-Dimensional resonance of sediment-filled valleys, *Bulletin of the Seismological Society of America*, 75(2): 519-541.
- Dassault Systèmes, Simulia Corporation, 2013, Abaqus 6.13.
- Kramer, S. (1996). Geotechnical Earthquake Engineering, Prentice Hall, Upper Saddle River, New Jersey, N. J., USA.
- Kapuskar, M., G. R. Martin, and J. Proubet, (1989). Site-Response analyses
- Makra, K., and D. Raptakis, 2007. How sensitive the effects of lateral heterogeneity on seismic ground motion are?, *4th International Conference on Earthquake Geotechnical Engineering*, (1687):13.
- Nielsen, A. H., (2006). Absorbing boundary conditions for seismic analysis in Abaqus, *Abaqus Users' Conference*, 359-376.
- Nielsen, A. H., (2014). Towards a complete framework for seismic analysis in Abaqus, *Proceedings of the ICE-Engineering and Computational Mechanics*, 167(1): 3-12.
- Paolucci, R., and L. Morstabilini, (2006). Non-dimensional site amplification functions for basins edge effects on seismic ground motion, *Third International Symposium on the Effects of Surface Geology on Seismic Motion*, 823-831.
- Sanchez-Sesma, F. J., and S. A. Velazquez, (1987). On the seismic response of a dipping layer, *Wave Motion*, 9(5): 387-391
- Toro, G.R.(1995). Probabilistic models of site velocity profiles for generic and site specific ground-motion amplification studies, Technical Report 779574, Brookhaven National Laboratory, Upton, New York, N.Y., USA

Appendix 2: Conference paper “Assessing earthquake site amplification for deep soil sites with uncertain bedrock conditions”

Carolina Volpini & John Douglas

*University of Strathclyde, Department of Civil and Environmental Engineering,
Glasgow (UK)*

ABSTRACT: Site-response analysis is commonly performed using shallow (<50m) shear-wave velocity profiles. The depth at which the bedrock motion is input into the analysis is one of the main parameters that influences the site response. Deciding on the appropriate depth can be difficult because of a lack of information (the “dark zone”) below a few tens of meters of depth due to the high cost of investigating greater depths. However, the deep part of the profile can have a large impact on the site response.

Here we use a database of over 1,000 shear-wave velocity profiles from strong-motion stations in the USA, Europe and Japan to develop a procedure to generate deep profiles that are consistent with observations and imposed constraints (e.g. presence of velocity inversions). By comparing the site response from the generated profile with the response of a known profile we demonstrate the importance of this “dark zone”.

INTRODUCTION

Ground motion site amplification is one the main topics of interest in geotechnical earthquake-engineering. The procedure usually adopted is to identify a shear-wave velocity profile (V_s), describing the site, the depth of the seismic bedrock and the mechanical characteristics of the soil deposit. Then, after choosing the most

appropriate approach from a mechanic point of view (i.e linear, equivalent-linear or fully non-linear) and from a geometric point of view (i.e. one-dimensional, two-dimensional or three-dimensional), a site-response analysis is performed.

It is common to restrict the geotechnical investigations, which are expensive, to the shallowest part of the soil deposit (depths < 50m), unless the site presents particular characteristics or the planned construction is particularly important.

The site characteristics that may mean deeper geotechnical investigations are undertaken include:

- Deep soil deposits, which brings uncertainties in the determination of the true bedrock;
- Presence of a second, deeper bedrock, with a higher V_s than the shallow bedrock;
- Uncertainty in the soil profile of the deeper zone, which we call the “dark zone”;

Whenever these types of site condition are encountered, it is important to move the investigation forward in order to understand the implication of these characteristics in site response analysis.

This study aims to provide some advice on this kind of issue. Starting from a well-known profile, for Memphis, Tennessee (USA) (Gomberg et al., 2003; Cramer et al., 2004), we undertake an investigation on the impact of the previous cited parameters on the results of a site response analysis.

We have chosen this site because: it appears to be a peculiar situation where the seismic bedrock can be found at an unusual high depth, it presents an inversion of velocity in

the so-called “dark zone” and, in general, there are many uncertainties in the definition of the whole profile. Figure B-1 displays the considered shear-wave profile (taken from Campbell, 2009).

According to Douglas et al. (2009), the list of important parameters, for site characterization, includes:

- Velocity of the seismic bedrock ($V_{s,bedrock}$), which can be defined as where $V_s > 800\text{m/s}$ (Pitilakis et al., 2018);
- Maximum depth, D , or thickness of the soil deposit, which is the depth corresponding to $V_{s,bedrock}$;
- V_0 , or the surface shear-wave velocity;
- $V_{s,30}$, the time-averaged shear-wave velocity of the top 30m;
- Minimum thickness of the layers (H_{min});
- Maximum thickness of the layers (H_{max});
- Deep bedrock shear-wave velocity and its depth (crustal depth).

Many of these factors are relatively easy to determine, such as surface shear velocity, V_0 or $V_{s,30}$, which is one of the main parameters (along with N_{SPT} blow count, plasticity index PI and undrained shear strength, S_u) used in Eurocode 8 to define the site classification. Others, such as maximum depth, D , and the velocity of the seismic bedrock are more difficult to determine and because of that, they can introduce great uncertainty in the resulting profile used for site response analysis.

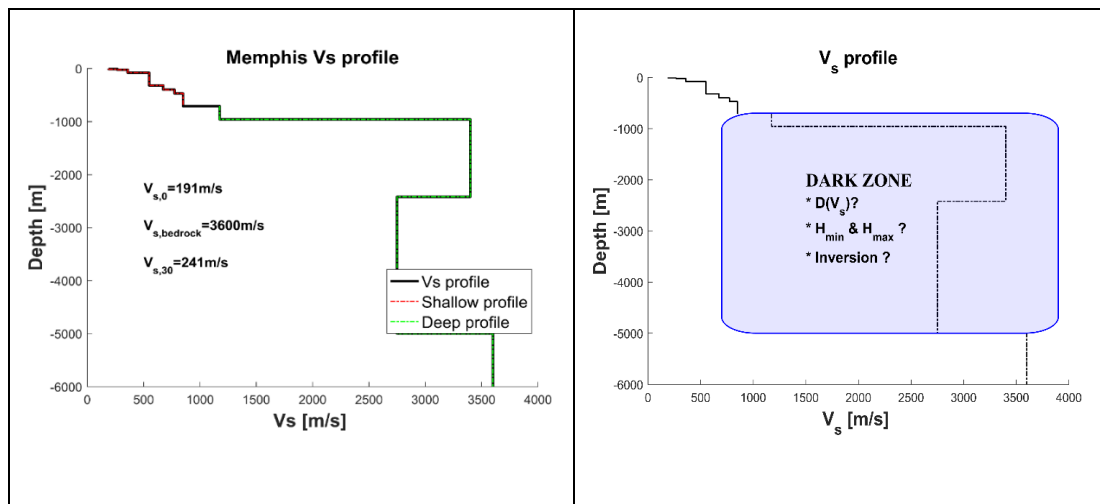


Figure B-1. Left: Memphis Vs profile, as shown in Campbell (2009). Right: Range of “Dark zone” where uncertainties are high

Let us consider that we do not know the deep Memphis profile and we need to make a hypothesis on its shape and key characteristics. To do that, we need to impose some constraints on the generic shape a deep profile could have. In particular, we focus on the zone between D and the crustal depth, which we call the “dark zone” (Figure 1, right). Using the Douglas et al. (2009) shear-wave velocity database (857 profiles) plus the ones kindly provided by INGV from the ESM strong-motion database (Luzi et al., 2016) (245 profiles), we aim to model deep profiles more accurately.

Obtaining information from the database

As explained above, we have a total of 1102 shear wave velocity profiles at our disposition. We have developed a taxonomy based on these parameters:

- $V_{s,\text{bedrock}}$;
- Depth of $V_{s,\text{bedrock}}$, which we will indicate by D ;
- Presence of a velocity inversion within the profile;

- Maximum and minimum thickness of the layers between D and the crustal depth; and
- Length of the profile after D;

First of all, we search for two of these parameters, simultaneously. They are $V_{s,bedrock}$ and the presence of a velocity inversion. One cannot exclude the other. As a matter of fact, despite the engineering concept of $V_{s,bedrock}$ as the velocity beyond which we no longer have an inversion, we could, for instance, have one before reaching D . Or, we could have an inversion that does not decrease below $V_{s,bedrock}$ (case A of figure B-2). This is the case for the Memphis profile. According to the concept of $V_{s,bedrock}$ the one we should eliminate from our analyses is only case B of figure B-2, i.e. an inversion that occurs after reaching $V_{s,bedrock}$ and decreases the velocity below this value. The other two groups can be included into the macro-group of $V_s > 800$ m/s.

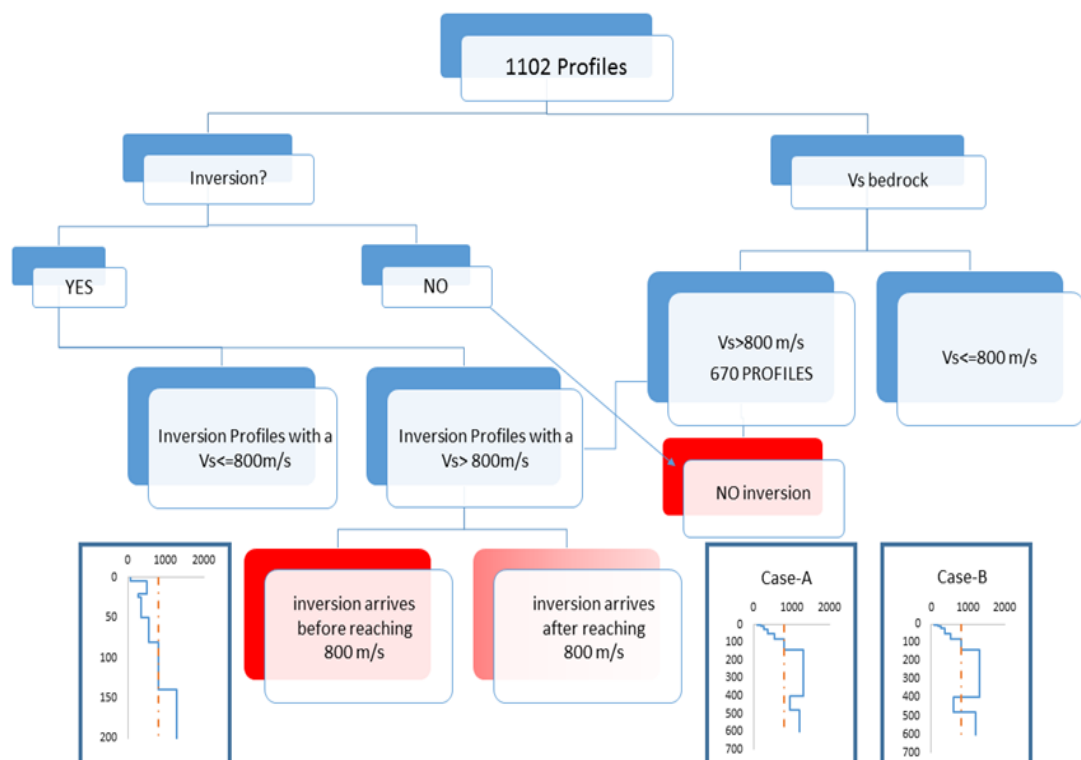
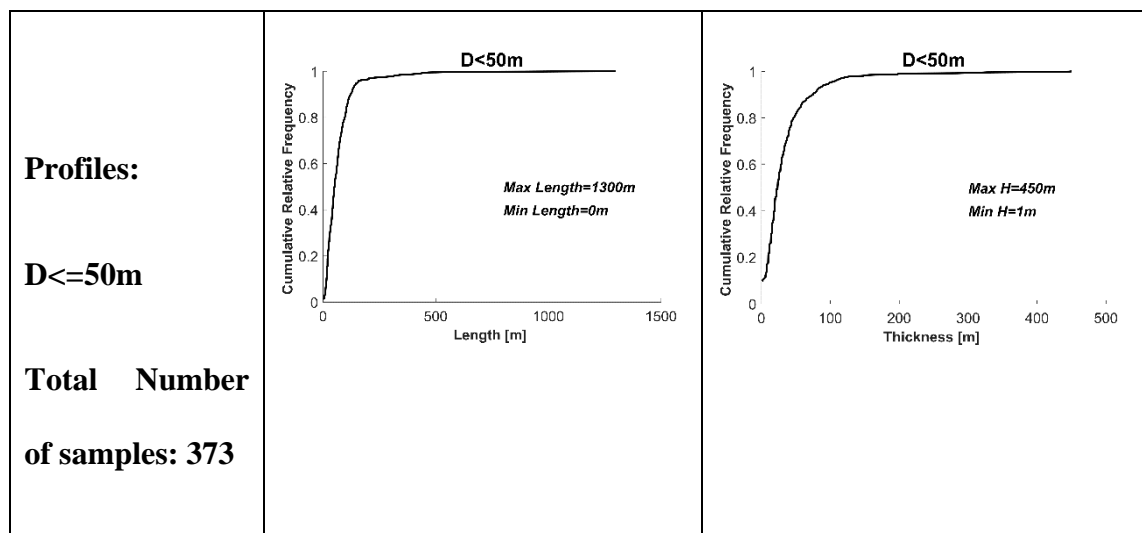


Figure B- 2. Taxonomy of the shear-wave velocity profile database

Once we have the final set of profiles, we proceed with the definition of some parameters.

Figure B-3 displays the cumulate relative frequency of profiles total length after D and thickness of layers. As mentioned above, the majority of the profiles in this database have a shallow D. The peak of total length is always located in a range smaller than 50m. This can be because the measurements have been stopped, once a certain value of V_s was reached (seismic bedrock), even though sometimes it leads to misrepresentation of the whole deposit. In fact, encountering a stiff material does not mean we always have an increasing V_s , from that point until the crustal depth. Instead, we could face an inversion of velocity.

According to the cumulative relative frequency thickness plots, the peak is always located between 0m and 50m. Actually, there are lot of values between 0-1 and this is why all the three cumulative relative frequencies start in a range between 0.1-0.4.



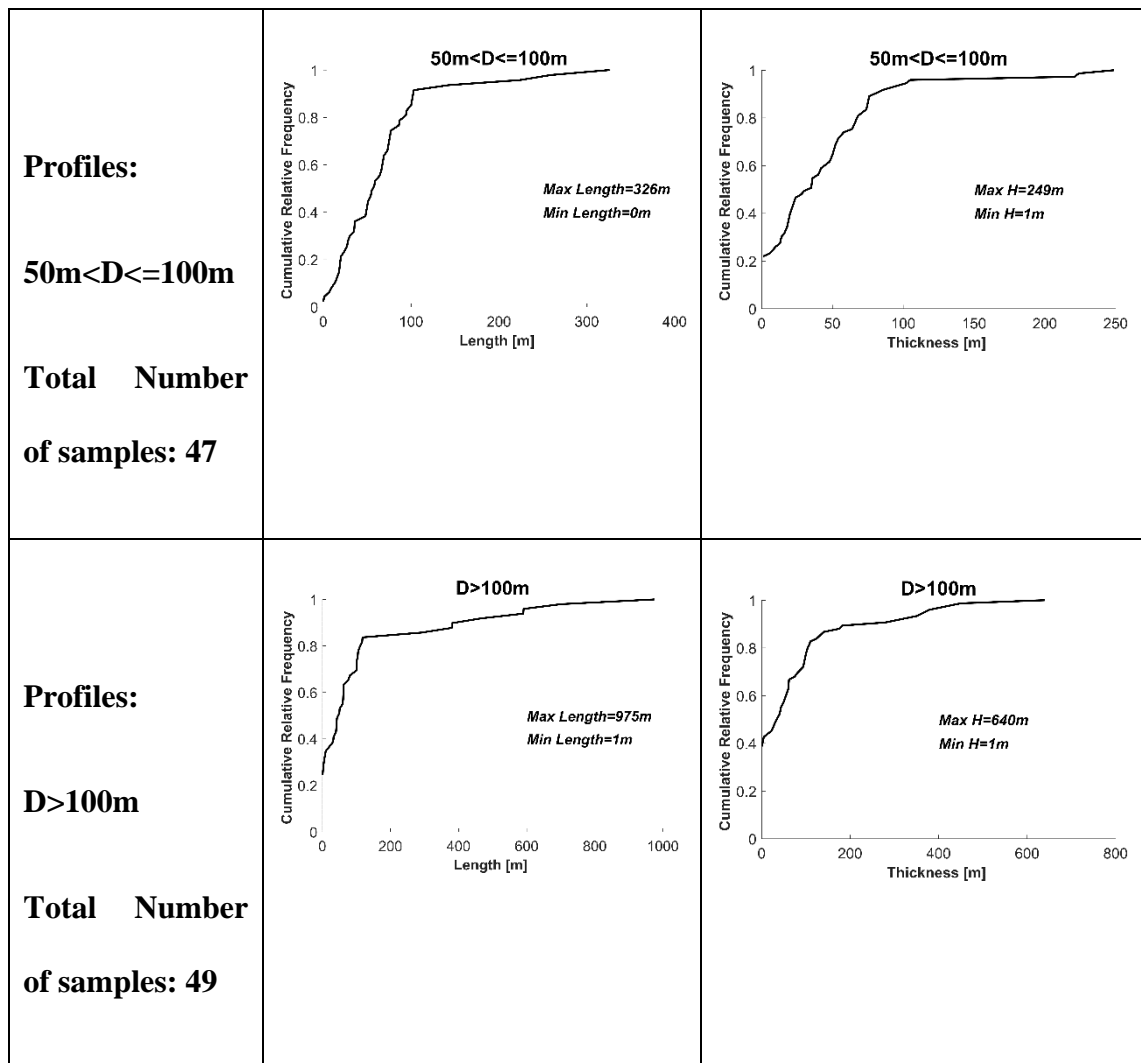


Figure B-3. Cumulative relative frequency plots of length after D and thickness of the layers. Top: $D \leq 50m$ profiles, center: $50m < D \leq 100m$, bottom: $D > 100m$

Figure B-3 misses the profiles with velocity inversions completely. For this group of profiles, we are going to characterize:

- Thickness of the layer with an inversion;
- Thickness of the top layer; and the
- Velocity step.

The chosen procedure aims to account for the effect of these three factors on site response. In particular, the thickness should shift the transfer function peaks, whereas the velocity step should modify the maximum amplification.

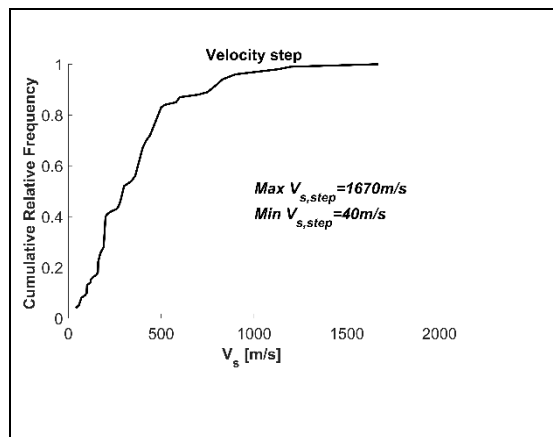
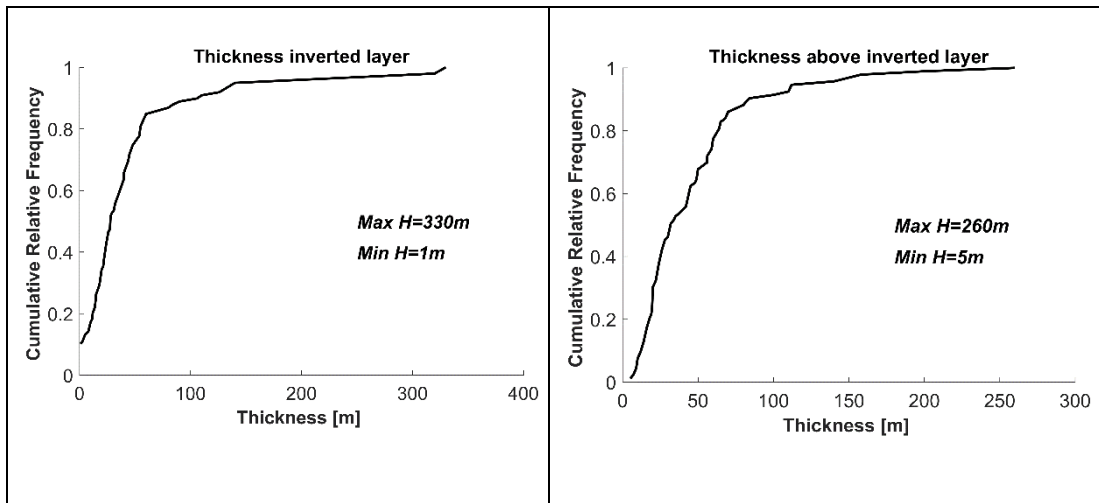


Figure B-4. Top left: Thickness of velocity inversion; top right: Thickness of the top layer; bottom: velocity step in the inversion.

Building a profile from the given information

Based on the given information (Figures B-3-4), our aim is to generate realistic shear wave velocity profiles for the deep portion of the Memphis site, as we are assuming that would not know it. Let us say that the only information we have is the shallow

portion of it (Figure 1) and the crustal velocity. We will use the data from $D > 100\text{m}$, as for the Memphis profile $D = 400\text{m}$.

The procedure is explained in Figure B-5, where two set of profiles are generated. The first kind does not present an inverted velocity. Indeed, it follows an increasing trend of V_s between $V_{s,\text{bedrock}}$ and the crustal velocity. Conversely, in the other one, which allows an inversion, the velocity actually decreases until a value that remains above $V_{s,\text{bedrock}}$. The basis of this procedure is to choose values in a random manner that is consistent with the frequency distribution plots given above.

Once these profiles have been generated, a full site response analysis is performed. As figure 5 shows, the most uncertain response is the one with the inversion.

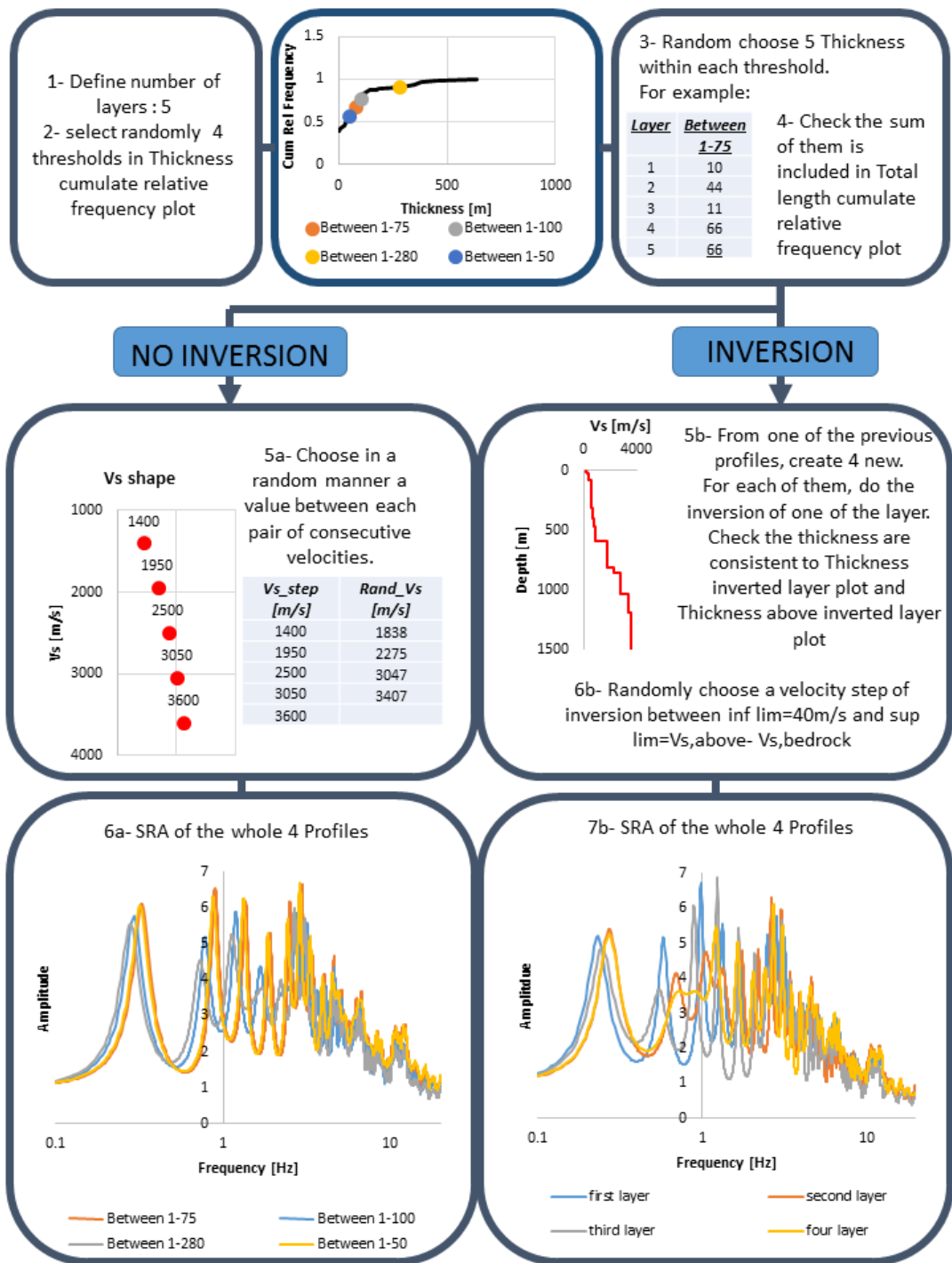


Figure B-5. Procedure to create invented deep portion of Memphis shear wave profile.

CONCLUSIONS

How much does the “dark zone” affect the final response? To answer this, we can compare the response from the:

- generated profile;
- the full original profile;
- quarter wavelength method profile, created using the procedure of Cotton et al. (2006) and the $V_{s,30}$ for this site; and
- the shallow profile;

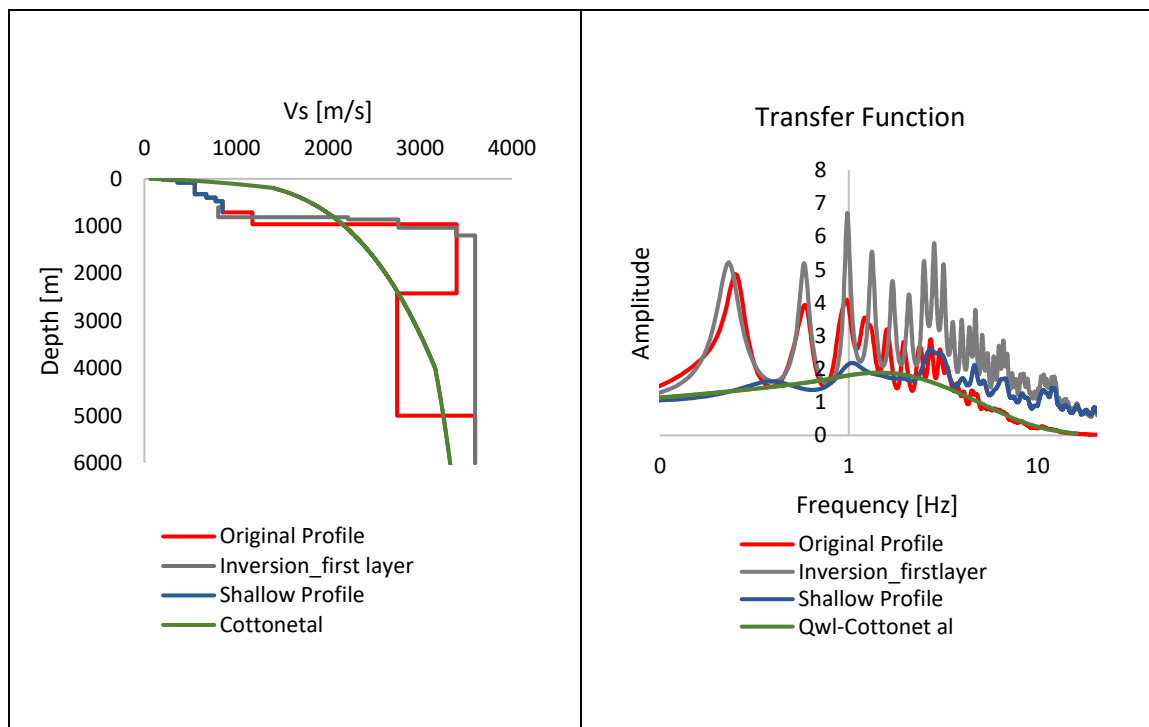


Figure B- 6. Comparison among original and shallow Memphis profiles, Cotton et al profile and the generated one with an inversion (left) and their transfer functions (right).

Figure B-6 shows this comparison. Considering just the shallow portion of the Memphis profile, we are actually ignoring the impedance ratio. That is why we do not have large peaks. We can say the same for the Cotton et al. (2006) profile because, although it reaches stiffer materials, it does so gradually. Conversely, comparing the original full profile and the generated one, we are comparing two similar results, at least for the first two peaks, although we observe a difference starting from 1Hz.

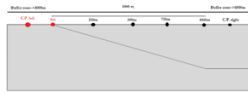
It appears to be important to study the deep portion of a shear-wave velocity profile, despite the fact that most of the time we do not have sufficient information about it. Therefore, a taxonomy, like the one in this work, can help to bridge this gap and give satisfactory results.

BIBLIOGRAPHY

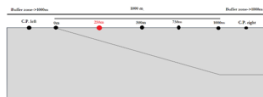
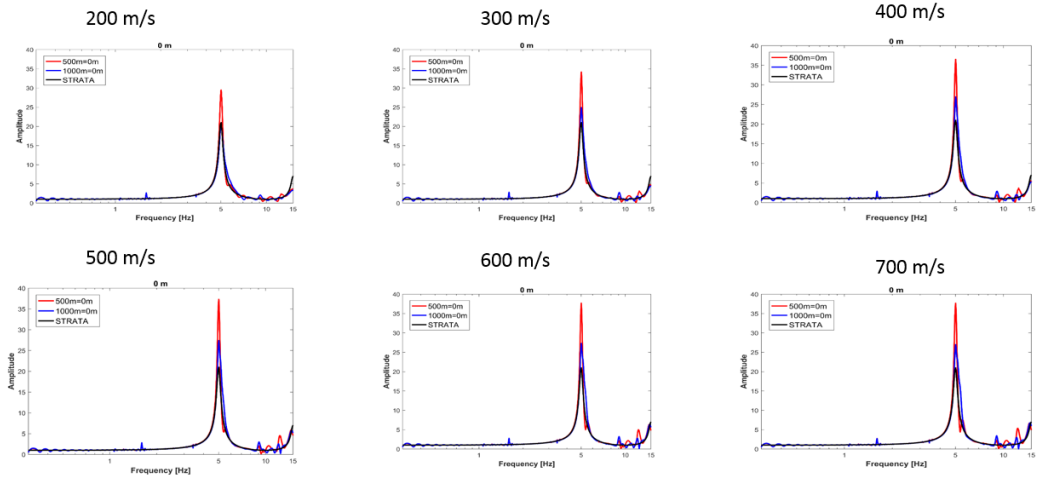
- Campbell K. W. (2009), Estimates of shear-wave Q and k_0 for Unconsolidated and Semiconsolidated Sediments in Eastern North America, *Bulletin of the Seismological Society of America*, 99(4): 2365-2392, doi: 10.1785/0120080116
- Cotton, F., F. Scherbaum, J.J. Bommer, and H. Bungum, (2006). Criteria for selecting and adjusting ground-motion models for specific target regions: Application to central Europe and rock sites, *Journal of Seismology* 10:137-156 doi:10.1007/s10950-005-9006-7
- Cramer, C. H., J. S. Gombert, E. S. Schweig, B. A. Waldron, and K. Tucker, (2004). The Memphis, Shelby County, Tennessee, seismic hazard maps, U.S. Geol. Surv. Open-File Rept. 04-1294.
- Douglas, J., P. Gehl, L. F. Bonilla, O. Scotti, J. Regnier, A. M. Duval, and E. Bertrand, (2009). Making the most of available site information for empirical ground-motion prediction, *Bulletin of the Seismological Society of America*, 99(3):1502-1520, doi: 10.1785/0120080075.
- Gombert, J., B. Waldron, E. Schweig, H. Hwang, A. Webbers, R. Van Arsdale, K. Tucker, R. Williams, R. Street, P. Mayne, W. Stephenson, J. Odum, C. Cramer, R. Updike, S. Hutson, and M. Bradley, (2003). Lithology and shear-wave velocity in Memphis, Tennessee, *Bulletin of the Seismological Society of America*, 93, 986–997.
- Luzi, L., R. Puglia, E. Russo, and ORFEUS WG5, (2016). Engineering Strong Motion Database, version 1.0. Istituto Nazionale di Geofisica e Vulcanologia, Observatories & Research Facilities for European Seismology. doi: 10.13127/ESM

- Pitilakis, K., E. Riga, A. Anastasiadis,, S. Fotopoulou, S. Karafagka, (2018). Towards the revision of EC8: proposal for an alternative site classification scheme and associated intensity dependent spectral amplification factors, *Soil Dynamics and Earthquake Engineering*, <http://doi.org/10.1016/j.soildyn.2018.03.030>

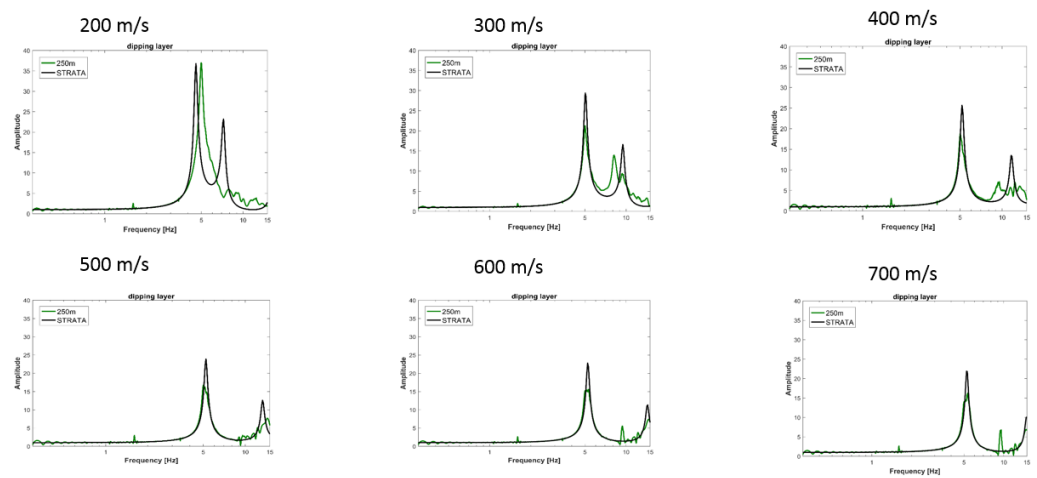
Appendix 3: Results of Abaqus simulations:

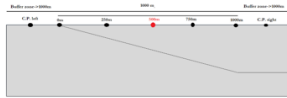


2 DEGREES: C.P. Left & 0m

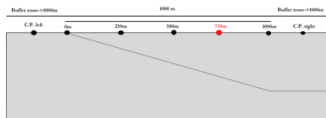
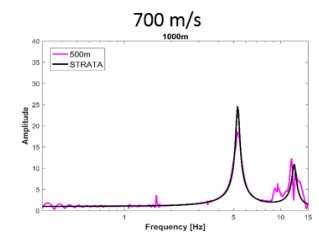
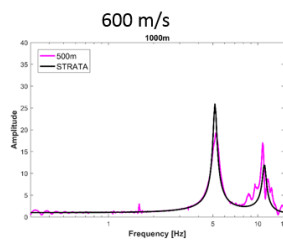
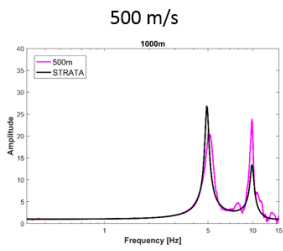
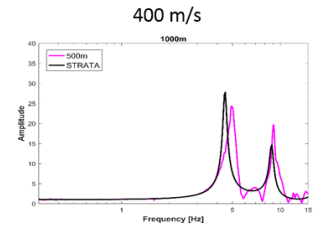
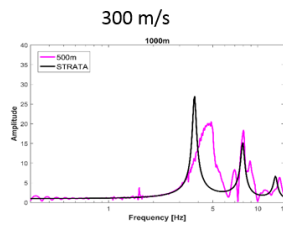
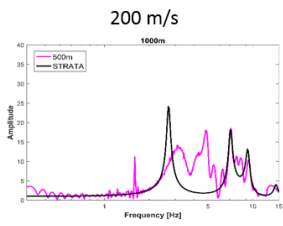


2 DEGREES: 250m

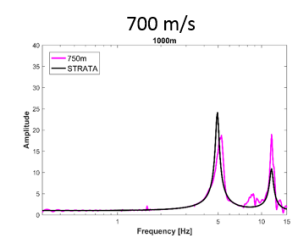
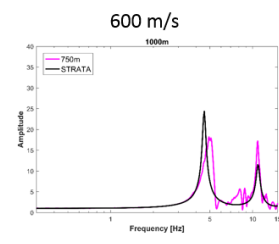
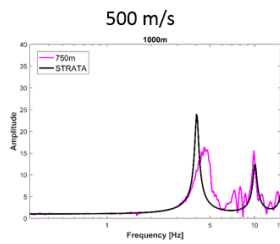
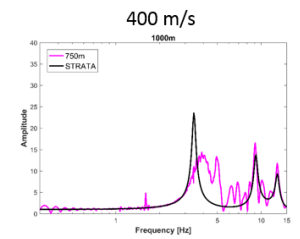
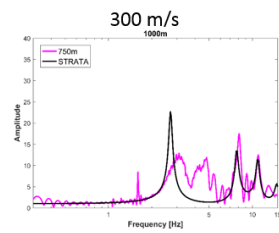
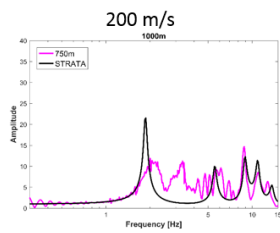


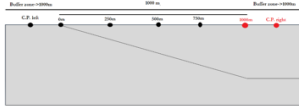


2 DEGREES: 500m

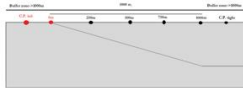
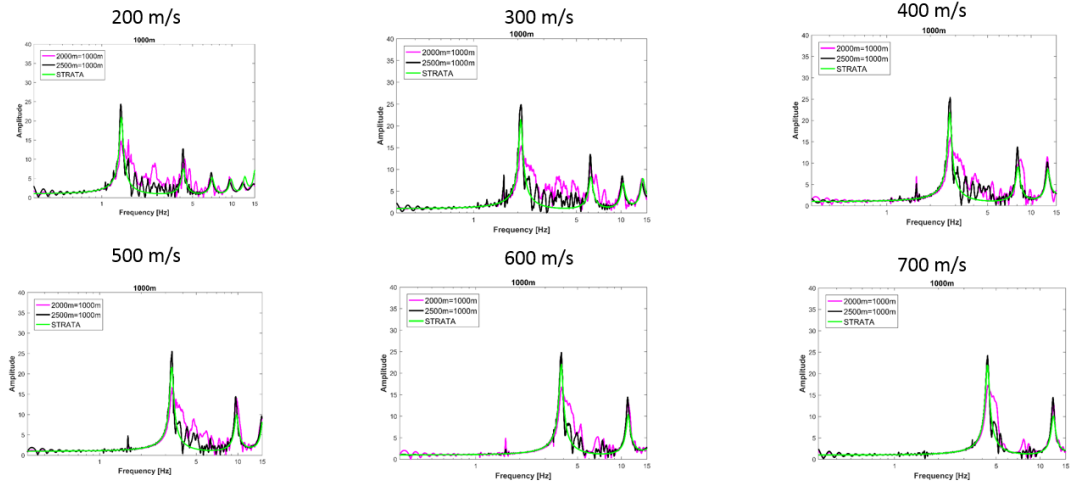


2 DEGREES: 750m

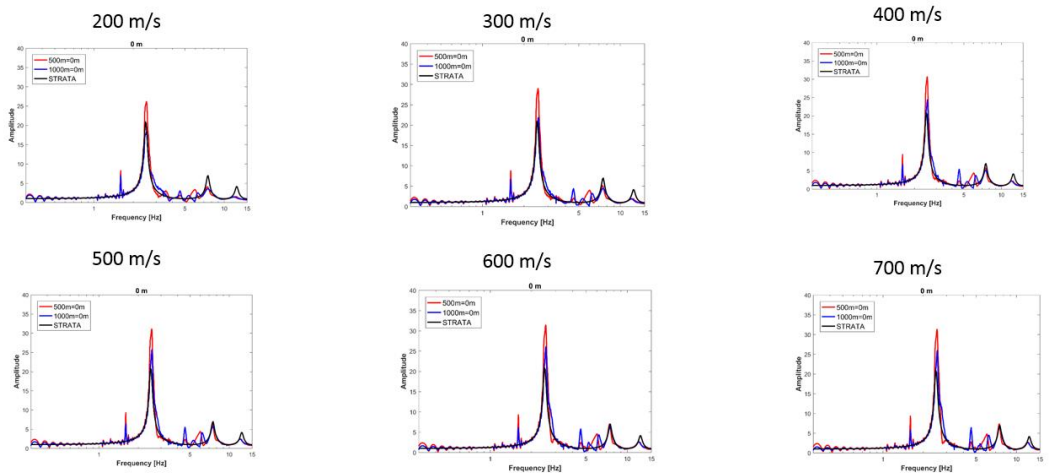


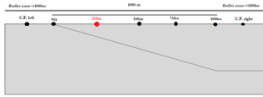


2 DEGREES: 1000m & C.P. right

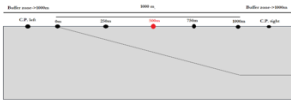
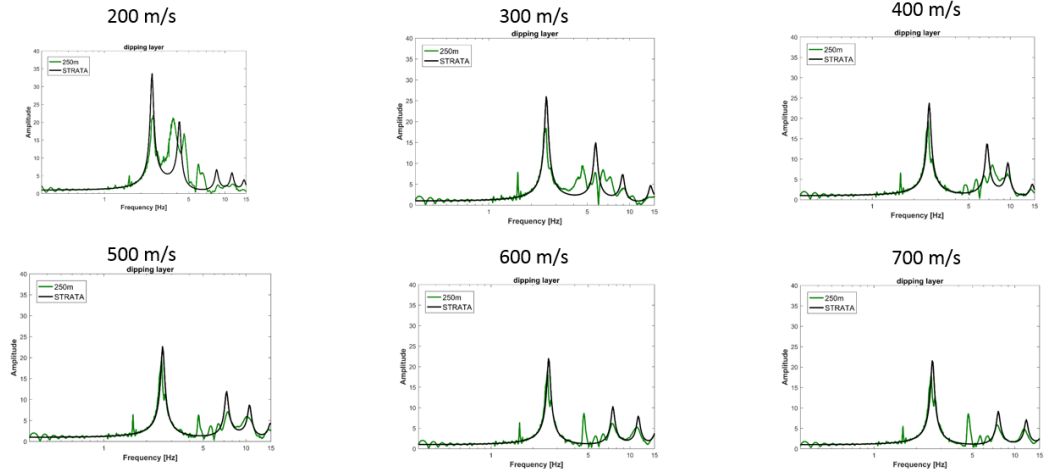


3 DEGREES: C.P. Left & 0m

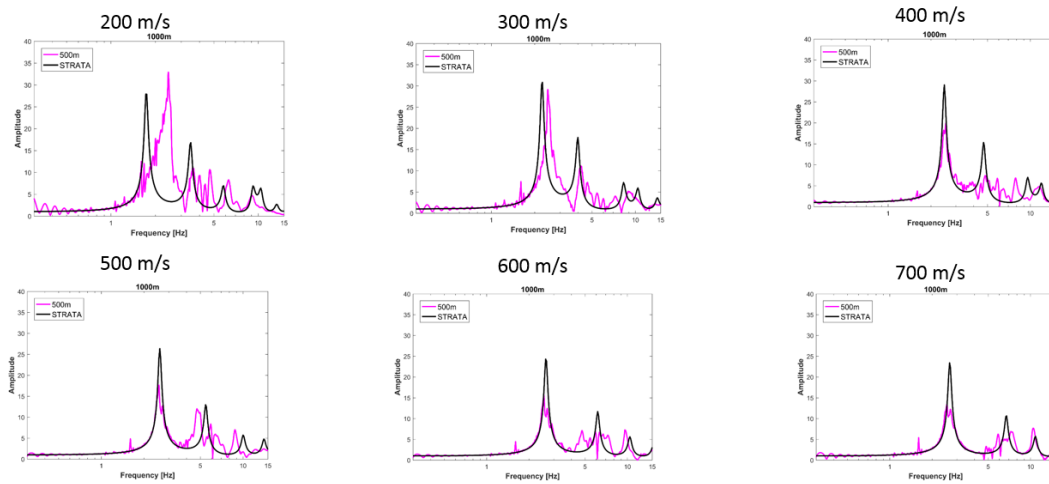


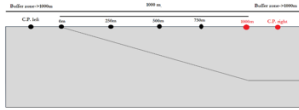


3 DEGREES: 250m

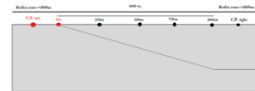
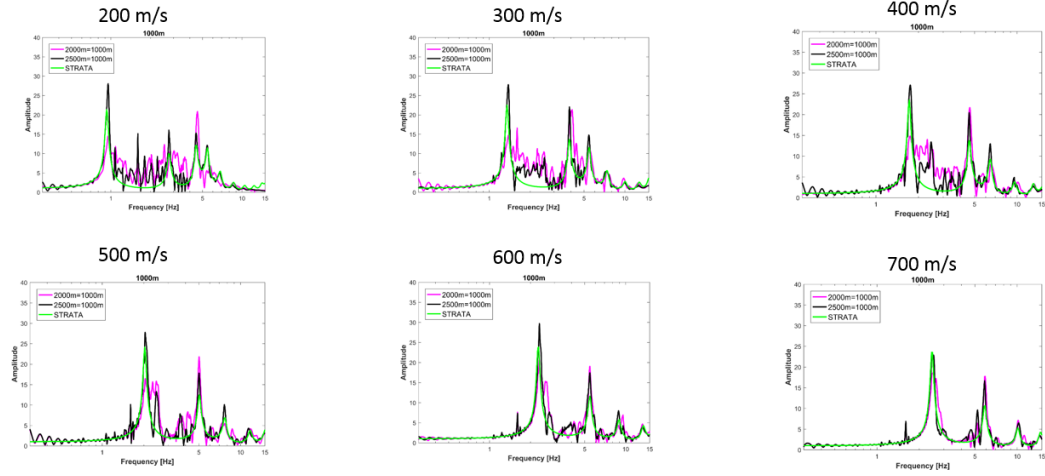


3 DEGREES: 500m

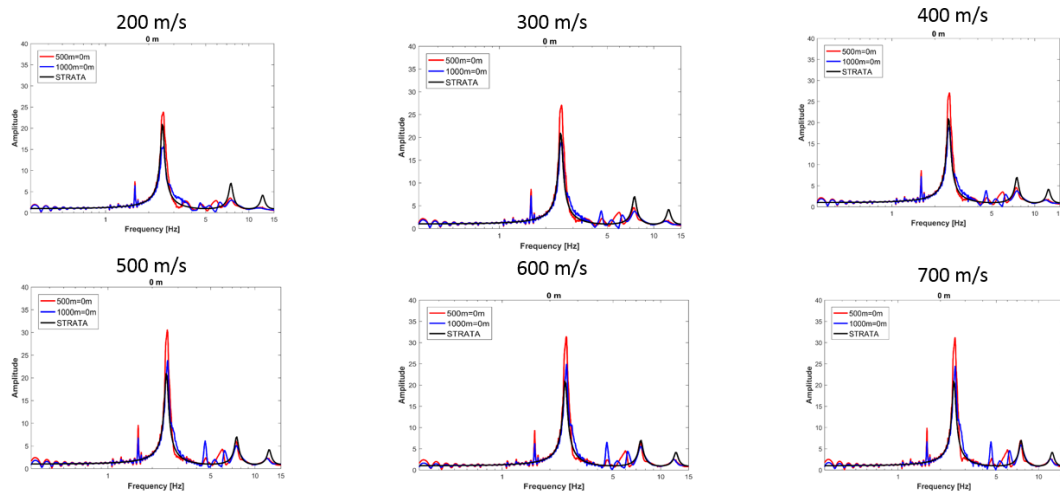


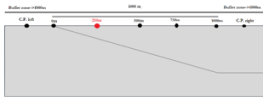


3 DEGREES: 1000m & C.P. right

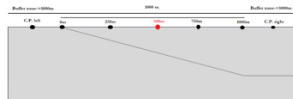
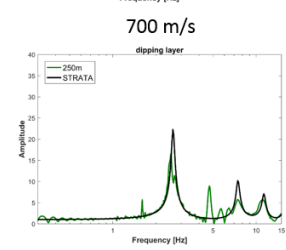
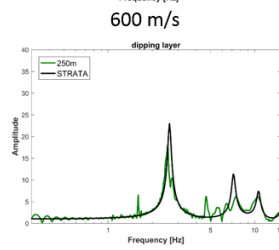
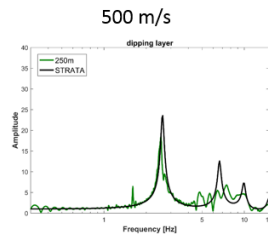
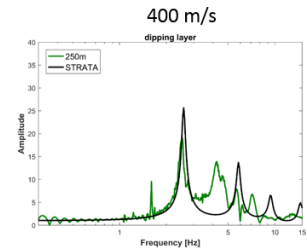
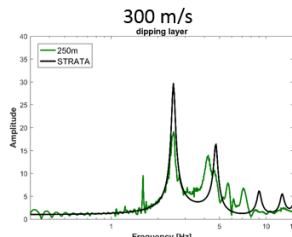
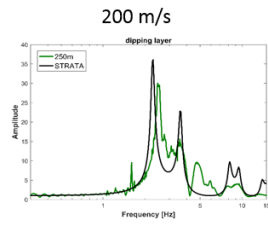


4 DEGREES: C.P. Left & 0m

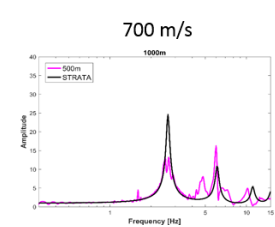
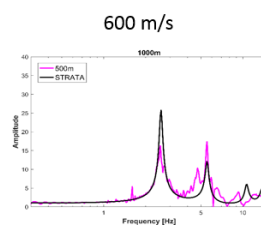
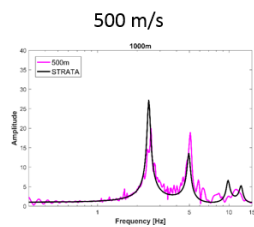
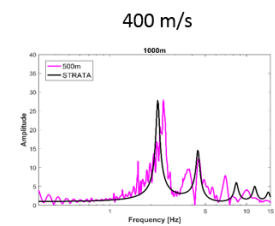
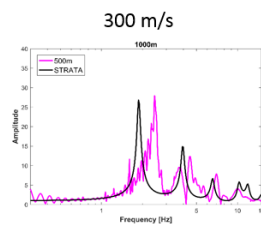
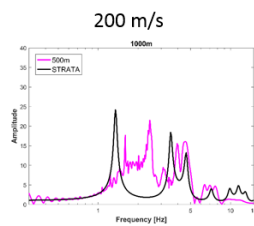


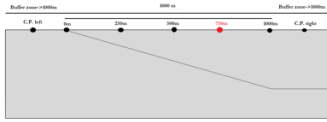


4 DEGREES: 250m

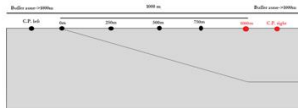
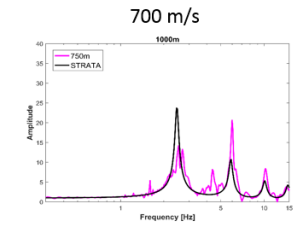
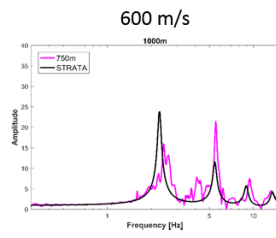
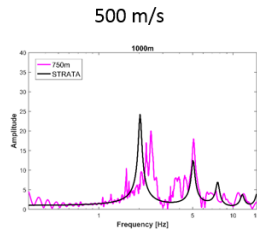
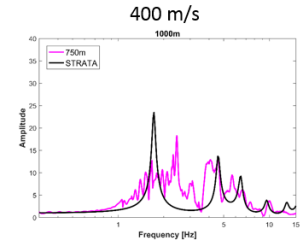
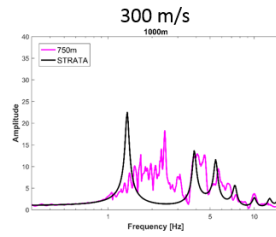
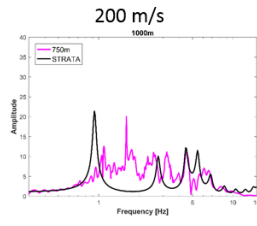


4 DEGREES: 500m

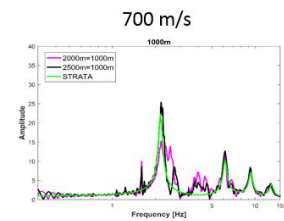
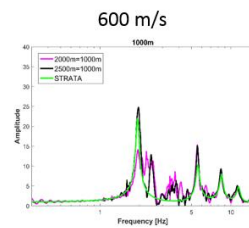
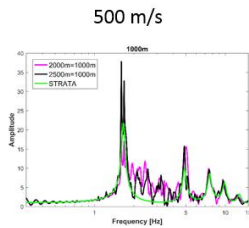
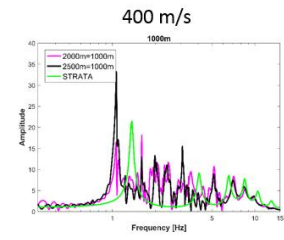
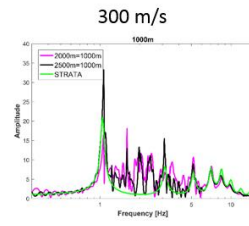
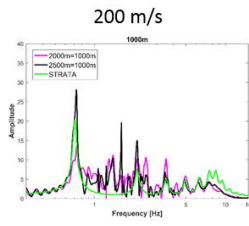


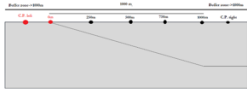


4 DEGREES: 750m

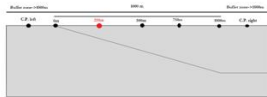
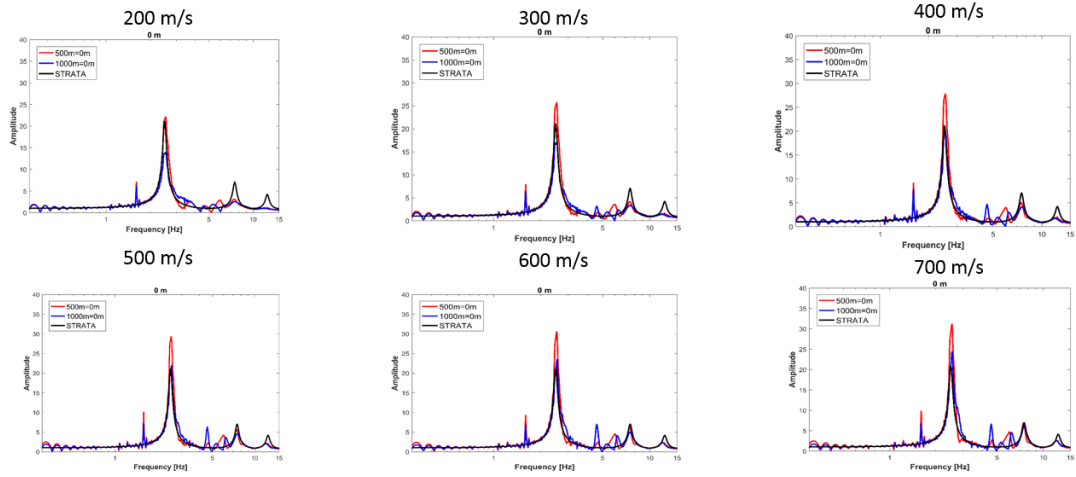


4 DEGREES: 1000m & C.P. right

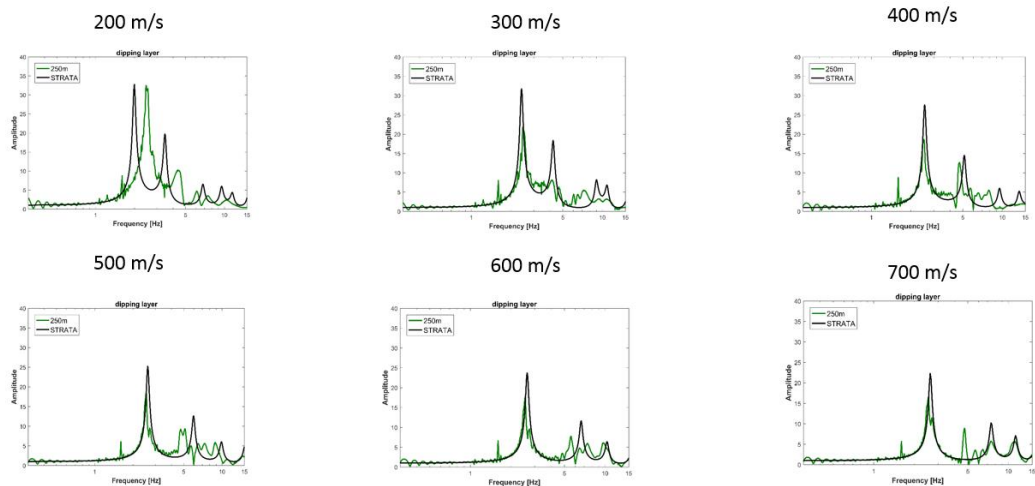


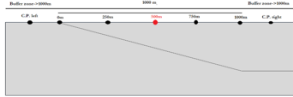


5 DEGREES: C.P. Left & 0m

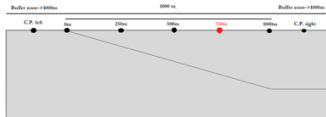
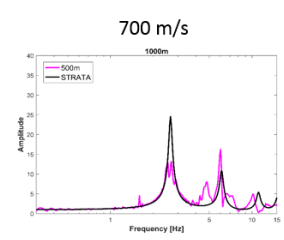
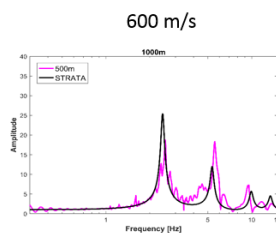
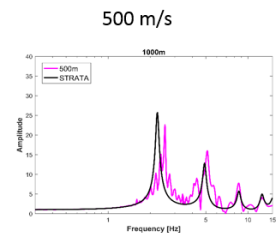
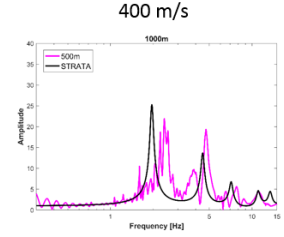
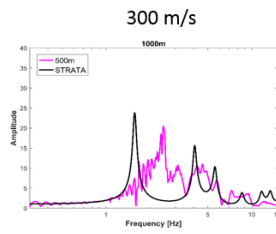
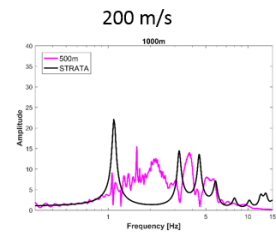


5 DEGREES: 250m

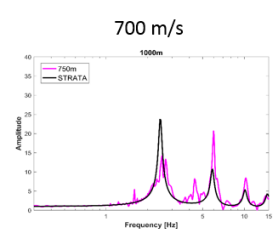
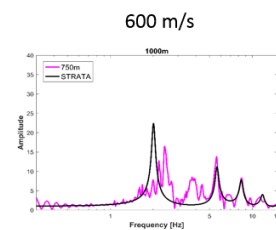
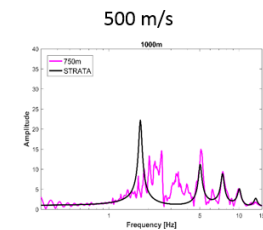
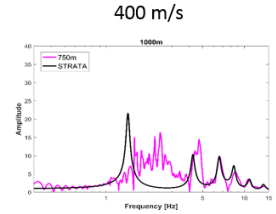
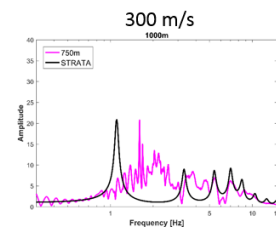
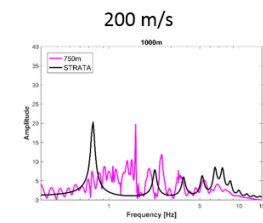


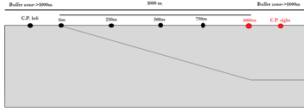


5 DEGREES: 500m



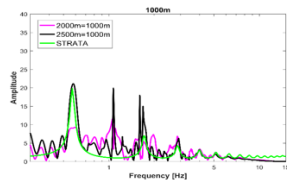
5 DEGREES: 750m



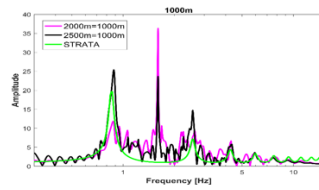


5 DEGREES: 1000m & C.P. right

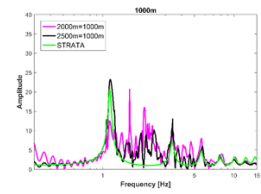
200 m/s



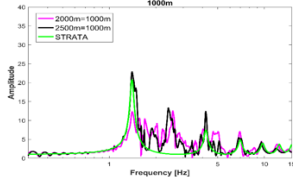
300 m/s



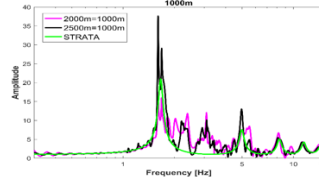
400 m/s



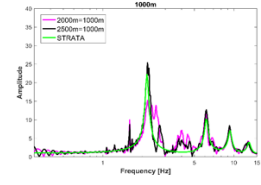
500 m/s



600 m/s



700 m/s



Appendix 4: Validation of the software used in Chapter 4

The procedure we develop uses a combination of Matlab and Seismo-soil, a software developed by Asimaki and Shi (2017). The first one generates the random profiles and the second one is needed for SRA. To validate the second program, we used Deepsoil (Hashash et al., 2006), a well-known software for SRA. We selected two different randomized Vs profiles (Figure D-1) and we have performed SRA using both software. In both cases, a damping of 0.01 and a density of 2800 Kg/m³ were assumed.

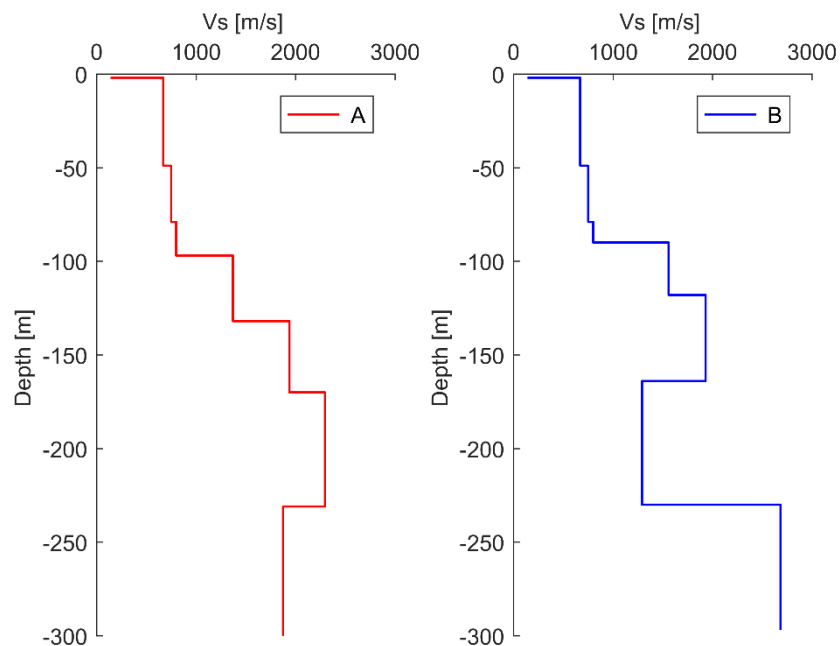


Figure D-1. Vs profiles used to validate Seismo-soil

Results show a perfect match between the two software (Figure D-2), demonstrating that Seismo-soil can be trusted as the main software for the calculations.

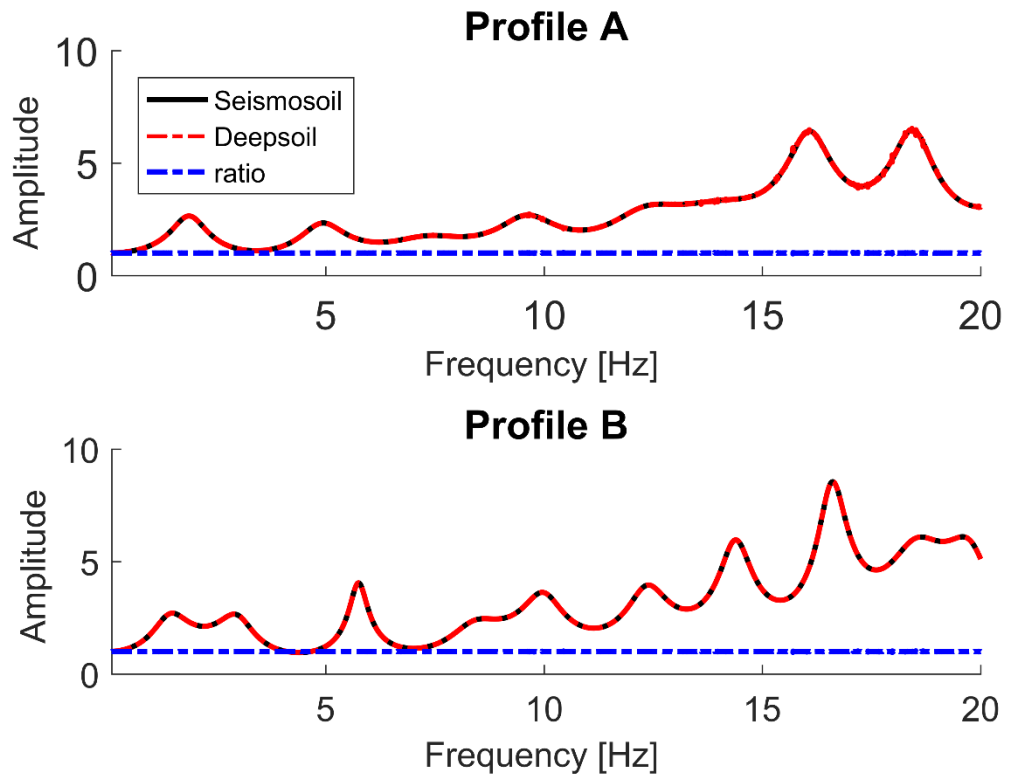


Figure D-2. Comparison between Seismo-soil and Deepsoil transfer functions of the two Vs profiles (A and B). The blue curve indicates the ratio between the results of the two programs.